IRF6 loss-of-function causes disturbances in epithelial polarity, enamel formation, and root patterning

Emily Y.Chu

A dissertation

Submitted in partial fulfillment of the

requirements for the degree of

Doctor of Philosophy

University of Washington

2015

Reading Committee:

Timothy Cox, Chair

Martha Somerman, Co-Chair

Michael Cunningham

Avina Paranjpe

Tracy Popowics

Program Authorized to offer Degree:

Oral Biology

University of Washington

Abstract

IRF6 loss-of-function causes disturbances in epithelial polarity, enamel formation, and root patterning

Emily Chu

Chairs of Supervisory Committee:

Timothy Cox

Martha Somerman

Interferon regulatory factor 6 (*IRF6*) variants are associated with common isolated forms of cleft lip with or without clefting of the palate (CLP). Based on high sequence and structural homology with other IRFs, IRF6 has been predicted to act as a transcription factor, but its function and role in CLP is largely unknown. Studies in the Cox lab have found that IRF6 binds, in a phosphorylation-enhanced manner, to the NME (non-metastatic) complex, which has been reported to interact with factors that activate the PAR (PARD3-PARD6) polarity complex. This provides a novel mechanism in which IRF6 may contribute to proper epithelial function. NME regulated PARD3 activation stimulates establishment of epithelial apical and basolateral domains (i.e. polarity), ultimately impacting epithelial cell adhesion, shape, and behavior. Thus, **via protein-**

protein interactions, IRF6 is hypothesized to contribute to the regulation of epithelial polarity, which when disrupted, leads to epithelial defects observed in CLP.

Specific aims were developed to investigate the contribution of IRF6 to primary palate and tooth development. Using site-directed mutagenesis, reported CLP associated VWS patient mutations were introduced into yeast and mammalian expression constructs and subsequently compared with wild type IRF6 in their ability to interact with NME. Out of the twelve mutations tested, nine mutations disrupted the IRF6:NME interaction. Additionally, mutating three conserved serines to alanines resulted in loss of IRF6:NME binding and lowered nuclear levels of IRF6. Potential effects of the IRF6:NME interaction on epithelial polarity were assessed by measuring activity of the GTPases Rac1 and RhoA, in HEK293T cells ectopically expressing either a wild type or mutant IRF6. Disruption of the IRF6:NME complex also caused active Rac1 and RhoA up-regulation.

In human patients, CLP is often associated with tooth abnormalities, and in mice, Irf6 was detected in ameloblasts and has roles in tooth epithelial invagination. A murine model with *Irf6* conditionally ablated in ameloblasts (driven by the *Pitx2-Cre* promoter) was developed. *Irf6* conditional knockouts-(*Irf6 cKO*) exhibited a variety of crown morphological alterations, including loss of cusp patterning. Hypodontia was also observed; 3rd molars were occasionally missing. Additionally, *Irf6-cKO* molars displayed

rapid enamel attrition with wear reaching dentin 7 days post-eruption. *Irf6-cKO* enamel was hypomineralized compared to controls ($p<0.05$), and a delay in maturation was observed. Histological sections revealed persistence of an immature enamel matrix in *Irf6-cKO* samples (not present in controls) in addition to disruptions in ameloblast polarity. Immunohistochemistry revealed upregulation of amelogenin and downregulation of kallikrein-like 4 in *Irf6-cKO* P14 molars. Root patterning defects were also observed in *Irf6-cKO* mice, including severely taurodontic mandibular second molars. In P4 *Irf6-ckO* molars, mRNA expression of enamel matrix proteins was unchanged, yet *Wnt10b* and *Osterix* were downregulated ($p<0.05$). By P13, *Wnt10b* and *Osterix* expression in *Irf6-cKO* mice were comparable to controls.

Overall, our findings contributed toward the understanding of the role of *Irf6* in CLP, as well as tooth abnormalities associated with epithelial disorders. Disruptions of IRF6:NME complex and altered Rac1/RhoA expression by IRF6/NME mutations suggest IRF6 can impact processes such as epithelial polarity. Tooth-targeted *Irf6* deletion in mice demonstrated enamel and root patterning defects consistent with CLP patients featuring *IRF6* mutations. These results identified a critical and non-redundant role for IRF6 in crown and root formation, suggesting diversity of *IRF6* function in epithelial-derived tissues.

The chapters in this thesis are organized by the following topics:

Chapter 1: Introduction to IRF6, palatogenesis, epithelial adhesion/polarity, and tooth development

Chapter 2: Materials and Methods

Chapter 3: Investigation of the IRF6:NME complex and its contribution to epithelial polarity: Tested IRF6 patient mutations and their ability to disrupt IRF6:NME binding, investigated factors regulating IRF6:NME complex and potential effects when it is disrupted,

Chapter 4: IRF6 loss-of-function causes defects in enamel formation and root patterning: characterization of *Irf6-cKO* model, investigated ameloblast polarity

Chapter 5: Towards understanding the role of IRF6 in tooth development: further characterization of *Irf6-cKO* model, investigated expression of enamel and dentin matrix proteins in *Irf6-cKO* samples versus controls

Chapter 6: Discussion: Propose pathways where IRF6 is a potential contributor

ABBREVIATIONS

λ: lambdoidal junction

AMBN: ameloblastin

AMEL: amelogenin

AP-2: adaptor protein complex 2

ARHGAP: Rho GTPase activating protein

ARF6: ADP-ribosylation factor 6

BMP: bone morphogenic protein

BPS: Bartsocas-Papas syndrome

cKO: conditional knockout

CLP: clefts with or without palatal involvement

Co-IP: Co-immunoprecipitation

Cre: Cre recombinase

DMP1: dentin matrix protein 1

DVL2: Dishevelled 2

EDA: Ectodysplasin A

EDTA: ethylenediaminetetraccetic acid

EMT: epithelial to mesenchymal transition

ENAM: Enamelin

FGF: fibroblast growth factor

GEF: guanine nucleotide exchange factor

GRHL3: Grainyhead-like 3

GTPase: guanosinetriphosphatase

HERS: Hertwig's epithelial root sheath

IAD: interferon association domain

IRF3: Interferon Regulatory Factor 3

IRF5: Interferon Regulatory Factor 5

IRF6: Interferon Regulatory Factor 6

K14: Keratin 14

KLK4: Kallikrein 4

KSR: kinase suppressor of Ras

LBC: A-Kinase Anchoring Protein-LBC

MEE: medial edge epithelium

MES: midline epithelial seam

MMP20: Matrix metalloproteinase 20

NDPK: nucleoside diphosphate kinase

OSX: osterix

OVOL1: OVO-like 1

PAR: PARD3-PARD6 polarity complex

PAGE: Polyacrylamide gel electrophoresis

PCR: Polymerase chain reaction

PDL: periodontal ligament

PFA: paraformaldehyde

PPS: popliteal pterygium syndrome

Rac1: Ras-related C3 botulinum toxin substrate 1

RGS19: regulator of G protein signaling 19

Rho: Ras homolog gene family

RhoA: Ras homolog gene family, member A

RIPK4: receptor interacting serine-threonine kinase 4

SDS: Sodium dodecyl sulfate

SHH: Sonic hedgehog

SMAD: mothers against decapentaplegic homolog

SRR: serine rich region

TIAM1: T-cell lymphoma invasion and metastasis 1

TGFβ: transforming growth factor beta

TGFB2: Tgfβ II receptor

TJs: tight junctions

TNAP: tissue non-specific alkaline phosphatase

TP63: tumor protein 63

UTR: untranslated region

VWS: Van der Woude Syndrome

Wnt: wingless type

Y2H: yeast two-hybrid

ACKNOWLEDGEMENTS

First, I would like to acknowledge my PhD mentors and chairs of my thesis supervisory committee, Dr. Timothy Cox and Dr. Martha Somerman for their mentorship, support, encouragement, and especially for making me a better scientist. I am always impressed by their scientific knowledge, and I feel privileged to have worked with them. I feel that I am more equipped now to handle scientific issues. I have learned many new techniques in the lab, and my writing/presentation skills have improved. Working with them has reinforced to me that although challenging, science is exciting and thus, I credit a significant amount of my accomplishments in my PhD program to their mentorship. I would also like to extend my gratitude to my thesis supervisory committee, Dr. Michael Cunningham, Dr. Avina Paranjpe, Dr. Tracy Popowics, and Dr. Daniel Chan (Graduate School Representative). I am especially grateful for their advice and guidance throughout my PhD career. They provided a variety of perspectives, and I feel that I have really benefited from their support.

In working with Dr. Cox and Dr. Somerman, I have benefited from working with wonderful individuals in their labs, and I am also extremely grateful for the opportunities to work in environments such as the University of Washington, Seattle Children's Research Institute, and the National Institutes of Health. I would like to mention Dr. Brian Foster, who was my first unofficial mentor at the University of Washington, where I decided to pursue the DDS PhD program. Additionally, I would also like to acknowledge the University of Washington Department of Oral Health

Sciences for their support, especially Dr. Richard Presland, Jennifer Kohn, Kathy Hobson, Rosale Meriales, and Eileen Kakida. They were also significant contributors to my success in the program.

I would also like to acknowledge sources of my funding support: the National Institutes of Health (for the UW institutional grant as well as my individual F30 fellowship), the University of Washington (for travel awards), the American Cleft Palate Association (Junior Investigator Award), and the Magnuson family for the Magnuson Scholarship. This funding has allowed me to pursue my goals in science, and I am deeply indebted to all of these institutions.

To all my friends—I wish I had space to name you all. Thank you for adding another dimension to my life besides work, and I gained many wonderful memories.

Last, but not least, I would like to acknowledge my parents, Tung and Hui Chu, and my sister, Felicia Chu. Words cannot express how much love, understanding, and encouragement they have given me, and I would not be where I am today without them. Every accomplishment I made in my life would not have been possible without them.

Table of Contents

List of Figures

List of Tables

Chapter 1: Introduction

CLP as a global disease

Clefts of the lip with or without clefting of the palate (CLP) are the most common congenital deformities of the face, occurring with a global incidence of approximately 1 in every 600 to 700 live births (1-4). CLP has multiple etiologies, including a genetic basis (*1, 2*). Genome-wide association studies have implicated Interferon Regulatory Factor 6 (*IRF6*) variants as major contributors to CLP incidence. *IRF6* mutations cause van der Woude syndrome (VWS) and popliteal pterygium syndrome (PPS), which notably feature orofacial clefts (5-33). VWS is the most common form of syndromic CLP, predicted to account for 2% of all syndromic forms of CLP. Additionally, IRF6 variants are linked to approximately 12% of nonsyndromic forms of CLP (34).

CLP is a result of an aberration in the fusion of embryonic structures during facial development (*35, 36*). Development of the primary palate is dependent on proper fusion of the two maxillary processes with the medial nasal processes (37). This fusion occurs during the sixth week of human development and mouse embryonic day 10.5. A critical step in this fusion process is adhesion of epithelial surfaces, and as a result of, failure to fuse in embryonic facial primordia, clefting may present either as a unilateral or bilateral anomaly (*35, 38*). Depending on the severity, CLP can require many years of therapy and management.

CLP is a public health problem

CLP dramatically alters the quality of life of affected individuals, often resulting in eating, speaking, and auditory problems. The consequences of not repairing CLP includes velopharyngeal insufficiency, which compromises feeding and speaking (*39, 40*). Other orofacial and dental complications include midface retrusion, collapse of the alveolar arches, and malocclusion (*39, 40*). In concurrence with these complications, CLP patients are likely to experience negative psychological effects. In a study of school-aged children with CLP, 69% reported bullying (41). Of the 69%, 84% of the taunts were related to the facial clefts. In a study of adults who had undergone CLP repair, the incidence of anxiety and depression was twice as high in CLP individuals versus controls (*42, 43*). In these studies, contributors to the anxiety and depression included dissatisfaction with appearance, dentition, speech, as well as a desire for further treatment. The current standard of care for CLP is surgery, which may require multiple surgeries as the child ages.

For reference, a general timeline of CLP is provided (*39, 40*) with medical and dental procedures highlighted:

- Prenatal: medical diagnosis, genetic counseling, psychosocial issues
- Neonatal (0-1 month): continue above, feeding, hearing screening, monitor growth
- 1-4 months: continue monitoring hearing, feeding, and growth, ***repair cleft lip***
- 5-15 months: continue monitoring hearing, feeding, and growth, ***repair cleft palate***

- 16-24 months: assess speech and language development, monitor ears and hearing, place ear tubes if necessary
- 2-5 years: monitor speech and language development, manage velopharyngeal deficiency, consider lip/nose revision
- 6-11 years: monitor speech and language development, manage velopharyngeal deficiency, ***orthodontic evaluation and treatment***, ***alveolar bone graft***, monitor school and psychosocial needs
- 12-21 years: monitor school and psychosocial needs***, orthodontics and restorative dentistry***, ***rhinoplasty and orthognathic surgery*** (if needed)

Consequently, management of CLP is multidisciplinary and multistage process, often leading to financial and psychosocial challenges. Furthermore, timing of surgical procedures may affect the wellbeing of the affected individual; individuals receiving surgical procedure earlier were reported to have higher self-esteem compared to individuals receiving the surgery later (44). Identifying risk factors, genes, and pathways involved may assist in management of CLP by helping to identify susceptible populations and develop more targeted therapies.

Development of the face

Facial clefts occur as a result of abnormal merging or fusion events (*35, 38, 45*). In facial development, the joining of two processes occurs either through merging or fusion. Merging of two processes refers to the removal of a furrow in between two facial

processes. Proliferation of the underlying mesenchyme removes the furrow. Fusion occurs between two separate, distinct facial processes, and this requires adhesion of the epithelia overlying the facial processes, removal of the epithelial seam between the two processes, and merging of the underlying mesenchyme.

During the fourth week of human development, the face is composed of five separate mesenchymal prominences that encircle the stomodeum, or primitive mouth (*45, 46*). The two maxillary prominences appear lateral to the stomodeum, the mandibular prominences lie caudal to the stomodeum, and the frontonasal prominence is present on the upper border of the stomodeum. During the fifth week of human development, invagination of the nasal placodes gives rise to a ridge of tissue, which form the medial and lateral nasal processes. During the sixth and seventh weeks of human development, the maxillary prominences grow, and the medial nasal and maxillary prominences fuse. The junction at which the maxillary process, medial nasal process, and the lateral nasal process meet is termed the lambdoidal junction (λ) (47). Fusion of the medial nasal and maxillary prominences forms the upper lip, and merging of the mandibular processes forms the lower lip and jaw. Merging of the medial nasal processes results in formation of the intermaxillary segment, which gives rise to the philtrum of the upper lip and the primary palate.

Also during the sixth week of human development, the palatine shelves are present (*45, 46*). They are first oriented obliquely downward on either side of the tongue, and by the seventh week, they begin to assume a more horizontal position. Once the shelves are fully horizontal, proliferation of the palatal shelves brings the shelves closer together. The mesenchyme of the palatal shelves is covered by a layer of epithelium, termed the medial edge epithelium (MEE). When the palatal shelves contact, the midline epithelial seam (MES) is formed. Fusion requires removal of the MES, and the palatine shelves fuse in an anterior to posterior direction, forming the secondary palate. In the anterior region, the palatine shelves fuse with the primary palate.

Abnormal epithelial fusion results in a variety of orofacial clefts. Clefts of the lip can present unilaterally or bilaterally (45). Unilateral cleft lip is caused by failure of the maxillary and lateral nasal processes to fuse, and bilateral cleft lip is caused by failure of the maxillary and median nasal processes to fuse (45). Inadequate merging of medial nasal processes results in median cleft lip. Clefts of the lip frequently occur in conjunction with clefts of the palate; clefting of the lip often distorts the position of the palatine shelves, causing improper contact of palatine shelves during fusion. Clefts of the palate also occur without facial clefts, and these are caused by failure of fusion between the palatine processes (45).

Behavior of epithelia during fusion

During fusion of the facial processes, epithelia overlying the mesenchyme undergo morphological changes. In development, immature ectoderm is initially composed of a single layer of undifferentiated, cuboidal cells, which stratify and differentiate, ultimately forming the mature epidermis (48). Following the first stratification, the periderm, a single layer of flattened cells covering the developing epidermis, is formed over the basal layer (*48, 49*). Oral periderm development has been examined in mice (50). P63 is a marker for the basal layer, and keratin 17 (K17) is a marker for periderm, and a K17-GFP promoter has been used to trace periderm development (50). In E10.5 embryos, the periderm is formed over the developing facial processes, and by E12.5, the periderm overlying the palatal shelves were also K17-GFP positive. Additionally, the periderm is highly proliferative; the majority of its activity occurs between E11.5-E15.5 (50). In these studies, periderm cell proliferation was inversely related to epithelial differentiation. By E16, terminal differentiation of the epidermis has been initiated, foreshadowing periderm removal (50).

The periderm serves as a barrier between apposing epithelia, preventing premature fusion. As the facial processes approach each other, the periderm must be removed for proper adhesion of the underlying basal epithelial cells. Thus, prior to contact, periderm cells overlying the MEE bulge and desquamate (51-54). Subsequently, filopodia, cytoplasmic projections and lamellipodia, cytoskeletal actin projections, are induced

which facilitate recognition and contact of apposing epithelia (*35, 51, 54*). Adhesion of the epithelia generates the MES, which has to be removed for mesenchymal continuity. Three hypotheses have been proposed for this removal: epithelial to mesenchymal (EMT) of the MES, cell death of the MES (primarily by apoptosis), and migration of MES cells away from the midline. Studies have provided evidence toward each one of these hypotheses; thus, removal of MES is likely coordinated by multiple processes (55). Regardless, MES requires disintegration of cell-cell adhesion complexes (adherens junctions, tight junctions, desmosomes) and alterations in cytoskeletal components. E-cadherin, the main cell adhesion molecule in adherens junctions, is downregulated during breakdown of the MES (56). Persistence of E-cadherin impairs fusion and mesenchymal confluence. Loss of E-cadherin can also lead to a tumorigenic epithelial phenotype (57). E-cadherin deletions have also been detected in families with CLP (58). Consequently, dysregulation of adhesion complexes can disrupt fusion of facial primordia.

Roles of IRF6 in developing epithelia

Irf6 expression has been detected in ectoderm overlying facial processes during formation of the lip, primary palate, and secondary palate, suggesting that *Irf6* has roles in epithelial adhesion and fusion (5, 59, 60). Further, in situ hybridization has detected *Irf6* expression in the periderm. To study *Irf6* function in developing epithelia, $Irf6^{R84C/R84C}$ mutants were generated (61). R84C is the most common IRF6 mutation found in PPS patients. Epidermis from these *Irf6* mutants failed to differentiate

properly, and ectopic epithelial adhesions were observed. In controls, the basal layer and periderm were labeled as distinct layers with p63 and K17, respectively. In contrast, K17 expression was dramatically reduced in *Irf6*$^{R84C/R84C}$ mutants, and the basal layer appeared thickened and disorganized. In the zebrafish model, a dominant negative form of Irf6 inhibited the expression of Grainyhead-Like 3 (Grhl3), which also has roles in maintaining epithelial integrity (62).

Further suggesting roles of IRF6 in epithelial differentiation, the expression of adhesion molecules was altered in *Irf6*$^{R84C/R84C}$ mutants compared to controls. Markers such as desmoplakin (desmosomes) and E-cadherin (adherens junctions) have been used to gauge status of epithelial adhesion complexes and polarity in *Irf6*$^{R84C/R84C}$ mutants. Prior to periderm formation, *Irf6*$^{R84C/R84C}$ epidermis was comparable to wild-type controls. In normal periderm development, epithelial cells are polarized with respect to their distribution of adhesion complexes. However, desmoplakin and E-cadherin exhibited altered distribution in *Irf6*$^{R84C/R84C}$ mutants. Desmoplakin was observed on the outer surface of the *Irf6*$^{R84C/R84C}$ mutant epithelium, whereas in wild-type epithelium, it was absent. E-cadherin was detected in *Irf6*$^{R84C/R84C}$ basal cells, which was not detected in controls. TEM analysis revealed multiple membrane protrusions on the apical surface of exposed basal cells and found desmosomes in ectopic adhesions detected in *Irf6*$^{R84C/R84C}$ mutants.

IRF6 and signaling pathways involved in palatal fusion

A myriad of genetic pathways have been implicated in palatal fusion events; these include the sonic hedgehog (Shh), bone morphogenetic protein (Bmp), fibroblast growth factor (Fgf), transforming growth factor beta (TGFβ) and wingless type (Wnt) pathways (35, 38, 63). Participants in these pathways include extracellular signaling factors, transcription factors, protein modification factors, cell adhesion molecules, extracellular matrix members, and molecules involved in kinase cascades. Of these pathways, *IRF6* has most frequently been associated with TGFβ and Wnt pathways.

TGFβ members have several roles in palatogenesis. In the TGFβ pathway, TGFβ activates its serine/threonine kinase receptors, leading to phosphorylation of mothers against decapentaplegic homolog (SMAD) proteins (64-66). Phosphorylation of Smad2 and Smad3 allows them to form transcriptional complexes with Smad4. These complexes are subsequently translocated to the nucleus, leading to activation of TGFβ targets. TGFβ1 and TGFβ3 are expressed in the MEE during palatal development, and *Tgfβ3*-null mice exhibit persistence of the MES and disrupted palatal fusion (66, 67). Furthermore, in Keratin14-*Cre recombinase* (*K14-Cre*)*; Tgfβ II receptor* (*Tgfbr2)* conditional knockouts, complete clefting of the soft palate, epithelial outgrowths of the primary palate, and persistence of the MEE were observed (68). *Irf6* has been detected in MEE during palatal fusion, and *Tgfbr2* mutants exhibit decreased Irf6 expression in the MEE (60, 69). Additionally, $Smad4^{fl/fl}$*; K14-Cre;* $Irf6^{+/R84C}$ mice exhibited submucosal

cleft palate and persistence of MEE, and overexpression of *Irf6* rescued MEE degeneration in *K14-Cre; Tgfbr2*$^{fl/fl}$ mice (68). Thus, this data suggests that IRF6 and TGFβ members participate in the same pathway to regulate the MEE in palatal fusion.

Irf6 is also believed to participate with Wnt family members in palatogenesis. WNT9b has been implicated in CLP; *Wnt 9b null* mice exhibit clefts of the secondary palate (70). WNT9b is expressed in the epithelia of maxillary, medial, and lateral nasal processes in E9.5 through E11.5 mouse embryonic ages, and via Tumor Protein 63 (TP63), is believed to regulate *IRF6* activity. Loss of *Tp63* in mice also results in facial clefting (71). p63 has been found to bind to an enhancer region within the *Irf6* locus, thus directly regulating *Irf6 (71).* Palatal epithelium from *p63-null* mice also exhibit reduced *Irf6* levels, and *p63*$^{+/-}$*; Irf6*$^{R84C/+}$ mutants exhibited dysregulation of periderm, and palatal shelves failed to fuse (72). Knockdown of *p63* in mouse keratinocytes revealed a decrease in *Irf6 mRNA* expression. *Irf6* and *p63* are both expressed at the λ junction, suggesting that this *p63-Irf6* regulation participates in the fusion of facial primordia. Furthermore, lower levels of *Irf6* and *p63* were detected in the λ junction of *Wnt9b null* mice, thus linking the WNT pathway with *IRF6* regulation in facial epithelia (72).

Other roles of IRF6

Additionally, studies to date suggest that IRF6 has significant roles in skin, limb, and craniofacial development. All current Irf6 murine lines exhibit recessive inheritance

with homozygotes dying before or shortly after birth as a result of inadequate barrier function through the skin (73). On a gross level, compared to wild type littermates, Irf6 knockout mice lacked external ears, had shorter snouts and jaws, as well as lacked hindlimbs and tail. Histologic examination revealed that homozygous null embryos do not form all layers of the epidermis. Wild-type embryos form basal, spinous, granular, and cornified layers, whereas *Irf6* homozygous null embryos possess an expanded spinous layer while lacking granular and cornified layers of the epidermis. Terminal deoxynucleotidyl transferase dUTP nick end labeling (TUNEL) and 5-bromo-2'-deoxyuridine (BrdU) analyses suggest this expansion is a result of increased proliferation and defective terminal keratinocyte differentiation. In addition, similar to PPS patients, ectopic epidermal adhesions were noted in the oral cavity (ventral surface of the tongue and the floor of the mouth). Epidermal adhesions were also noted between the tail and hindlimbs, as well as in the esophagus, further indicating unregulated proliferation and keratinocyte differentiation.

NME2 has been identified as a potential IRF6 protein-protein interactor

In order to identify potential IRF6 interacting proteins and provide clues to possible roles in cellular processes, yeast two-hybrid screens were conducted in the Cox lab at Seattle Children's Research Institute (74). Yeast two-hybrid (Y2H) screen using N-terminally truncated IRF6 protein (Exons 7-9) retaining both the protein interaction domain and the serine rich region) identified NME2 as a potential protein-protein interactor.

NME2 belongs to a large family of highly conserved proteins that were first discovered for their involvement in metastasis (75). NME2 has numerous functions, including functioning as a nucleoside diphosphate kinase (NDPK) and as a histidine-dependent protein kinase. It functions as a hexamer with its close paralog NME1 and provides the majority of cellular GTP used by GTPases that regulate cell adhesion and behavior (76-78). In epithelia, NME1/2 has been implicated in the regulation of epithelial adhesion and polarity (discussed further in the next section). Initial studies of *NME* function were in *Drosophila*; *awd* mutants possess a NDPK dead mutation, and they exhibit loss of apical and basolateral domains accompanied by a redistribution of DE-Cadherin (79). In mammalian cells, NME1 also has roles in the regulation of E-cadherin levels in adherens junctions (80).

To date, a role in NME1/NME2 in CLP has not been reported. NME1 has been found to inhibit TGF-β1-mediated EMT in mammalian cells, and loss of NME1 led to increased TGF-β1 suppression of E-cadherin (81). Although this study were not conducted in palatal epithelia, it theorizes a role for the NME complex in the MES. Additionally, Regulator of G protein signaling 19 (RGS19), which has roles in MES removal, is believed to upregulate NME1/2 (82). Loss of Rgs19 delays palatal fusion, which may be a result of Nme alterations in epithelial polarity and adhesion (83, 84).

Epithelial polarity and adhesion

The presence of ectopic oral adhesions suggests dysregulation in epithelial adhesion. Epithelial cell-cell adhesion is a carefully regulated process, from initiation of cell to cell contact to full maturation of cell-cell junctional complexes. Mature epithelial cell-cell junctional complexes are composed of tight junctions and adherens junctions (85). Tight junctions and adherens junctions are both composed of transmembrane proteins (nectins and cadherins for adherens junctions, occludins and claudins for tight junctions), which alter cytoskeletal dynamics via interactions with cytoplasmic proteins (86-89). Via interactions with p120-catenin, β-catenin, and α-catenin, cadherins influence cytoskeleton reorganization (Figure 3.1) (85, 90, 91). Absence of these cytoplasmic proteins results in loss of cell-cell adhesion. Other contributors to E-cadherin mediated cell-cell adhesion include the family of Ras homolog gene family guanosinetriphosphatases (Rho GTPases), including Ras homolog gene family, member A (RhoA) and Ras-related C3 botulinum toxin substrate 1 (Rac1) (91-93).

RhoA has several roles in the epithelium. For example, RhoA is crucial in proper assembly of stress fibers at adhesion complexes (94) and regulates the actin cytoskeleton (95). Via RhoA, Irf6 has been hypothesized to impact epithelial cell shape and adhesion. Irf6 deficient keratinocytes exhibit more prominent stress fibers and elevation of activated RhoA compared to wild type cells (95). Similar to other GTPases, RhoA cycles between active (GTP-bound) and inactive (GDP-bound) forms. RhoA is activated by guanine nucleotide exchange factors (GEFs), which exchange GDP for GTP,

and inactivated by GTPase activating proteins (GAPs), which induce GTP hydrolysis (96). For example, Arhgap29, a GAP, has been identified as a downstream target of Irf6, and Irf6 deficient keratinocytes exhibit lower levels of Arhgap29 (83, 97). Additionally, RhoA has reported roles in keratinocyte differentiation (98, 99). RhoA has also been implicated in palatogenesis, via mediation of TGF-β signaling (100).

Along with other cytoplasmic proteins, Rac1 and RhoA are critical in other functions of Adherens junctions, including participation in intracellular signaling, transcriptional regulation, and establishment of epithelial cell polarity. The NME complex also regulates epithelial adhesion and migration via activation of Rac1 and RhoA GTPases. Activation of GTPases is controlled by the interaction of NME1 and NME2 with Rac1 and RhoA-specific guanine nucleotide exchange factors (GEFs): T-cell lymphoma invasion and metastasis 1 (TIAM1) and A-Kinase Anchoring Protein-LBC (LBC), respectively .(101-105). By altering the expression of Rac1 and RhoA, these GEFs are believed to regulate adhesion strength by controlling microtubule dynamics, reorganization of the actin cytoskeleton, and E-cadherin recruitment to and/or removal from the plasma membrane (106-108). Regulation of epithelial adhesion by NME likely occurs through the PAR (PARD3-PARD6) polarity complex, for which TIAM1 binding is required for PARD3 activation. PARD3 activation stimulates establishment of epithelial apical and basolateral domains (i.e. polarity), and its activity influences the dynamic nature of tight junctions and adherens junctions. Adherens junctions contain cell adhesion molecules such nectins and cadherins: the position and number of such adhesion molecules

regulates the strength of epithelial-epithelial cell adhesion and therefore cell shape and behavior (85, 91). Mutations in both nectin1 and E-cadherin have been identified in CLP patients (58, 109). Accordingly, the IRF6-NME complex is hypothesized to regulate establishment and/or maintenance of adherens junctions and tight junctions via GEFs, and mutation or complete loss of IRF6 would impact overall polarity and adhesion strength.

Importance of serine phosphorylation

Numerous IRF6 mutations have been documented in CLP cases, but mechanistic links between the reported mutations and the associated phenotypes have not been established. In patients with VWS, 60% of all IRF6 mutations are missense mutations (110). Fifty five percent of these reside in the helix-loop-helix domain and are predicted to affect DNA binding. Of the remaining 45% of missense mutations, 70% are found in the protein binding region/interferon association domain (IAD) and 25% in the serine-rich region (SRR) (110). Of note, 25% of nonsense mutations also occur within the SRR, further highlighting the importance of this small region in overall IRF6 function (110). Data from yeast two hybrid assays and co-immunoprecipitation experiments demonstrate that NME2 binds IRF6 via the IAD, and this interaction is enhanced by phosphorylation of serine 424 in the C-terminal SRR (74). Thus, we hypothesize that CLP-associated mutations in the IAD and SRR disrupt the ability of IRF6 to bind NME2, and that this subsequently affects epithelial adhesion and/or polarity (ultimately impacting fusion of maxillary and medial nasal processes that form the upper lip).

Serine phosphorylation has important roles in other members of the IRF family. For example, IRF3 resides in the cytoplasm until phosphorylated; upon viral infection, IRF3 is phosphorylated and enters the nucleus, subsequently activating interferon expression (111). The crystal structure of IRF3 suggests that N and C terminal autoinhibitory sequences interact to protect a hydrophobic surface present in the IAD (111). Phosphorylation is believed to rearrange the autoinhibitory interaction to expose the IAD hydrophobic surface, thus allowing for protein-protein interactions, including dimerization (111). When autoinhibitory sites are mutated in IRF3, IRF3 maintains a constitutive monomeric state. Similarly, phosphorylation activates transcriptional activity of IRF5 (112). When phosphorylation target residues were replaced with the phosphomimic aspartic acid, increased nuclear localization of IRF5 was observed (112). The crystal structure of IRF6 has not been resolved, but based on sequence homology, phosphorylation of IRF6 is expected to play a role in IRF6 activation.

Studies have identified potential serine residues involved in regulating IRF6 activation and nuclear localization. Serines 413 and 424, potential IRF6 phosphorylation sites, are conserved in IRF3 and IRF5 (Figure 3.2). Mutation of these serines to glutamic acid resulted in constitutive IRF6 activation, suggesting that similar to other IRF members, serine phosphorylation regulates IRF6 activity (113). Additionally, S413E/S424E results in increased IRF6 dimerization, although S413E/S424E did not appear to enhance nuclear localization. Receptor-interacting protein kinase 4 (RIPK4) is believed to

phosphorylate IRF6; a kinase-dead RIPK4 does not elicit the same trans-activator activity as a wild-type RIPK4 (114). Additionally, wild-type RIPK4 colocalizes with IRF6 in the cytoplasm and results in IRF6 nuclear translocation, whereas the kinase dead RIPK4 had no effect on IRF6 nuclear translocation (114). IL-1 receptor-associated kinase-1 (IRAK1), which is also implicated in the immune system roles of IRF5 and IRF7, has also been reported to activate IRF6 (113). Thus, evidence is building towards additional roles for IRF6 besides the epithelia—IRF6 has potential roles in the immune system.

CLP and tooth development

Dental abnormalities are frequently found in patients featuring epithelial disorders. The tooth has several origins; the cells and structures that form the enamel arise from oral ectoderm, and the cells and structures that form the dentin, pulp, and periodontium arise from neural-crest derived ectomesenchyme (45). Reported dental abnormalities associated with ectodermal dysplasias include enamel hypoplasia, conical crowns, taurodontic molars, and hypodontia (115). Furthermore, compared to the general population, patients with CLP exhibit higher rates of tooth agenesis, aberrations in tooth morphology, and enamel defects (116). Specifically, hypodontia and taurodontism are associated with VWS and isolated forms of CLP (117-119). Maxillary second premolars, mandibular second premolars, and maxillary lateral incisors are the most frequently absent; depending on the study, their absence is noted in 10 to 81% of VWS patients references. Thus, similar mechanisms likely control aspects of tooth development and palatal fusion.

Overview of crown development

Tooth development is a carefully coordinated and complex process. Development of the mandibular first molar has been well studied (45, 120-123). In mice, mandibular first molar development begins on embryonic day 11.5 (E11.5) with thickening of the oral epithelium. As the oral epithelium proliferates, the dental lamina is formed, and it invaginates into the underlying ectomesenchyme, resulting in formation of the tooth bud. The ectomesenchyme continues to condense around the developing tooth bud, and by E14.5, the tooth bud has progressed to the cap stage. In the cap stage, the epithelium has folded and formed the inner and outer enamel epithelium, which encircle the stratum intermedium (found adjacent to the inner enamel epithelium) and the stellate reticulum. Together, these layers comprise the enamel organ. The outer enamel epithelium is on the perimeter of the enamel organ, and the inner enamel epithelium gives rise to the ameloblasts, which eventually form enamel. Additionally, in the cap stage, the enamel knot is formed, which functions as a signaling center, although the cells present in the enamel knot do not proliferate. Molars also have secondary enamel knots, which are the tips of future cusps. Signals are sent to the ectomesenchyme, which has now formed the dental papilla. The dental papilla will eventually give rise to the dentin and the pulp. The ectomesenchyme surrounding the dental papilla and the enamel organ is termed the dental follicle, and it eventually develops into the supporting structures of the tooth. Mice are generally born around E19-E20, and by postnatal day 4 (P4), the tooth has progressed to the bell stage. In the

bell stage, the tooth begins to assume characteristics of its final shape as a result of folding of the inner enamel epithelium. Additionally, cells in the inner enamel epithelium and the dental papilla differentiate into ameloblasts and odontoblasts, respectively. The inner enamel epithelium cells elongate and signal to ectomesenchymal cells to differentiate into odontoblasts. The odontoblasts begin to deposit dentin, and the ameloblasts begin to deposit enamel.

Overview of root development

Following crown development, root development is initiated with formation of the Hertwig's epithelial root sheath (HERS) (45, 124-126). In the murine mandibular first molar, this occurs at P7. The HERS is derived from the inner and outer enamel epithelium and is believed to act as a guide for root elongation and separation (125, 127). As the HERS migrates inward and apically, it establishes a barrier between the mesenchyme-derived developing periodontium and pulp. The HERS extends apically and surrounds the pulp; at the very apical end of the pulp, the rim of the HERS encircles the apical foramen. For multi-rooted teeth, folding of the HERS generates secondary apical foramina (45). The HERS has also been found to induce differentiation of the root odontoblasts. Following deposition of the radicular mantle dentin, the epithelial sheath fenestrates, and individual cells migrate away from the root into the future periodontal ligament. This also allows for the initiation of cementum formation. In murine P14, root dentin and cementum deposition are visible in the mandibular first molar. As the root lengthens, the alveolar crests surrounding the crown are removed, and the tooth

socket undergoes resorption and apposition in order to position the tooth for eruption into the oral cavity at P21.

Overview of enamel development

During amelogenesis, or enamel development, the ameloblasts, which form enamel and are derived from the oral epithelium, undergo several morphological and functional stages: presecretory, secretory, transition, and maturation (128-132). In the presecretory stage, following odontoblast differentiation and predentin deposition, ameloblasts differentiate and begin enamel deposition. As ameloblasts progress toward the secretory stage, they elongate into tall, columnar cells, develop Tomes' processes, and secrete enamel matrix proteins, including amelogenin (AMEL), ameloblastin (AMBN), enamelin (ENAM), and matrix metalloproteinase (MMP20). During this stage, the ameloblasts move in a sliding pattern relative to one another, altering the strength of adherens junctions between ameloblasts. At the end of the secretory stage, the Tomes' process is lost as the enamel reaches its full thickness. In the transition stage, the ameloblasts lose their columnar shape and begin the transition between ruffle and smooth-ended cells. In the maturation stage, ameloblasts secrete enamel proteinases to remove enamel matrix proteins as well as transport ions to enhance mineral accretion. As the protein matrix is removed, the enamel crystals grow wider and larger as mineral is deposited. During the maturation stage, ameloblasts also undergo apoptosis prior to tooth eruption.

Ameloblast morphology

In amelogenesis, the ameloblasts feature distinct morphological characteristics in each stage (45, 128-132) . Prior to the presecretory stage, preameloblasts are cuboidal with large, centrally located nuclei. Distally, they are found adjacent to the basal lamina, which also contacts the predentin. At the proximal end, a junctional complex is found adjacent to the stratum intermedium. As ameloblasts differentiate and elongate in the presecretory stage, the organelles (e.g. the Golgi complex) migrate distally, and the nuclei become more proximally located. At the distal end, the basal lamina breaks down, the Tomes' process is visible, and a second junctional complex is formed adjacent to the differentiating odontoblasts. At the end of the presecretory stage, ameloblasts are fully differentiated and cannot undergo cell division. In the secretory stage, enamel matrix proteins are synthesized and are packaged into membrane-bound secretory granules, which migrate into the Tomes' process. The contents of the granules are released adjacent to the mantle dentin to form the initial layer of enamel. As the enamel matrix is deposited, ameloblasts move away from the dentin surface, and the Tomes' process lengthens. Eventually, the Tomes' process narrows, and by the time the enamel reaches its full thickness, the Tomes' process no longer extends into the enamel. The ameloblasts shorten and assume a more cuboidal appearance. In the transition stage, ameloblasts continue to synthesize and secrete proteins. The ameloblasts continue to shorten, and breakdown of organelles occurs. During this time, water and organic material are removed, and the distal end of the ameloblasts alternate between ruffle-ended and smooth-ended. Modulation between smooth and ruffled ends is

believed to alter permeability of the enamel organ, thus allowing for organic matrix removal and mineral deposition. Ruffle-ended ameloblasts have tight distal junctions and leaky proximal junctions, allowing for mineralization. In contrast, smooth ended ameloblasts feature the opposite and allow for the exit of protein fragments and water. Additionally, the basal lamina is re-deposited between the ameloblasts and the developing enamel, and ameloblasts attach to it via hemidesmosomes.

Amelogenin

Amelogenin (AMEL) is the most abundant extracellular matrix protein in developing enamel, and it is encoded by two single copy genes on the X chromosome and the Y chromosome (*AMELX* and *AMELY*, respectively) (45). AMEL expression ceases when enamel has reached its full thickness. Mutations in *AMELX* cause a range of enamel defects, including hypoplastic and hypomaturation phenotypes. Amelogenin-null mice exhibit chalky-white teeth with accelerated wear of incisor tips and molar occlusal surfaces (133, 134). Scanning electron microscopy revealed loss of prismatic structure in amelogenin-null mice, although elemental analysis suggested normal hydroxyapatite composition. Human patients with *AMELX* mutations have a spectrum of enamel disturbances that ranged from hypoplastic to hypomineralized forms.

Enamelin

Enamelin (ENAM) is the least abundant of the enamel matrix proteins (comprises about 5% of the total enamel matrix) and is encoded by the *ENAM* gene. Full length ENAM is

detected at the developing enamel surface, and following establishment of full thickness of enamel, small ENAM fragments linger within the enamel—these are believed to inhibit crystal growth. Human mutations in *ENAM* cause localized pitting of enamel or in more severe cases, hypoplastic enamel and loss of enamel rod structure. A murine *Enam* model has marked enamel hypoplasia and complete absence of normal prismatic structure (135). Secretory ameloblasts in *Enam*$^{-/-}$ incisors also lacked polarity and organization.

Matrix metalloproteinase 20

Matrix metalloproteinase 20 (MMP20) is a tooth specific matrix metalloproteinase. It is secreted into the enamel matrix during the secretory and transition stages of enamel development, and it is believed to cleave sites in amelogenin and enamelin. By the maturation stage, MMP20 is no longer secreted. Cleavage of amelogenin is believed to diminish amelogenin's affinity for hydroxyapatite (136). Individuals with MMP20 mutations have hypomineralized enamel, although it is of normal thickness (137-139). Clinically, the enamel appears mottled and wears easily. Radiographically, the enamel does not contrast well with dentin. Additionally, *Mmp20*$^{-/-}$ mice exhibit thinner, hypomineralized enamel, which fractures at the dentino-enamel junction (140-143). Histological sections revealed retention of organic matrix in *Mmp20*$^{-/-}$ enamel, which was not observed in controls. Furthermore, *Mmp20*$^{-/-}$ ameloblasts exhibited abnormal morphology; the Tomes' processes were not distinct, and nodule-like formations were

found in the ameloblast layer (143). *Mmp20*$^{-/-}$ enamel also lacks normal rod and inter-rod structure and delaminates from the dentin.

Kallikrein 4

Kallikrein 4 (KLK4) is another proteinase critical toward enamel mineralization. KLK4 is expressed by transition and maturation stage ameloblasts. KLK4 is believed to be secreted into enamel after the enamel has reached its full thickness in order to degrade amelogenins and other extracellular matrix proteins. Similar to individuals with MMP20 mutations, individuals with KLK4 mutations exhibit hypomineralized enamel of normal thickness (144, 145). Loss of KLK4 results in enamel hypomaturation and fracturing above the dentin-enamel junction (146, 147). Enamel thickness is normal, although enamel from molars of *Klk4*$^{-/-}$ mice chips away at occlusal surfaces, resulting in dentin exposure. *Klk4*$^{-/-}$ null mice also exhibit increased ENAM and AMEL immunostaining, suggesting that loss of Klk4 leads to improper removal of enamel matrix proteins. Micro-CT analysis revealed that *Klk4*$^{-/-}$ enamel density was lower compared to *Klk4*$^{+/+}$ enamel. Furthermore, scanning electron microscopy (SEM) reveals decussating enamel rods with prismatic structure (146, 147). However, the crystallites within the rods are more loosely packed in *Klk4*$^{-/-}$ enamel, thus leading to weaker enamel and further indicating KLK4's role in enamel maturation.

Polarity and enamel development

The tooth serves as an isolated system to examine epithelial-derived tissues. Ameloblasts, which form enamel and are derived from oral epithelium, exhibit easily visualized polarity. When p120 catenin, Rac1, and RhoA, molecules critical toward the establishment of epithelial adhesion and polarity, are ablated in teeth, mice exhibit severe enamel structure defects, including disorganized and hypomineralized enamel (148-150). For example, when p120 catenin was ablated in the murine enamel organ, secretory stage ameloblasts lost polarity, flattened, and detached from surrounding tissues. The resultant enamel was rough and hypomineralized. Furthermore, loss of p120 catenin resulted in downregulation of E and N cadherins. p120 catenin has been reported to prevent internalization and degradation of cadherins, which directly affect the status of adherens junctions. Adherens junctions are also found in cell-cell contacts between secretory ameloblasts, thus, in addition to polarity, loss of p120 catenin altered adhesion in the enamel organ (151). Rac1 conditional knockouts also exhibited detachment of ameloblasts from the developing enamel matrix, and enamel matrix proteins such as amelogenin and ameloblastin were reduced. Enamel was severely hypomineralized, and abraded quickly following tooth eruption. Similarly, transgenic mice expressing a dominant-negative RhoA exhibited downregulation of amelogenin and E-cadherin, leading to hypomineralized enamel (152). Thus, disruption of ameloblast polarity often leads to enamel defects, and ameloblasts offer an alternative model to further validate the impact of IRF6 on epithelial cell adhesion and polarity.

Hypothesis and Specific Aims

The aims of this research project were designed to investigate the role of IRF6 in proper primary palatal development and in ameloblast function, and specifically its contribution to epithelial polarity in these two tissues. Based on current reports and studies in the Cox lab, **I hypothesized that the interaction of IRF6 with the NME complex is required to properly regulate polarity of oral epithelium in developing facial primordia and ameloblasts during mineralization.** The following aims were pursued:

Aim 1: Assess effects of IRF6 mutations found in CLP patients on localization of polarity effector proteins.

Strategies: The potential role of IRF6-NME2 in establishing polarity was assessed *in vitro* using HEK293T epithelial cells. Cells were transfected with IRF6 mutant sequences in order to generate cells that ectopically expressed mutant IRF6 forms. Activity and expression of polarity markers were assayed.

Aim 2: Investigate contributions of IRF6 to polarity in a tooth model.

Strategies: Using a conditional murine model in which *Irf6* is ablated in ameloblasts, the impact on ameloblast polarity were assessed by morphological observations and assessment of the quantity/quality of enamel formed using microCT analysis.

Aim 3: Define the role of IRF6 in tooth development.

Strategies: Tooth tissues will be harvested from *Irf6* conditional knockout mice, and a histological time course will be conducted to determine affected stages of tooth

development. Gene and protein expression of enamel matrix proteins were evaluated using qPCR and immunohistochemistry.

Chapter 2: Materials and Methods

Yeast two hybrid

Competent MAV203 cells were prepared using the Frozen-EZ Yeast Transformation II kit (Zymo Research; Irvine, California). Co-transformation was performed using Frozen EZ Solution III solution. Constructs were tested for self-activation by co-transforming competent MAV203 yeast cells with either pDEST^{TM}32-hIRF6 and the empty pDEST^{TM}22 vector or pDEST^{TM}22-hNME1/2 and the empty pDEST32 vector. Full length IRF6 self-activates; cell growth was detected when transformed with an empty vector. Based on studies in the Cox lab (Seattle Children's Research Institute), Exons 7-9 were deemed essential for IRF6:NME2 binding and did not result in self-activation when co-transformed with an empty vector. Thus, truncated human IRF6 (Exons 7-9) sequences were used in subsequent yeast two hybrid assays to assess for possible disruptions to the IRF6:NME2 interaction. To assess potential effects of patient missense mutations on IRF6:NME2 binding, competent MAV203 cells were co-transformed with wild type NME1/NME2 and wild-type/mutant IRF6 sequences. Cells were plated on SD-Leu-Trp plates, which selected for transformants that had taken up both plasmids. MAV203 cells were also transformed with an empty vector for a negative control. Plates were incubated at 30^{o} C for three days; from these plates, colonies were picked and grown up in SD-Leu-Trp liquid media overnight at 30^{o} C.

Transformants were assessed for reporter gene activity: *HIS3*, *lacZ*, *URA3.* A strong interaction will exhibit activity for at least two of the three genes. Optical density of

liquid cultures was measured at 600nm (OD_{600}), and 2µL of each culture at OD_{600} of 0.100 was spotted on selection plates. To assess for *HIS3* activity, 3-amino-1,2,4 triazole (3AT) was added to SD-Leu-Trp-His plates at 50mM and 75mM. 3AT inhibits histidine biosynthesis, via transcription of *HIS3*, strong yeast-two hybrid interactions are able to overcome this inhibition. Concentrations of 50mM and 75mM were deemed sufficient to limited background activity (negative controls did not exhibit growth). *URA3* activity was assessed by evaluating growth of transformants on SD-Leu-Trp-Ura plates. To assess for *lacZ* activity, transformants were first grown on a nylon membrane, which was placed on a YPAD media plate. SD-Leu-Trp-His+3AT and SD-Leu-Trp-Ura plates were incubated 48 hours at 30°C, and the YPAD plate was incubated overnight at 30°C. Transformants were assessed for growth on the –His and –Ura selection plates, and cultures grown on the nylon membrane were lysed for the X-Gal assay. Transformants positive for *lacZ* turned blue in the X-Gal assay.

Selection of IRF6 patient mutations

Twelve specific IRF6 missense mutations in the IAD were compared to wild type IRF6 in ability to interact with NME2. The specific mutations were selected based on the following criteria: 1) found in familial cases of VWS/PPS, 2) unlikely to cause secondary structure disruptions (PSIPRED prediction), 3) less than a 30% molecular weight discrepancy between original and substituted amino acid, 4) does not change isoelectric point by more than 0.32 (accepted discrepancy between predicted and measured values, (153)), and 5) no change in grand average of hydropathicity index. Each of these

mutations was introduced into yeast (pDEST32) IRF6 expression constructs to test for interaction with NME2. Wild type IRF6-NME2 interaction will be used as a positive control.

Selection of conserved serines

Based on sequence alignment between IRF6 and the well-studied IRF5 and IRF3, three C-terminal serine residues were found to be completely conserved in position within the SRR. For example, the Cox lab has already shown that the chick homolog to serine 424, which is conserved, regulates the strength or stability of interaction with NME2. Here, the role of two other conserved serines (S413 and S418) in IRF6 function will be investigated. Using site-directed mutagenesis, phosphoinhibitory (Ser to Ala) and phoshomimic (Ser to Asp) substitutions were generated.

Investigating NME1/NME2 sequence conservation

Various NME2 mutant constructs were tested for interaction with IRF6 using Y2H and co-immunoprecipitation. To determine specific sites to target, NME2 and NME1 protein sequences were compared. NME1 and NME2 are small, closely related proteins that exhibit over 90% amino acid identity within and between species, yet have been reported to interact with different protein partners(76, 77, 154). To identify key residues in NME2 that confer this specificity of interaction with IRF6, residues that differ between the NME1 and NME2 sequences will be targeted for mutation. Additional

hybrid constructs, in which portions of NME1 and NME2 are interchanged, were tested in case more than one residue is responsible for this specificity in binding.

Selection of NME1/NME2 patient mutations

Screens for NME1/NME2 polymorphisms were conducted on CLP patients, and two variants were identified: R18Q in NME1 and G71V in NME2. These were also tested for ability to disrupt the IRF6:NME interaction.

Generation of mutant constructs

For each of the IRF6 mutations selected, forward and reverse primers were designed with either single or double nucleotide substitutions for use in overlap PCR (Table 2.1, Table 2.2, Table 2.3). Overlap PCR was used to generate full length and truncated (Exons 7 through 9) DNA templates encoding mutant sequences, which were subsequently A-tailed using standard Taq polymerase and cloned into the entry pCR®8/GW TOPO® vector with Top10 *E.coli* cells (Life Technologies; Carlsbad, California). Following transformation, cells were plated on LB+Spectinomycin agar plates and incubated at 37°C overnight. Colonies were picked, grown in liquid LB+Spectinoymcin and incubated at 37°C overnight for plasmid DNA isolation and purification using the QIAprep Spin Miniprep Kit (Qiagen; Valencia, California). Plasmid DNA was digested with restriction enzymes EcoRV and BamHI (LifeTechnologies; Carlsbad, California) to check for orientation of insert. DNA that exhibited predicted

digest pattern was submitted for sequencing (Eurofilms Operon; Huntsville, Alabama) to verify presence of mutated sequence.

For Y2H, the pCR®8/GW-TOPO® clones were subsequently cloned into pDEST™32 destination vectors using the Gateway® LR Clonase II Enzyme mix (Life Technologies; Carlsbad, California) for use in the ProQuest™ Two-Hybrid System (Life Technologies; Carlsbad, California). Plasmid DNA from pDEST™32 clones was also submitted for sequencing to verify identity of sequences. For use in immuoprecipitation studies, the entry clones were cloned into pDEST-myc vectors. Clones containing pDEST-myc plasmids were selected using LB+Ampicillin plates, and colonies were subsequently grown in liquid LB+Ampicillin for plasmid DNA isolation and purification using the QIAGEN Plasmid Midi kit (Qiagen; Valencia, California). Presence of insert was verified using digestion with restriction enzymes and sequencing (Eurofilms Operon).

Similarly, for NME1/NME2 mutations, forward and reverse primers were designed (Table 2.4 and Table 2.5). Overlap PCR products were A-tailed and cloned into entry pCR®8/GW TOPO® vectors. These clones were then cloned into the pDEST™22 destination vectors using the Gateway® LR Clonase II Enzyme mix (Life Technologies; Carlsbad, California) for use in Y2H. For use in immunoprecipitation, NME1/NME2 entry clones were cloned into pcDNA™DEST53 destination vectors.

Primer name	Missense mutation	Sequence (5’ to 3’)
hIRF6-A958G-K320E-f	K320E	TGCCAGTGCGAGGTGTACTGGTCTGGGC
hIRF6-A958G-K320E-r	K320E	CCAGTACACCTCGCACTGGCACAGCC
hIRF6-A1162G-K388E-f	K388E	TTGGAAAGGGAACTCATCTTGGTTCAGG
hIRF6-A1162G-K388E-r	K388E	CAAGATGAGTTCCCTTTCCAATGGTTTCCC
hIRF6-C772T-P258S-f	P258S	GACCTGGGTTCCATGCCTGACCAGG
hIRF6-C772T-P258S-r	P258S	GTCAGGCATGGAACCCAGGTCCCC
hIRF6-G749A-R250Q-f	R250Q	CAGGGCTGCCAACTCTTCTATGGGGACC
hIRF6-G749A-R250Q-r	R250Q	CATAGAAGAGTTGGCAGCCCTGAGGG
hIRF6-G799T-G267C-f	G267C	GAGCTCTTTTGTCCCGTCAGCCTGG
hIRF6-G799T-G267C-r	G267C	GCTGACGGGACAAAAGAGCTCCTCCT
hIRF6-G961A-V321M-f	G961A	CAGTGCAAGATGTACTGGTCTGGGCC
hIRF6-G961A-V321M-r	G961A	AGACCAGTACATCTTGCACTGGCACAG
hIRF6-G1016T-R339I-f	G1016T	CTGATTGAGATACAAAAGAAGGTCAAGC
hIRF6-G1016T-R339I-r	G1016T	CTTCTTTTGTATCTCAATCAGGTTGGG
hIRF6-G1141T-D381Y-f	G1141T	GAATGGCCATATGGGAAACCATTGG
hIRF6-G1141T-D381Y-r	G1141T	TGGTTTCCCATATGGCCATTCTTCCCC
hIRF6-G1199A-R400Q-f	G1199A	GTAGTGGCTCAGATGATCTACGAGATG
hIRF6-G1199A-R400Q-r	G1199A	GTAGATCATCTGAGCCACTACTGGAATG
hIRF6-T752C-L251P-f	T752C	GGCTGCCGACCCTTCTATGGGGACC
hIRF6-T752C-L251P-r	T752C	CATAGAAGGGTCGGCAGCCCTGAGG

hIRF6-T881C-L294P-f	T881C	CACTAGCAAGCCGCTGGACGTCATGGAC
hIRF6-T881C-L294P-r	T881C	GACGTCCAGCGGCTTGCTAGTGAA
hIRF6-T1118C-L373S-f	T1118C	GAGATCTACTCATGCTTTGGGGAAGAATCG
hIRF6-T1118C-L373S-r	T1118C	CCCAAAGCATGAGTAGATCTCAAACGG

Table 2.1: Primers used in site-directed mutagenesis to generate constructs with IRF6 mutations.

Each mutation has a corresponding forward and reverse primer.

Primer name	Mutation	Sequence (5' to 3')
hIRF6-S407Af	S407A	GAGATGTTTGCTGGTGATTTCACACGA
hIRF6-S407Ar	S407A	GAAATCACCAGCAAACATCTCGTAGATC
hIRF6-S407Df	S407D	GAGATGTTTGACGGTGATTTCACACG
hIRF6-S407Dr	S407D	GAAATCACCGTCAAACATCTCGTAGATC
hIRF6-S413Af	S413A	TTCACACGAGCCTTTGATAGTGGCAGTG
hIRF6-S413Ar	S413A	CTATCAAAGGCTCGTGTGAAATCACCAG
hIRF6-S413Df	S413D	TTCACACGAGACTTTGATAGTGGCAGTG
hIRF6-S413Dr	S413D	CTATCAAAGTCTCGTGTGAAATCACCAG
hIRF6-S416Af	S416A	TCCTTTGATGCTGGCAGTGTCCGCCTG
hIRF6-S416Ar	S416A	GACACTGCCAGCATCAAAGGATCGTGTG
hIRF6-S416Df	S416D	TCCTTTGATGACGGCAGTGTCCGCCTG
hIRF6-S416Dr	S416D	GACACTGCCGTCATCAAAGGATCGTGTG

hIRF6-S418Af	S418A	ATAGTGGCGCTGTCCGCCTGCAGATCTC
hIRF6-S418Ar	S418A	GCAGGCGGACAGCGCCACTATCAAAGGATC
hIRF6-S418Df	S418D	ATAGTGGCGATGTCCGCCTGCAGATCTC
hIRF6-S418Dr	S418D	GCAGGCGGACATCGCCACTATCAAAGGATC
hIRF6-S424Af	S424A	CTGCAGATCGCAACCCCAGACATCAAGGA
hIRF6-S424Ar	S424A	CTGGGGTTGCGATCTGCAGGCGGACACTG
hIRF6-S424Df	S424D	CTGCAGATCGATACCCCAGACATCAAGGA
hIRF6-S424Dr	S424D	CTGGGGTATCGATCTGCAGGCGGACACTG

Table 2.2: Primers used in site-directed mutagenesis to generate constructs either abolishing a phosphorylation site (serine to alanine) or acting as a phosphomimic (serine to aspartic acid).

Primer name	**Region targeted/purpose**	**Sequence (5' to 3')**
hIRF6start	Places IRF6 in same open reading frame with destination vector cloning sites	CATATCATGGCCCTCCACC
hIRF6stop	Spans IRF6 stop codon	CACAATTACTGGGGAGGCAG
hIRF6-ex7f	Used to generate constructs that only include Exons 7-9	ATGACTGACCTGGACATCAAGTTTC

Table 2.3: Primers used to generate IRF6 wild type and mutation-containing PCR products, which were subsequently A-tailed and cloned into TOPO vectors.

Primer name	Mutation	Sequence (5' to 3')
NME1R18Qf	R18Q	GGGGTCCAGCAGGGTCTTGTG
NME1R18Qr	R18Q	CACAAGACCCTGCTGGACCCC
NME2G71Vf	G71V	ATGAACTCAGTGCCGGTTGTG
NME2G71Vr	G71V	CACAACCGGCACTGAGTTCAT

Table 2.4: Primers used in site-directed mutagenesis to generate constructs with NME1 or NME2 mutations. Each mutation has a corresponding forward and reverse primer.

Primer name	Region targeted/purpose	Sequence (5' to 3')
hNME1 start	Places NME1 in same open reading frame with destination vector cloning sites	ACCATGGCCAACTGTGAGCGTACC
hNME1 stop	Spans NME1 stop codon	CTGTCATTCATAGATCCAGTTCTGAG
hNME2 start	Places NME2 in same open reading frame with destination vector cloning sites	ACCATGGCCAACCTGGAGCGCACC
hNME2 stop	Spans NME2 stop codon	CTCTTATTCATAGACCCAGTCATGAG
hNME1-2overlapf	Used to generate PCR products that could be overlapped to create NME1/NME2 hybrid sequences	GCCATGGTCTGGGAGGGGCTG

hNME1-2overlapr	Used to generate PCR products that could be overlapped to create NME1/NME2 hybrid sequences	CAGCCCCTCCCAGACCATGGC

Table 2.5: Primers used to generate NME1 wild type and hybrid PCR products, which were subsequently A-tailed and cloned into TOPO vectors.

Addition of 5' Untranslated Region (UTR)

Sequencing of the mouse Nme2 clone identified revealed a long 5' untranslated region (UTR); this UTR was in frame with the coding sequence. When this untranslated region was absent, the IRF6:NME interaction could not be recapitulated using human sequences. In the GAL4BD fusion protein, comparatively, the NME protein is much smaller than the GAL4BD, and the GAL4BD is likely to interfere with proper folding of the NME protein. The untranslated region is believed to act as a spacer between the GAL4BD and the NME protein, thus allowing NME to fold properly.

The murine Nme2 clone was part of a library in which pPC86 was used as the vector backbone (pPC86-mNme2). Analysis of possible restriction enzyme sites revealed that NcoI and BamHI sites could be used to add the 5'UTR to human sequences. An internal NcoI site was found in the NME1 and NME2 sequences; therefore, overlap primers were designed to eliminate the internal NcoI site (Table 2.6). Subsequently, primers were designed to amplify the NME1/NME2 sequences in order to include the NcoI and BamHI sites in the PCR products (Table 2.6). PCR products were subsequently poly A-tailed and

cloned into pCR®8/GW TOPO® vectors (Life Technologies; Carlsbad, California). The mouse Nme2 (including the 5'UTR) and the pCR®8/GW TOPO® Nme1/2 clones were digested with NcoI and BamHI to generate sticky ends. The digested, linearized pPC86-mNme2 was gel purified and ligated with the digested pCR®8/GW TOPO® Nme1/2 products. Ligation products were transformed into Top10 *E.coli* cells, and plasmid DNA was extracted and purified (Qiagen Plasmid Midi kit, Qiagen; Valenica, California). These constructs were co-transformed with IRF6 constructs in MAV203 cells to assess for impact on IRF6:NME binding.

Primer name	**Region targeted/purpose**	**Sequence (5' to 3')**
hNME2startNcoI	Added a NcoI restriction enzyme site to NME2 sequence	CCTTACCATGGCCAACCTGGAGCGC
hNME1start-NcoI	Added a NcoI restriction enzyme site to NME1 sequence	CCTTACCATGGCCAACTGTGAGCGTACC
hNME2delNcoI-f	Used in overlap PCR to remove internal NcoI site	GCCGGTTGTGGCTATGGTCTGGGAGGGGC
hNME2delNcoI-r	Used in overlap PCR to remove internal NcoI site	CTCCCAGACCATAGCCACAACCGGCCTG

hNME1delNcoI-f	Used in overlap PCR to remove internal NcoI site	CCGGTAGTTGCTATGGTCTGGGAGGGGCTG
hNME1delNcoI-r	Used in overlap PCR to remove internal NcoI site	CAGCCCCTCCCAGACCATAGCAACTACCGG
ADH-BamHI	Added a BamHI site to NME1/NME2 sequences	TTGGGATCCGTGTGGAAGAACGATTAC

Table 2.6: Primers used to add 5'UTR to human NME1/NME2 sequences.

Selection of epithelial cells

Human embryonic kidney 293T (HEK293T) cells

HEK293T cells are derived from HEK293 cells, and unlike the original HEK293 cells, contains the SV40 T-antigen. The original HEK293 line was derived from primary cultures of human embryonic kidney cells transformed with sheared adenovirus DNA (155). The Cox Lab (Seattle Children's Research Institute) have used HEK293T cells for a number of experiments, and these cells have been found to have high transfection efficiency and grow as an adherent monolayer on tissue culture treated dishes. Thus, these were used in our *in vitro* studies.

LS8 cells

To investigate the effects of IRF6 on ameloblasts *in vitro*, the LS8 cell line, an ameloblast-like cell line was selected. LS8 cells were kindly provided by Dr. Malcolm Snead, USC, and they have been used to study amelogenin promoter activities for a number of years (156-159). Similar to HEK293T cells, LS8 cells have a high transfection efficiency and grow as an adherent monolayer on tissue culture dishes.

Co-immunoprecipitation

Full length human IRF6 sequences (wild-type and mutant) were cloned into pDESTMYC vectors, which effectively added a c-myc tag. Adherent mammalian (HEK293T) cells at 70% confluency were transfected with plasmids either containing GFP-tagged NME1/NME2 or c-myc tagged wild type/mutant hIRF6. After twenty four hours, cells were lysed with M-PER™ Mammalian Protein Extraction Reagent (Life Technologies; Carlsbad, California) and 1X protease inhibitor cocktail (Life Technologies; Carlsbad, California), and cell lysate was collected. Protein concentrations were obtained using either the Pierce™ Coomassie (Bradford) Protein Assay Kit (Life Technologies; Carlsbad, California) or the Pierce™ BCA Protein Assay Kit (Life Technologies; Carlsbad, California). To confirm successful transfections, SDS-PAGE and Western blots were used with GFP and myc primary antibodies (antibody dilutions: 1:1000). The Pierce c-myc Tag IP/Co-IP (Life Technologies; Carlsbad, California) kit was used to assess the IRF6:NME2 interaction. SDS-PAGE and Western blots (with NME2 as the primary antibody) were used to assess protein-protein interactions and characterize protein-protein complexes.

SuperSignal™ West Femto Maximum Sensitivity Substrate (Life Technologies; Carlsbad, California) or fluorescent secondary antibodies (Odyssey) were used for detection.

Rac1 Pull down assays

RhoA activity was measured to assess the contribution of IRF6:NME complex to maintenance of epithelial adhesion and polarity. HEK293T cells were transfected with either wild type or mutant IRF6 constructs. Twenty-four hours following transfection, cells were serum starved (DMEM+0.1.% FBS, Penicillin/Streptomycin, and GlutaMax) for sixteen hours to reduce GTPase levels to a basal state, therefore enhancing detection of effects on their activity. Following serum starvation, cell lysate was harvested, and all active Rac1 activity measurements were performed using an Active Rac1 Pull-Down and Detection kit (Life Technologies; Carlsbad, California) followed by SDS-PAGE and Western blotting using an anti-Rac 1 antibody (dilution 1:1000).

RhoA Pull down assays

RhoA activity was measured to assess the contribution of IRF6:NME complex to maintenance of epithelial adhesion and polarity. HEK293T cells were transfected with either wild type or mutant IRF6 constructs. After twenty four hours, cells were serum starved for sixteen hours to reduce GTPase levels to a basal state, therefore enhancing detection of effects on their activity. Following serum starvation, cell lysate was harvested, and active RhoA activity measurements were performed using a RhoA Pull-

down Activation Assay Biochem Kit (Cytoskeleton; Denver, Colorado) followed by SDS-PAGE and Western blotting using an anti-RhoA antibody (dilution 1:500).

Generation of IRF6 conditional knockout

A conditional knockout mouse driven by the Pitx2 promoter was generated. Mice possessing Irf6 exons 3 and 4 flanked by LoxP sites were crossed with mice possessing the Pitx2 promoter linked to *Cre* recombinase. Floxed Irf6 mice were kindly provided by Dr. Brian Schutte (Michigan State University), and $Pitx2^{Cre}$ mice were kindly provided by Dr. James Martin (Baylor College of Medicine). All mice were housed at Seattle Children's Research Institute according to IACUC policies. *Pitx2* is specific to the oral epithelium is expressed in the dental lamina, enamel knot, undifferentiated cervical loops, and pre-ameloblasts (160). $Pitx2^{Cre/Cre}$ mice are embryonic lethal. Thus, our *Irf6* conditional knockout mice (*Irf6-cKO*) were heterozygous for the $Pitx2^{Cre}$ allele and homozygous for the $Irf6^{fl}$ allele ($Pitx2^{Cre/+}$; $Irf6^{fl/fl}$). Controls had either $Pitx2^{+/+}$; $Irf6^{fl/+}$, $Pitx2^{Cre/+}$; $Irf6^{fl/+}$, or a $Pitx2^{+/+}$; $Irf6^{fl/fl}$ genotype.

Genotyping for $Irf6^{fl/fl}$ and $Pitx2^{Cre}$ mice was performed. At time of either weaning or sacrifice, tail tips were obtained. Tails were digested with 50mM sodium hydroxide (30 minutes at 95°C, then treated with Tris-HCl, pH 8.0). Samples were centrifuged to remove debris from digested tissue, and resultant supernatant was used for genotyping. Samples were prepared for PCR according to KAPA Mouse Genotyping Kit (Kapa Biosystems; Wilmington, Massachusetts) instructions. Primers are listed in Table 2.7,

and the annealing temperature for genotyping *Pitx2*^{Cre} mice was 60°C, and the annealing temperature for genotyping *Irf6*^{fl} mice was 55°C. Following PCR, products were run on a 1% Agarose/Sodium Borate gel and visualized using ultraviolet light. *Pitx2*^{Cre} mice exhibited a 900bp band, and *Pitx2*$^{+/+}$ mice did not exhibit a band when genotyped with MHOX and PITX2 primers. *Irf6*$^{fl/fl}$ mice exhibited a 379bp band, and *Irf6*$^{fl/+}$ mice exhibited 222 bp and 379bp bands.

Primer name	**Allele targeted**	**Sequence (5' to 3')**
MHOX	Pitx2-Cre	GCCACTCCCACTGTCCTTTC
PITX2-FLEXB	Pitx2-Cre	TTCTGGAGGGTTTTCTTGTTCTAGG
3318	Irf6-floxed	TGGCAAAATCTATTTCGAGTGG
3319	Irf6-floxed	CACACTGACCTCAATGCCTCCAA

Table 2.7: Genotyping primers used in our study.

Histology

Heads were harvested at postnatal ages 4, 7, 14, 28, and 84 (P4, P7, P14, P28, and P84). Heads were skinned and split sublingually to allow for penetration of the fixative, either 4% paraformaldehyde (PFA) or Bouin's fixative (Sigma Aldrich; St. Louis Missouri. Samples were fixed at room temperature for two to three days under rotary motion. Samples were then rinsed and stored in 70% ethanol at 4° C. For histology, samples were demineralized in either 14% EDTA solution (pH 7.1) or a mixture of 10% acetic

acid, 4% formalin, and 0.86% sodium chloride. Following decalcification, samples were processed and embedded in paraffin for microtome sectioning. 5µm sections were obtained. Sections were deparaffinized and stained with hematoxylin and eosin. Images were obtained using a Zeiss Axio Imager 2 microscope (Zeiss; Peabody, Massachusetts).

Immunohistochemistry (IHC)

Standard IHC procedures were used. Tissues were processed for paraffin-embedding and microtome sectioning (5uM). Primary antibodies used were: Anti-NME2 (LS-B9880, Lifespan Biosciences), Anti-IRF6 (LS-B3231, Lifespan Biosciences), Anti-amelogenin (sc-32892, Santa Cruz Biotechnology), and Anti-KLK4 (LS-B1736, Lifespan Biosciences). All primary antibodies were used at a 1:150 dilution. IHC was performed using biotinylated secondary antibodies and peroxidase substrate (Vectastain Elite ABC Kit; Vector Labs, Burlingame, California). AEC Peroxidase Substrate Kit (3-amino 9-ethylcarbazole) (Vector Labs) was used for detection. Slides were mounted using VectaMount AQ Aqueous Mounting Medium (Vector Labs; Burlingame, California) and imaged using a Zeiss Axio Imager 2 microscope (Zeiss; Peabody, Massachusetts).

Immunocytochemistry

Madin-Darby Canine Kidney (MDCK) cells were cultured on either chambered coverslips (Life Technologies; Carlsbad, California) or Poly-d-lysine coated dishes (MatTek Corporation; Ashland, Massachusetts) at 37°C with 5% CO_2 in DMEM (ThermoScientific)

supplemented with 10% fetal bovine serum (FBS; Thermo Scientific) and 1% GlutaMAX (GIBCO by Life Technologies; Carlsbad, California). At 70-80% confluency, cells were transfected with c-myc-IRF6 wild type or mutant constructs. Twenty-four hours following transfection, cells were fixed in 4% paraformaldehyde, rinsed with PBS, and permeabilized with 0.25% Triton X-100. Cells were blocked and stained with a goat anti-IRF6 antibody (LifeSpan Biosciences; Seattle, Washington) and a rabbit anti-NME2 antibody (Abcam; San Francisco, California) at 1:200 dilutions. Following primary antibody incubation, cells were incubated with AlexaFluor donkey anti-rabbit 488 and AlexaFluor donkey anti-goat 633 (Life Technologies; Carlsbad, California) at 1:2000 dilutions. Following staining, cells were visualized with a Zeiss LSM510 confocal microscope (Zeiss; Peabody, Massachusetts).

Silencing IRF6

LS8 and HEK293T epithelial cells were cultured on either six or twelve well plates at 37°C with 5% CO_2 in DMEM (Life Technologies; Carlsbad, California) for 24 hours. At 50-60% confluency, cells were transfected with either 100nM negative control (scrambled sequence purchased from Life Technologies; Carlsbad, California) or 100nM siRNA (three different siRNAs were tested: s79447, s79448, and s79449). Twenty-four hours following transfection, cells were homogenized (QIAshredder; Qiagen; Valencia, California), and RNA was isolated and purified (RNeasy Micro Kit; Qiagen; Valencia, California). RT-PCR and qPCR were performed (Roche Lightcycler 480) with IRF6 as the target and GAPDH as the reference. Using Roche480 software, relative quantification

was performed, and IRF6/GAPDH ratio was compared between cells transfected with the negative control versus the siRNAs. For experiments with two groups, student's t-test was performed, and for experiments with more than two groups, one way analysis of variance (ANOVA) was used. All statistical analyses were performed with GraphPad Prism 6.01 (GraphPad Software; La Jolla, California). Graphs were also created using GraphPad Prism 6.01. See Table 2.8 for primer sequences used.

Primer name	**Species/purpose**	**Sequence (5' to 3')**
mGAPDH-f	Mouse (for LS8 cells)	ACCACAGTCCATGCCATCAC
mGAPDH-r	Mouse (for LS8 cells)	TCCACCACCCTGTTGCTGTA
mIRF6-f	Mouse (for LS8 cells)	GCGGTGTGAACTCTTGTGC
mIRF6-r	Mouse (for LS8 cells)	GGTGGAGGGCCATGATCT
hGAPDH-f	Human (for HEK293T cells)	TCGGAGTCAACGGATTT
hGAPDH-r	Human (for HEK293T cells)	CCACGACGTACTCAGC
hIRF6-f	Human (for HEK293Tcells)	GGCATAGCCCTCAACAAGAA
hIRF6-r	Human (for HEK293T cells)	CACCCCTTCCTGGTACTTCC
hNME1-f	Human (for HEK293T cells)	CAGCCGGAGTTCAAACCTAA
hNME1-r	Human (for HEK293T cells)	CAGGCTGACTTAGTCCTGTGTAGA
hNME2-f	Human (for HEK293T cells)	TGACCTGAAAGACCGACCAT
hNME2-r	Human (for HEK293T cells)	GTTCAGCCCCTCCCAGAC

Table 2.8: Primers used to check *Irf6* mRNA expression in LS8 and HEK293T cells. Each gene has a forward and reverse primer.

Whole tooth dissections (P4 samples)

Immediately after mice were sacrificed, heads were hemisected and immersed in RNALater (Life Technologies; Carlsbad, California) for 24 hours at 4°C. Samples were subsequently transferred to -20°C for storage. Prior to dissection of teeth, samples were thawed at 4°C, and molars were dissected from the surrounding tissues. Samples were homogenized (MP FastPrep; MP Biomedicals; Santa Ana, California), and RNA was extracted using TriPure Isolation Reagent (Roche Life Science; San Francisco, California). Next, RNA was purified (RNEasy kit; Qiagen; Valencia, California) and quantitated (Nanodrop). RNA was used for RT-PCR and qPCR (Roche Lightcycler 480; Roche Life Science; San Francisco, California). See Table 2.9 for primers.

Whole tooth dissections (P13 samples)

Immediately after mice were sacrificed, mandibles were dissected out, flash frozen, and stored at -20°C. Prior to dissection of teeth, mandibles were thawed in RNALater (Life Technologies; Carlsbad, California) for 30 minutes at room temperature. Samples were homogenized (MP FastPrep; MP Biomedicals; Santa Ana, California), and RNA was extracted using TriPure Isolation Reagent (Roche Life Science; Roche Life Science; San Francisco, California). Next, RNA was purified (RNEasy kit; Qiagen; Valencia, California) and quantitated (Nanodrop; Wilmington, Delaware). RNA was used for RT-PCR and qPCR (Roche Lightcycler 480; Roche Life Science; San Francisco, California). See Table 2.9 for primers.

Enamel organ dissections

Immediately after sacrifice of animals, mandibles were dissected out and flash frozen for storage and transport. Prior to enamel organ dissections, samples were thawed out in RNALater (Life Technologies; Carlsbad, California). Basal bone was removed from inferior aspect of mandibles, and enamel organ was extracted. Enamel organs were homogenized (MP FastPrep; MP Biomedicals; Santa Ana, California), and RNA was extracted using TriPure Isolation Reagent (Roche Life Science; San Francisco, California) and purified using Qiagen RNEasy kit (Qiagen; Valencia, California). RNA was used for RT-PCR and qPCR (Roche Lightcycler 480; Roche Life Sciences; San Francisco, California). See Table 2.9 for primers.

Primer name	**Sequence (5' to 3')**
AMBN-f	TCCCACCGCATAACTCT
AMBN-r	GATATTGAACGGGCGAT
AMEL-f	ATCGGATCAAGCATCCC
AMEL-r	GGGTTCGTAACCATAGG
DMP1-f	GCGCGGATAAGGATGA
DMP1-r	GTCCCCGTGGCTACTC
ENAM-f	ACTATGATGCGGCCAG
ENAM-r	GGTTGAGGCGTAGTGC

GAPDH-f	ACCACAGTCCATGCCATCAC
GAPDH-r	TCCACCACCCTGTTGCTGTA
IRF6-f	GCGGTGTGAACTCTTGTGC
IRF6-r	GGTGGAGGGCCATGATCT
KLK4-f	GTTCCTGGGGTGCCTCAT
KLK4-r	ATCCGGCTGCTGACACTT
MMP20-f	GGAGCCTCAGAAGACCCTTT
MMP20-r	TTTGGGTAGTCTTTTTCCATTTTC
OSX-f	CGGGTCAGGTACAGTG
OSX-r	ACCATGACGACAAGGG
TGFβ1-f	CACCATCCATGACATGAAC
TGFβ-r	ACCCACGTAGTAGACGA
TNAP-f	GGGGACATGCAGTATGAGTT
TNAP-r	GGCCTGGTAGTTGTTGTGAG
WNT3A-f	CTTAGTGCTCTGCAGCCTGA
WNT3A-r	GAGTGCTCAGAGAGGAGTACTGG
WNT10B-f	CGGATTTCTGTCTAGGG
WNT10B-r	AGGTAGAGAAGACGCTAAC

Table 2.9: Primers used to check mRNA expression of genes involved in amelogenesis and odontogenesis.

Scanning electron microscopy (SEM)

(Methods provided by Dr. Hanson Fong, University of Washington Department of Materials Science and Engineering)

Samples were fixed in 4% paraformaldehyde for 2 to 3 days at room temperature and subsequently stored in 70% ethanol. For incisor samples, alveolar bone was removed prior to mounting in epoxy for the purpose of polishing. Samples were first dried in ambient air for 15 minutes followed by mounting in room-temperature-cure epoxy (Allied High Tech Products, Inc., Rancho Dominguez, CA). After overnight curing at room temperature, the samples were polished sequentially with 600 grit SiC paper, followed by diamond lapping films of 6 um and 1 um to a mirror finish (Allied High Tech Products, Inc., Rancho Dominguez, CA). All samples were polished sagittally. After polishing, the samples were lightly etched with 0.5% aqueous HCl for 30 seconds to reveal the enamel rod structure under SEM imaging. SEM sample preparation involved mounting the etched samples on SEM stubs and sputter coated with ~5 nm of Pt (SPI Module Sputter/Carbon Coaters, SPI Supplies, Inc., West Chester, PA). SEM imaging was performed in a JSM 6010 SEM (JEOL USE, Inc., Peabody, MA) at 10kV acceleration voltage in secondary electron imaging mode.

Micro-CT

Samples were harvested at P4, P7, P14, P21, P28, P84, and 6 months following birth. Following sacrifice of animals, samples were either immediately placed in -20°C or in 4% paraformaldehyde. Heads were scanned using a Skyscan 1076 scanner; 9um scans were

obtained using the following settings: 55kV, 180uA, 1450ms with an Aluminum 1.0 filter (Skyscan; Kontich, Belgium). Scans were reconstructed using NRecon (beam hardening correction at 60°) (Bruker; Kontich, Belgium) and reoriented in DataViewer (Bruker; Kontich, Belgium). Regions of interest were defined in CTAnalyser (Bruker; Kontich, Belgium), and a grayscale threshold was set for enamel. Following thresholding, enamel mineral density was calculated using built in CTAnalyser functions using attenuation coefficients obtained from scans of 0.25 g/cm^3 and 0.75 g/cm^3 phantoms. One way ANOVA with Tukey's post hoc tests was performed with significance at $p<0.05$. (GraphPad Prism, Version 6.01). Graphs were also generated using GraphPad Prism. 3D reconstructions of samples were created using Drishti Volume Exploration and Presentation Tool (Ajay Limaye), CTVox (Bruker), and CTVol (Bruker; Kontich, Belgium).

Distance between mesial and distal roots of the mandibular first molar was measured using reconstructed scans (NRecon, Bruker; Kontich, Belgium). Coronal slices were obtained after reorientation in DataViewer (Bruker; Kontich, Belgium). One Way ANOVA with Tukey's post hoc tests was performed with significance at $p<0.05$ (GraphPad Prism, Version 6.01). Graphs were also created using GraphPad Prism.

Chapter 3: The IRF6:NME complex contributes to epithelial maintenance and polarity

INTRODUCTION

Clefts of the lip with or without clefting of the palate (CLP) are the most common congenital deformities of the face, occurring with a global incidence of approximately 1 in every 600 to 700 live births (1-4). Genome-wide association studies and investigations of familial inheritance have implicated Interferon Regulatory Factor 6 (*IRF6*) variants as major contributors to CLP incidence. *IRF6* mutations cause van der Woude syndrome (VWS) and popliteal pterygium syndrome (PPS), which notably feature orofacial clefts (5-33). VWS is the most common form of syndromic forms of CLP, predicted to account for 2% of all syndromic forms of CLP. IRF6 variants are linked to approximately 12% of other nonsyndromic forms (34). VWS is autosomal dominant, has high penetrance, and exhibits variable expression; cardinal signs of VWS are lower lip pits with or without CLP (5-33). Familial recurrence has been found in approximately 60% of VWS patients, and lip pits occur in conjunction with orofacial clefts in approximately 50% of the cases (161). Other orofacial abnormalities include intraoral synechiae between the mucosal surfaces of the upper and lower alveolar ridges and commissural pits (161). PPS patients exhibit all of the characteristics of VWS in addition to syndactyly of digits and pterygium of the lower limbs. Severity of symptoms is highly variable in VWS and PPS patients, and not much is known about the contributors to this variability. Similar to management of other orofacial clefts, the orofacial aberrations

found in VWS and PPS are managed by surgery, and VWS patients have a higher incidence of severe wound complications compared to CLP patients without VWS (162).

Despite IRF6's association with syndromic and nonsyndromic forms of CLP, IRF6's function in CLP presentation remains largely unknown. Targeted alleles of murine *Irf6* have been generated, but none display the classic CLP phenotype (59, 61, 73, 163, 164). IRF6 belongs to the interferon regulatory factor (IRF) family of transcription factors, which have critical roles in innate and adaptive immune responses, e.g. regulating growth and regulation of many cell types, including B and T cells (165-167). Nine members comprise the IRF family (IRF1-IRF9); they all possess an N-terminal helix-loop-helix motif that is presumed to be the DNA binding domain, and IRFs 3-9 also possess a C-terminal region that includes a SMAD-like binding domain, or IRF association domain (IAD) (167-169). In a number of IRF family members (unknown in IRF6), the C-terminus is required for interactions with other IRFs, additional transcription factors, and non-nuclear proteins. In addition, several IRFs possess a serine rich region (SRR) in the C-terminus, which is influential in nuclear transport, dimerization, and interactions with other proteins. IRF6 has been proposed to act as a transcriptional activator based on analogies with other IRFs (28, 71, 72, 170, 171). However, IRF6 is unique among the IRF family in that its major role is outside the immune system. Recent studies in keratinocytes found IRF6 primarily localized in the cytoplasm, suggesting that IRF6

either has other roles besides acting as a transcription factor or is sequestered outside the nucleus until needed (61, 95, 163, 164).

The Cox lab (Seattle Children's Research Institute) has found that IRF6 binds, in a phosphorylation-enhanced manner, to the NME complex (non-metastatic), which has been shown to influence regulation of epithelial cell-cell adhesion and polarity. The NME complex has not been implicated in the formation of CLP, thus the research proposed here aims to investigate a novel mechanism in which IRF6 contributes to CLP. Via interactions with the NME complex, IRF6 has potential roles in the establishment and maintenance of epithelial polarity (Figure 3.1) (79). The NME complex is composed of NME2 and NME1, which are nucleoside diphosphate kinases. NME1 is reported to interact with the widely expressed T-cell lymphoma invasion and metastasis 1 (TIAM1) (172). TIAM1 has been found to regulate the PARD3-PARD6 (PAR) epithelial polarity complex, which is also found in primordial adhesions. The PAR complex is also dependent on signals from adherens junctions; mature adherens junctions are critical in delineating apical and basolateral domains. Adherens junctions contain nectins and cadherins adhesion molecules, whose surface expression is dynamically regulated to influence adhesion strength and ultimately epithelial polarity. In addition, NME2 has been reported to interact with plakoglobin, which interacts with E-cadherin and alpha catenin, providing another mechanism in which IRF6 and NME2 can participate in epithelial cell-cell adhesion and polarity (80).

Our studies here were designed to further elucidate the role of IRF6 on CLP by investigating molecular contributions of IRF6 on epithelial adhesion and polarity. We hypothesize that IRF6, via interaction with the NME complex, contributes to the establishment and maintenance of epithelial polarity in developing facial primordia. Ultimately, these studies are expected to provide novel insight into the molecular and cellular consequences of IRF6 mutations that underlie orofacial clefting disorders.

MATERIALS AND METHODS

Selection of VWS patient mutations and conserved serines

Twelve specific IRF6 missense mutations in the IAD were compared to wild type IRF6 in ability to interact with NME2. These mutations were found in patients with VWS and CLP. Each mutation was introduced into yeast pDEST32 IRF6 expression constructs to test for interaction with NME2. Wild type IRF6-NME2 interaction was used as a positive control.

Based on sequence alignment between IRF6 and the well-studied IRF5 and IRF3, three C-terminal serine residues were found to be completely conserved in position within the SRR (Figure 3.2). These were serines 413, 418, and 424. Using site-directed mutagenesis, phosphoinhibitory (Ser to Ala) and phoshomimic (Ser to Asp) substitutions were generate.

RESULTS

IRF6 also binds to NME1

NME1 and NME2 are small, closely related proteins that exhibit over 90% amino acid identity within and between species, yet have been reported to interact with different protein partners(76, 77, 154). When NME1 and NME2 protein sequences were compared, NME1 and NME2 share over 90% identity (Figure 3.3). To identify key residues in NME2 that confer this specificity of interaction with IRF6, residues that differ between the NME1 and NME2 sequences were targeted for mutation. Hybrid constructs, in which portions of NME1 and NME2 are interchanged, were tested in case more than one residue is responsible for this specificity in binding. For example, the N-terminal half of NME1 was fused with the C-terminal half of NME2 and vice versa. NME1/NME2 mutant constructs were tested for interaction with IRF6 using Y2H and co-immunoprecipitation (Co-IP). NME1, NME2, as well as NME1/NME2 hybrids interacted with IRF6 with comparable strength (Figure 3.4).

VWS patient mutations disrupt IRF6:NME binding

Twelve specific IRF6 missense mutations in the IAD were compared to wild type IRF6 in ability to interact with NME2. Using the Y2H assay, co-transformants were assessed for *HIS3* and *lacZ* activity, and several missense mutations disrupted the IRF6:NME interaction as demonstrated on SD-Leu-Trp-His+3AT plates and the X-Gal assay. Similar results were obtained when cells were co-transformed with NME1 instead of NME2

(Figure 3.5 and Table 3.3). Co-immunoprecipitation studies further validated the IRF6:NME interaction and demonstrated that certain patient mutations disrupted this interaction. In addition, the two NME variants identified by our collaborators in individuals with CLP (J. Murray group), R18Q in NME1 and G71V in NME2, were also tested for ability to interact with IRF6. These NME mutations also disrupted the IRF6:NME interaction, further supporting the importance of the IRF6:NME complex in CLP.

Importance of C-terminal phosphorylation in regulation of IRF6 function

Sequence alignment between IRF6 and the well-studied IRF5 and IRF3 revealed three C-terminal serine residues to be completely conserved in position within the serine rich region (SRR) of exon 9. Here, the role of these conserved serines (S413, S418, and S424) along with two other serines not conserved in position (S407, S416) in IRF6 function was investigated. Contribution of phosphorylation toward IRF6 function was tested for ability to disrupt IRF6:NME2 binding and assessed for impact on IRF6 nuclear localization. When each of these serines (S407, S413, S416, S418, and S424) was singly mutated to either alanine or aspartic acid, none of them demonstrated an effect on IRF6:NME2 binding in the Y2H or in Co-IP studies (data not shown). Double serine phosphoinhibitory and phosphomimic mutants also did not show an appreciable effect on IRF6:NME2 binding. However, when all three of the conserved serines (S413-418-424AAA) were mutated to alanines, the IRF6:NME2 interaction was weakened as shown

on the SD-Leu-Trp-His+3AT plates and X-Gal assay (Figure 3.6A). When co-immunoprecipitation studies were conducted with S413-418-424AAA mutants, the IRF6:NME2 interaction was weakened. Similar results were observed when NME2 was replaced with NME1 (data not shown).

Disrupting serine phosphorylation alters nuclear translocation of IRF6

Because ablation of three conserved serines (S413, S418, and S424) disrupted IRF6:NME2 binding, we examined whether disruption of the IRF6:NME2 altered IRF6 localization. LS8 cells were transfected with wild type, S413-418-424AAA, or S413-418-4424DDD constructs. Cells were stained with an anti-IRF6 and an anti-NME2 antibody. IRF6 was detected primarily in the nucleus with lower levels in the cytoplasm in cells overexpressing wild type IRF6 (Figure 3.7). In these same cells, NME2 was primarily detected in the cytoskeleton and cytoplasm with low levels in the nucleus. In comparison, cells transfected with S413-418-424AA exhibited lower IRF6 levels in the nucleus and higher levels in the cytoplasm. Furthermore, these cells exhibited lower levels of NME2 in the cytoskeleton and cytoplasm (Figure 3.7). This suggests that in addition to regulating IRF6 nuclear translocation, IRF6 serine phosphorylation regulates NME2 expression.

Rac1 and RhoA are altered when IRF6:NME2 are disrupted

Select IRF6 mutations that disrupted the IRF6:NME2 complex were assayed for Rac1 and RhoA expression. These mutations exhibited a weaker interaction with NME2 compared to the wild-type IRF6 in co-immunoprecipitation studies. Compared to cells ectopically expressing wild-type IRF6, cells expressing a mutated IRF6 exhibited higher levels of active Rac1 and RhoA, particularly RhoA (Figure 3.8).

siRNA knockdown of IRF6 results in decrease of NME1/NME2 in 293T epithelial cells

To test the effects of IRF6 ablation in epithelial cells, HEK293T cells were transfected with siRNA specific for IRF6 or a negative scrambled siRNA. RT-qPCR was performed with IRF6 and GAPDH to verify successful knockdown of IRF6 (Figure 3.9). Greater than 75% IRF6 knockdown was considered successful. NME1 expression was significantly lower with knockdown of IRF6, whereas NME2 expression was lower, but not significant. Cells were plated in triplicate, and qPCR was repeated twice for each plate.

DISCUSSION

Mutations in *IRF6* are associated with syndromic and nonsyndromic cleft lip with/without clefting of the palate, yet many aspects of its function remains elusive. Here, we present data demonstrating that the IRF6:NME complex may have a role in the establishment and maintenance of epithelial polarity.

Via the interferon association domain (IAD), IRF6 was found to bind to NME2, and here, using the same protein sequences, we show that IRF6 binds to NME1. Many documented VWS IRF6 patient mutations have been identified in the IAD, and out of the twelve mutations tested here, nine of them disrupted the IRF6:NME complex. Moreover, NME1/NME2 mutations found in CLP patients also disrupted the IRF6:NME interaction, further suggesting specificity of the IRF6:NME interaction and participation in the cause of CLP. Although the twelve mutations were not predicted to alter secondary structure, the position of the mutated residues may change tertiary structure. The crystal structure of IRF6 has not been resolved, although the crystal structure of IRF3 yields some clues (173). The IAD is conserved among IRFs 3 through 9, and it has been implicated in protein-protein interactions (167, 169). Structurally, the IAD is similar to the MH2 domain of Smad proteins; both participate in protein-protein interactions, have transactivation functions, and are mediated by phosphorylation (174). The IAD in IRF3 is flanked by autoinhibitory sequences, which interact to protect a hydrophobic core. When the autoinhibition is relieved, the DNA binding domain (DBD) is repositioned, allowing it to bind DNA regulatory downstream transcriptional targets (111). None of the mutations that disrupted IRF6:NME binding are part of the hydrophobic core, but they are conserved in identity and position among at least three other IRFs, suggesting that they are important for IRF function. Because all of the mutations did not result in loss of IRF6:NME binding, other protein-protein interactors not yet identified may be involved.

Serine phosphorylation is critical towards function of other IRFs, including IRF3 and IRF5. When IRF3 is phosphorylated in the C-terminus serine rich region (SRR), the configuration of the IAD is changed, unmasking the hydrophobic core (111). Subsequently, IRF3 is able to interact with other IRFs and other proteins. Here, when three conserved serines (S413, S418, and S424) were mutated to alanines (abolishing the phosphorylation sites), IRF6:NME binding was lost. Thus, IRF6 protein-protein interactions may also be mediated by serine phosphorylation. Additionally, phosphorylation activates transcriptional activity of IRF5 (112). When phosphorylation target residues were replaced with the phosphomimic aspartic acid, increased nuclear localization of IRF5 was observed. Similarly, nuclear localization was altered when HEK293T cells were transfected with S413-418-424AAA constructs, indicating that serine phosphorylation may also regulate IRF6 nuclear translocation and subsequent regulation of transcriptional targets. When IRF6 was silenced in HEK293T cells, the resultant decrease in NME1/NME2 suggests that IRF6 may regulate transcription of NME1/NME2 in addition to acting as a binding partner.

Although NME is known to act as nucleoside diphosphate and histidine-dependent kinases, it is not believed to be responsible for IRF6 phosphorylation. A kinase dead NME2 did not have any effects on IRF6 serine phosphorylation (74). Receptor interacting serine-threonine kinase 4 (RIPK4) has been proposed to phosphorylate IRF6. RIPK4 is a member of the receptor-interacting serine threonine kinase (RIP) family, which has important roles in immune function (175). Notably, IRF5 is believed to be

phosphorylated by RIPK2, another member of the RIP kinase family, and both RIPK2 and RIPK4 participate in the nuclear factor kappa-light-chain-enhancer of activated B cells (NF-κB) and c-Jun N-terminal kinase (JNK) pathways (112, 175). RIPK4 mutations have been found in individuals with PPS and Bartsocas Pappas syndrome (BPS), which exhibit epidermal adhesions (176-178). *Ripk4-null* mice feature a similar phenotype to *Irf6-null* mice; both feature a hyperproliferative epidermis and loss of epidermal differentiation, suggesting that RIPK4 and IRF6 participate in the same pathway (179, 180).

Co-immunoprecipitation studies have also demonstrated that RIPK4 and IRF6 interact (181). Truncation of IRF6 proximal to the serine rich region results in loss of binding between RIPK4 and IRF6. Furthermore, a kinase-dead RIPK4 does not interact with IRF6 and does not promote IRF6 nuclear translocation (114). In the nucleus, IRF6 has known transcriptional targets, including Grainyhead-like 3 (GRHL3) and OVO-like 1 (OVOL1), which have roles in keratinocyte differentiation (62, 182). GRHL3 has roles in keratinocyte differentiation and establishment of the oral periderm; in the absence of *IRF6*, *GRHL3* expression is downregulated. OVOL1 also promotes keratinocyte differentiation, and *IRF6* knockdown results in *OVOL1* downregulation. Knockdown of RIPK4 also resulted in downregulation of GRHL3 and OVOL1, suggesting that the phosphorylation state of IRF6 influences keratinocyte differentiation.

Via an interaction with NME, IRF6 has the potential to impact other processes crucial towards proper epithelial function, e.g. adhesion and polarity. In the adherens

junctions, via interactions with NME and other cytoplasmic proteins, IRF6 has the potential to influence E-cadherin recruitment and removal from the cell membrane. Disruption of E-cadherin cell-cell adhesion complexes leads to increased cell proliferation, disrupted cell shape, and altered cytoskeletal architecture (88, 183). E-cadherin endocytosis is essential in disassembly of adherens junctions and occurs through clathrin-dependent and independent pathways (184, 185). Clathrin-dependent endocytosis, in which E-cadherins are removed from the cell membrane and packaged into vesicles, is mediated by adaptor proteins, e.g. adaptor protein complex 2 (AP-2) (186, 187). Additionally, AP-2 translocation to the cell membrane is mediated by ADP-ribosylation factor 6 (ARF6), which also recruits NME1 during adherens junctions disassembly (188, 189). Increased, uncontrolled E-cadherin endocytosis would likely lead to disruptions in epithelial polarity and hyperproliferation of the epithelia as seen in *Irf6* mutants. This hyperproliferation can also lead to the ectopic adhesions observed in individuals with VWS and PPS. Furthermore, when IRF6 is knocked down in chick epithelia, E-cadherin expression decreases and assumes a more irregular appearance compared to controls, which may be a reflection of unregulated E-cadherin endocytosis (74). Thus, IRF6, which promotes keratinocyte differentiation, may bind to the NME complex in order to regulate E-cadherin endocytosis.

Additionally, NME has several known roles in the establishment of epithelial polarity, particularly via the Rho GTPases Rac1 and RhoA. Rac1 is activated by the PAR polarity complex in epithelial cells during the establishment of apical-basal polarity (107). NME1

inhibits TIAM1, and TIAM1 activates Rac1, which normally regulates the PAR polarity complex. Binding of NME2/NME1 to the GEFs, LBC, and TIAM1, suppresses their activity and results in activation of RhoA and Rac1, respectively (104, 190). Thus, Rac1/RhoA is expected to increase when the NME complex is unable to interact with LBC/TIAM1. In our studies here, HEK293T cells ectopically expressing a mutation in which the IRF6:NME interaction is disrupted, exhibited higher levels of Rac1 and RhoA compared to cells ectopically expressing a wild-type IRF6 (Figure 3.8). Thus, the IRF6:NME complex may be needed for LBC/TIAM1 inhibition of Rac1/RhoA. Irf6 deficient keratinocytes also express higher RhoA levels as a result of downregulation of RhoA GTPAse Activating Protein 29 (ARHGAP29) (191). This suggests that the IRF6:NME complex can affect the expression of Rho GTPases, which can cause alterations in epithelial polarity. Although basal levels of activated Rac1 are required for adherens junctions assembly, sustained Rac1 activation results in adherens junctions disassembly and loss of polarity (192, 193). Similarly, sustained RhoA activity results in disassembly of tight junctions, but not adherens junctions. Irf6 null mice and chicks in which IRF6 expression is ablated exhibit reduced E-cadherin and altered epithelial shape; these may be consequences of Rac1 or RhoA alterations (60). Additionally, wound closure is dependent on RhoA modulated actin cytoskeletal dynamics (194). An ARHGAP29 variant is associated with poor scarring, suggesting that the elevated active RhoA levels contribute to the poor wound healing observed in VWS patients (195).

Furthermore, studies have identified roles of NME in other pathways. NME1/2 has been implicated in the Raf/MEK/ERK pathway (94, 196). The Raf/MEK/ERK pathway is regulated by Ras GTPase signaling, which is inhibited by RSG19, a Gα Interacting Protein (115, 161). Active Ras stimulates the formation of the Raf/MEK/ERK complex, which is anchored by the kinase suppressor of Ras (KSR). Assembly of the complex promotes phosphorylation of Raf/MEK/ERK, leading to nuclear translocation of ERK and activation of ERK target genes. RGS19, which ultimately inhibits Ras signaling, upregulates NME1/2. Presence of NME1/2 in the cytoplasm promotes the formation of the RGS19/NME/KSR complex. Formation of this complex inhibits formation of the Raf/MEK/ERK complex and thus, transcriptional activation of ERK targets does not occur. Rgs19 has been implicated in palatal fusion; Rgs19 is detected in palatal epithelial prior to palatal fusion, specifically in the MEE (83). Once palatal fusion has occurred, Rgs19 ceases to be detected in the epithelium. Knockdown of Rgs19 resulted in delay of palatal fusion as well as alteration of cell proliferation and apoptosis in palatal shelves (83). RGS19 is expected to upregulate NME1/2; thus, loss of RGS19 is expected to result in NME1/2 downregulation. This downregulation may inhibit formation of the IRF6:NME complex, subsequently contributing to the epithelial abnormalities observed in patients with IRF6 mutations.

Here, we presented data suggesting that the IRF6:NME complex contributes to the presentation of CLP. We have found that CLP patient mutations disrupt normal IRF6 protein-protein interactions and cause alterations in polarity effector molecules,

including Rac1 and RhoA. Furthermore, IRF6 nuclear translocation and the RF6:NME interaction appears to be mediated by serine phosphorylation. Because of NME's diverse functions, the IRF6:NME complex has the potential to impact many processes required for proper epithelial function.

FIGURES AND TABLES

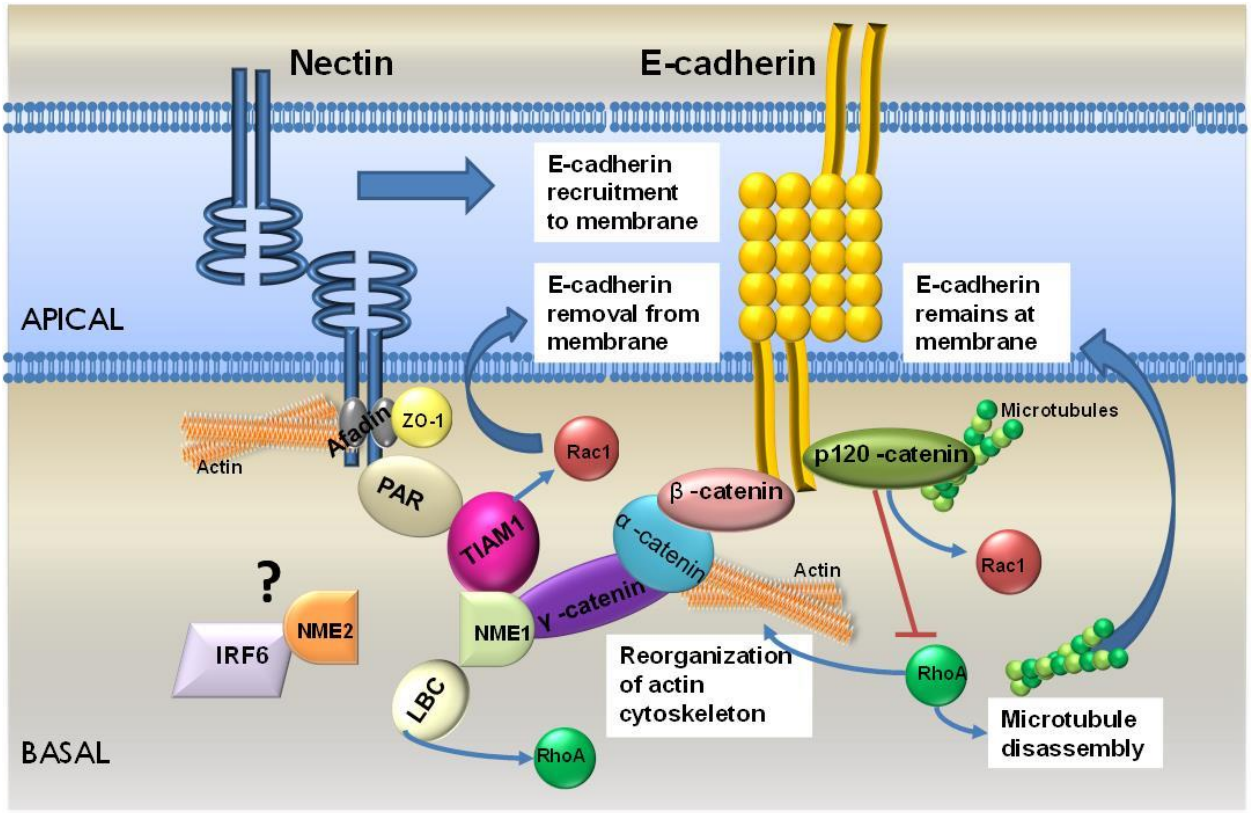

Figure 3.1: Schematic of contributors to epithelial polarity in adherens junctions.

Although the cell adhesion molecules Nectin and E-cadherin do not interact directly, they are connected via interactions with other proteins. This schematic depicts one potential relationship between Nectin and E-Cadherin and suggests a possible interaction between IRF6 and adherens junction proteins, i.e. contribution to epithelial polarity.

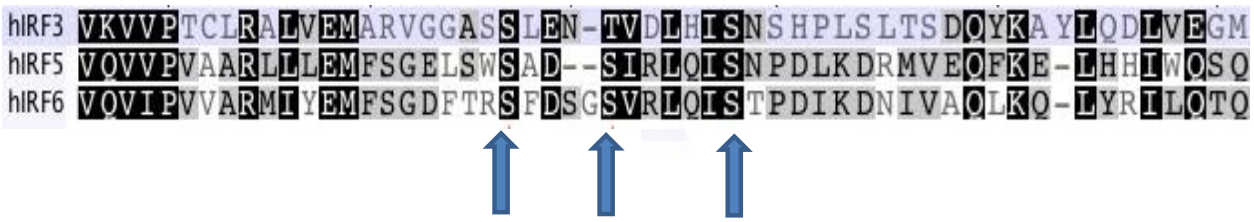

Figure 3.2: Serines absolutely conserved in position among IRF3, IRF5, and IRF6.

Serines absolutely conserved in position correspond to S413, S418, and S424 in IRF6 (indicated by blue arrows).

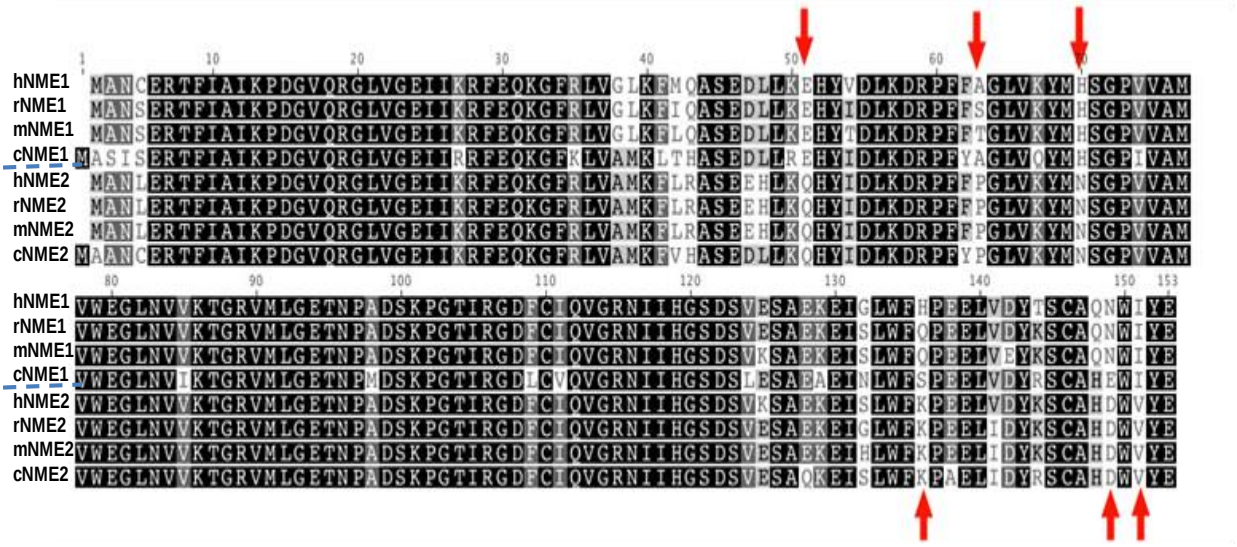

Figure 3.3: Comparison of NME1 and NME2 in human (h), rat (r), mouse (m), and chick (c). High sequence homology exhibited between all sequences; amino acids that are not conserved between NME1 and NME2 are indicated with red arrows.

		SD-Leu-Trp	SD-Leu-Trp-His +3AT	X-Gal Assay
Wild-type	IRF6+NME1			
	IRF6+NME2			
Domains switched	IRF6+NME1(N)-NME2 (C)			
	IRF6+NME2 (N)-NME1(C)			
Negative control				
Positive control				

Figure 3.4: IRF6 also binds to NME1. Abbreviations: N= N-terminal half of either NME1 or NME2, C= C-terminal half of either NME1 or NME2. In the yeast two hybrid system, NME1, NME2, as well as NME1/NME2 hybrids interacted with IRF6 as demonstrated by growth on the SD-Leu-Trp+3AT selection plate and blue color in the X-Gal assay.

A

		SD-Leu-Trp	SD-Leu-Trp-His +3AT	X-Gal Assay
Wild-type	IRF6+NME1			
	IRF6+NME2			
IRF6 mutations	G749A+NME			
	T752C+NME			
	G1016T+NME			
	A1162G+NME			
NME1 mutation	IRF6+R18Q			
NME2 mutation	IRF6+G71V			
Negative control				
Positive control				

B

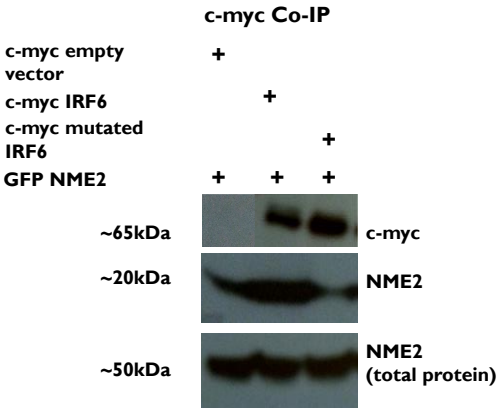

Patient Mutations	
G749A (R250Q)	G961A (V321M)
T752C (L251P)	G1016T (R339I)
C772T (P258S)	T1118C (L373S)
G799T (G267C)	G1141T (D381Y)
T881C (L294P)	A1162G (K388E)
A958G (K320E)	G1199A (R400Q)

Figure 3.5 and Table 3.1: Evaluating effect of IRF6 missense mutations on the ability of IRF6 to bind NME1/NME2 using yeast two-hybrid. Wild-type human and mouse IRF6 were cloned into pDEST32 vectors; wild-type NME2 was cloned into pPC86. **(A)** Selected results from yeast two-hybrid assay, demonstrating loss of IRF6:NME interaction when certain patient mutations were tested. Positive interaction demonstrated by growth on the SD-Leu-Trp+3AT selection plate and blue color in the X-Gal assay **(B)** Representative co-immunoprecipitation results validating results from yeast two-hybrid.

Table 3.1: Summary of IRF6 missense mutations that disrupted IRF6:NME binding. IRF6 patient mutations that disrupted IRF6:NME binding are highlighted in red.

		SD-Leu-Trp	SD-Leu-Trp-His +3AT	X-Gal Assay
Wild-type	IRF6+NME1			
	IRF6+NME2			
Serine mutations	S413-418AA			
	S413-424AA			
	S418-424AA			
	S413-418-424AAA			
Negative control				
Positive control				

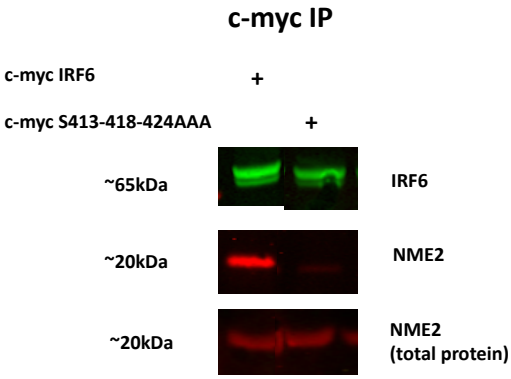

Figure 3.6: Testing effects of conserved serines on IRF6:NME binding. (A) Selected results from the testing of phosphoinhibitory (S to A). Double serine (S413-418AA, S413-424AA, and S418-424AA) mutants did not disrupt IRF6:NME binding. When all three of the conserved serines were mutated (S413-418-424AAA), the IRF6:NME interaction was lost as shown by lack of growth on the SD-Leu-Trp-His+3AT media and a negative result on the X-gal assay. **(B)** Immunoprecipitation results showing lower amounts of NME2 being precipitated in cells ectopically expressing S413-418-424AAA compared to cells ectopically expressing a wild type IRF6 (compare lane 2 with lane 1).

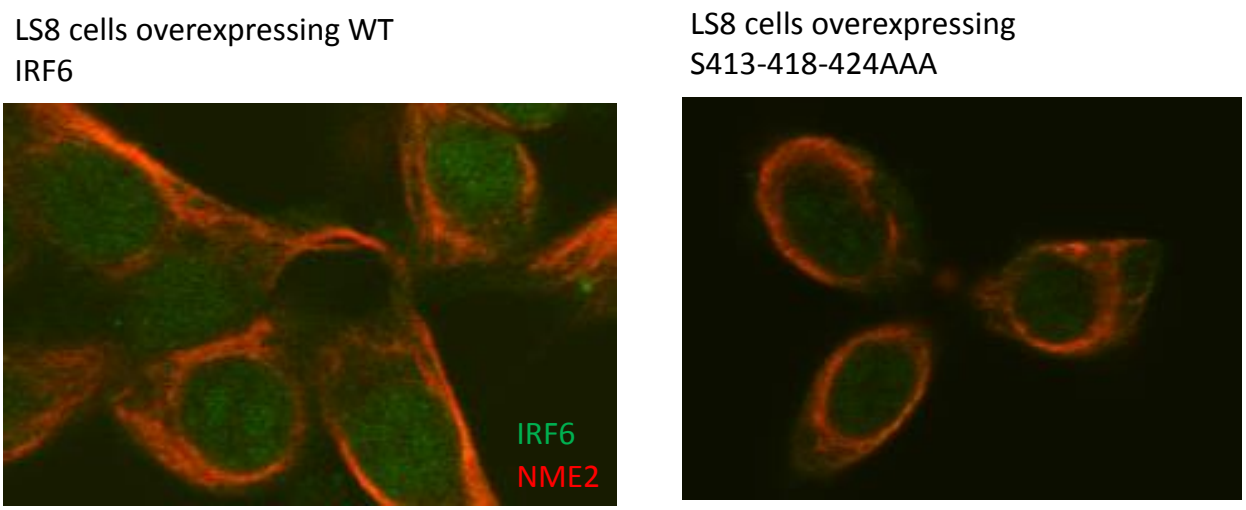

Figure 3.7: Serine phosphorylation alters nuclear translocation. Lower amounts of IRF6 (green) observed in the nucleus of LS8 cells ectopically expressing S414-418-424AAA (B) compared to cells ectopically expressing wild type (WT) IRF6

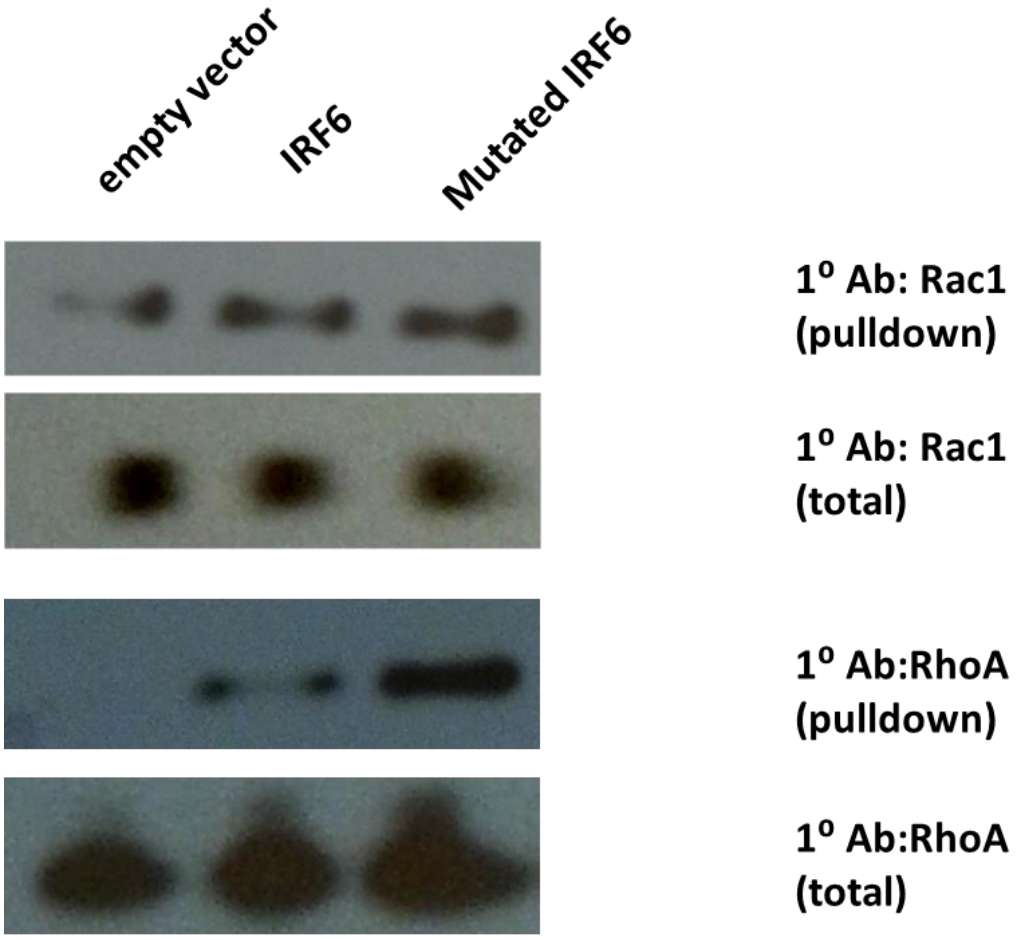

Figure 3.8: Rac1 and RhoA increase when the IRF6:NME2 interaction is disrupted in HEK293T cells. HEK293T expressing a mutated IRF6 exhibited higher levels of active Rac1 and RhoA compared to cells expressing a wild type IRF6 (compare lane 3 with lane 2).

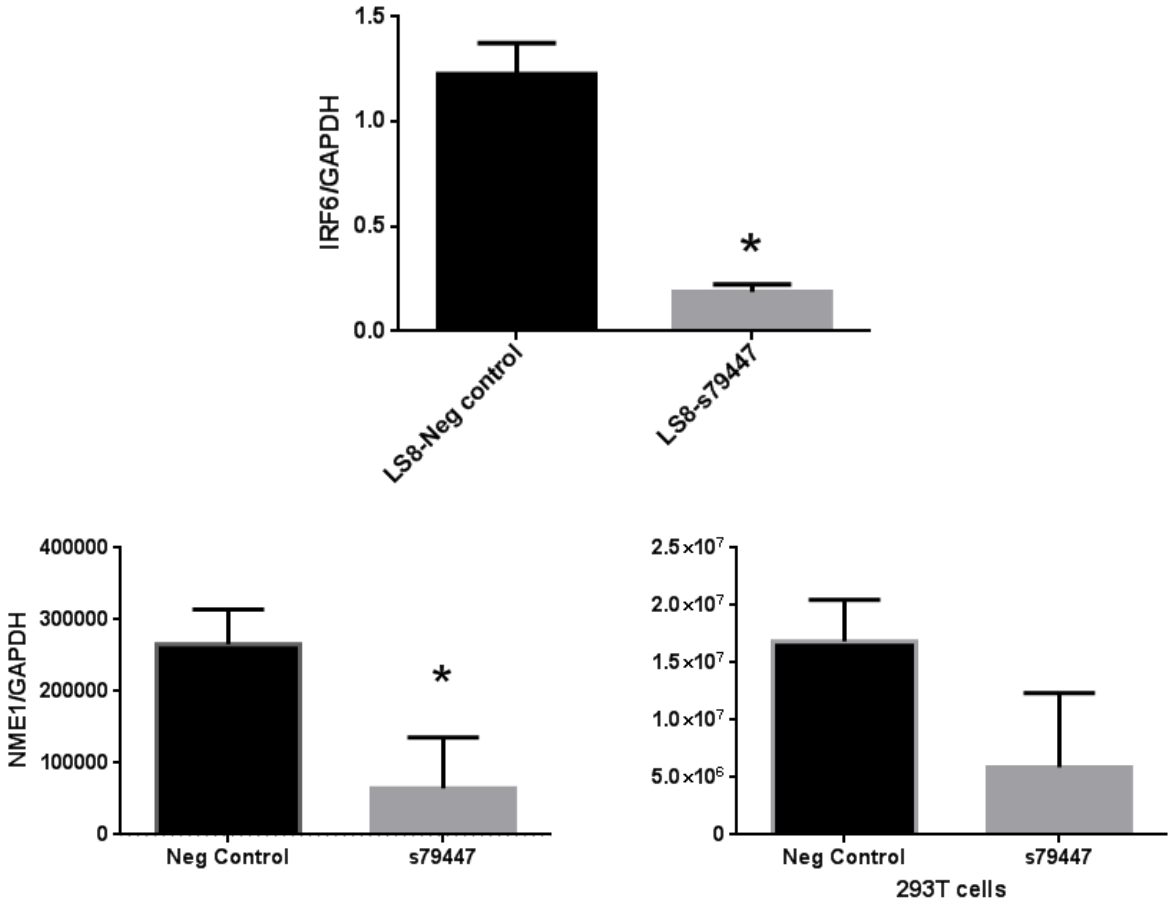

Figure 3.9: Knockdown of IRF6 HEK293T cells results in decrease in NME1 and NME2 mRNA expression. (A) Cells transfected with siRNA specific to IRF6 (s794447) exhibited greater than 75% knockdown of *IRF6* compared to cells transfected with a scrambled sequence (Compare right column with left column). qPCR results were normalized to *GAPDH* as an internal control. **(B)** qPCR analysis shows significant downregulation of *NME1* in HEK293T cells where *IRF6* was silenced. **(C)** qPCR analysis shows downward trend, although not statistically significant reduction of *NME2* in HEK293T cells where *IRF6* was silenced. Student's t-test performed with *: $p<0.05$

Chapter 4: IRF6 loss-of-function results in defects in enamel formation and root patterning

INTRODUCTION

Dental abnormalities are frequently found in patients featuring epithelial disorders. Tooth tissues have several origins; the cells and structures that form the enamel arise from oral ectoderm, and the cells and structures that form dentin, pulp, and periodontium arise from neural-crest derived ectomesenchyme. Reported dental abnormalities associated with ectodermal dysplasias include enamel hypoplasia, conical crowns, taurodontic molars, and hypodontia (115). Furthermore, compared to the general population, CLP patients exhibit higher rates of tooth agenesis, aberrations in tooth morphology, and enamel defects (116). Specifically, hypodontia and taurodontism are associated with VWS and isolated forms of CLP (117-119). Maxillary second premolars, mandibular second premolars, and maxillary lateral incisors are the most frequently absent; depending on the study, their absence is noted in 10 to 81% of VWS patients (161). Thus, similar mechanisms likely control aspects of tooth development and proper palatal fusion.

IRF6 in situ hybridization revealed IRF6 expression in dental and oral epithelium in embryonic ages (59, 115). At E12.5, *Irf6* was detected in the oral epithelium, and in E14.5, *Irf6* was expressed in the enamel organ with higher intensity in the tissues that would become the cervical loop. In later stages, *Irf6* was detected in the outer enamel epithelium, the stellate reticulum, the stratum intermedium, and the preameloblasts. In

Irf6 null mutant mice, incisor tooth buds exhibited abnormal epithelial protrusions into the oral cavity, whereas, in wild-type control mice, the epithelium invaginated into the condensing mesenchyme. Molars exhibited comparable invagination in the *Irf6* null and wild-type mice. Thus, in the tooth, *Irf6* expression is restricted to epithelial derived tissues.

Irf6 mutant strains die before completion of tooth development (73); thus, to investigate the role of *Irf6* on tooth development, an *Irf6* conditional knockout model was generated. Because of its restricted expression in epithelial tissues, the paired-like homeodomain2 (Pitx2) promoter was selected to investigate the effects of Irf6 on ameloblast polarity and enamel development (197). *Pitx2*, specific to the oral epithelium is expressed in the dental lamina, enamel knot, undifferentiated cervical loops, and pre-ameloblasts (160). During the progression from oral epithelium to differentiated ameloblasts, the epithelial derived tissues undergo morphological changes, likely influenced by epithelial polarity and adhesion. *Irf6* is expressed in the oral epithelium; thus, our murine model is expected to help elucidate the role of *Irf6* in epithelial-derived tooth structures directly, as well as effects on associated tissues.

RESULTS

Loss of Irf6 causes defects in tooth patterning and initiation

Irf6-cKO mice survived past birth and were indistinguishable from control littermates in regards to physical and behavioral appearance. Gross examination of skulls at six

months postnatal did not yield any appreciable craniofacial differences between *Irf6-cKO* mice and controls (Figure 4.1). On closer examination, *Irf6-cKO* mice exhibited defects in tooth patterning and initiation, resulting in an array of crown abnormalities at post-eruptive ages (P28 and P84) (Figure 4.2). Overall, molars were smaller in the *Irf6-cKO* samples (microdontia) compared to controls. In 25% of samples examined (5 out of 20), abnormal cusp patterns were noted, including significantly smaller crown shapes, and loss of cusp patterning with single peg-shaped roots. In 10% of samples (2 out of 20), 3rd molars were missing (Table 4.1). Alterations in *Irf6-cKO* molar cusp shape were observed in P7 and P14 samples, ages prior to tooth eruption. In these ages, cusps appeared shallower in *Irf6-cKO* samples compared to the controls (Figure 4.3).

Loss of Irf6 causes alterations in root formation

Irf6-cKO mice presented root patterning defects, including severely taurodontic mandibular second molars in 100% of *Irf6-cKO* samples (N=20) examined (Table 4.1). None of the other genotypes exhibited taurodontic mandibular second molars. Teeth were characterized as taurodonts using the following criteria: enlarged pulp chamber, apical displacement of the pulpal floor, reduction of separation between or fusion of mesial and distal roots, and reduced constriction at the cementoenamel junction. When teeth were removed from the alveolar bone, *Irf6-cKO* mandibular first molars (that did not exhibit peg shaped roots) had comparable root morphology to controls (Figure 4.4,

C' versus A' and B'). In contrast, mandibular second molars completely lost separation of mesial and distal roots and exhibited an elongated root trunk (Figure 4.4, C").

Enamel maturation defect observed in *Irf6-cKO* samples

Irf6-cKO mice displayed rapid enamel attrition with wear reaching dentin seven days post-eruption. (Figure 4.5). By P84, the occlusal surfaces of the *Irf6-cKO* molars were almost worn completely flat (Figure 4.5, C"). Micro-CT analysis of P28 and P84 samples revealed that *Irf6-cKO* enamel was hypomineralized compared to controls in incisors and molars (Figure 4.6). Thresholds were set for mature enamel, and enamel mineral density was measured for mandibular molars. One way ANOVA with post hoc tests were performed with $p<0.05$). Enamel mineral density was statistically significantly lower in *Irf6-cKO* samples compared to $Pitx2^{+/+}; Irf6^{fl/+}$ samples ($p<0.05$), whereas the $Pitx2^{Cre/+}; Irf6^{fl/+}$ and $Pitx2^{+/+}$; $Irf6^{fl/fl}$ were not statistically different from the $Pitx2^{+/+}; Irf6^{fl/+}$ samples.

Cross sections of the incisors were examined below four landmarks in postnatal day 28 (P28) samples: alveolar crest, mental foramen, mesial root of the mandibular first molar, and mesial root of the mandibular second molar. Incisor enamel at the alveolar crest and the mental foramen landmarks was comparable between *Irf6-cKO* and control samples, whereas micro-CT and histological analysis revealed that incisor enamel at the mandibular molar landmarks was less mineralized in *Irf6-cKO* samples. Additionally, the

transition zone between mature and immature enamel (Figure 4.7, red arrows) was located more cervically in *Irf-cKO* samples compared to controls.

Scanning electron microscopy (SEM) analysis revealed comparable prismatic structure between *Irf6-cKO* and control samples at mature enamel sites (Figure 4.8). However, at higher magnification, shearing of enamel rods was observed in *Irf6*-cKO samples (Figure 4.8, D, red arrow). This was not observed in any of the control samples. Structure of immature enamel was comparable between *Irf6-cKO* and control samples (Figure 4.8, E and F).

Disturbances in ameloblast polarity observed in *Irf6-cKO* samples

Histological sections obtained at the mesial root of the mandibular first molar revealed presence of immature enamel matrix in *Irf6-cKO* samples, which was absent in comparable control samples (Figure 4.9, B'). In P28 *Irf6-cKO* samples, incisor ameloblasts showed clear disturbances in morphology and polarity, appearing shortened and irregular (Figure 4.9, B" versus A"). In P28 sagittal sections of the incisor, significantly shorter and disorganized ameloblasts were also observed (Figure 4.10).

Altered NME2 protein expression detected in *Irf6-cKO* samples

Sections from P14 incisors were immunolabeled using primary anti-IRF6 and NME2 antibodies. IRF6 and NME were detected in developing ameloblasts, specifically adjacent to the developing enamel matrix, suggesting that IRF6 and NME are involved in amelogenesis (Figure 4.11). IRF6 was detected in the nuclei and cytoplasm of ameloblasts, with stronger localization at the distal end of the Tomes' processes. NME2 appeared to be distributed evenly throughout the cytoplasm of ameloblasts. NME2 expression exhibited altered distribution in ameloblasts of P14 *Irf6-cKO* incisors and molars compared to controls (Figure 4.12). In P14 control samples, NME2 was distributed throughout the cytoplasm of the ameloblasts, although there appears to be slightly increased localization at the proximal and distal ends of the ameloblasts (Figure 4.12). In contrast, the Irf6-cKO P14 ameloblasts exhibit lower amounts of NME2 in the cytoplasm, and NME2 appears to aggregate at the distal end of the ameloblasts.

DISCUSSION

Ablation of Irf6 in oral epithelium demonstrates tooth defects commonly found in CLP and amelogenesis imperfecta patients, suggesting importance of Irf6 in epithelial-derived tooth tissues (116-119, 198). Enamel defects, hypodontia, and taurodontism occur at a higher prevalence in CLP patients compared to the general population. Additionally, increased wear observed in *Irf6-cKO* molars resembles amelogenesis imperfecta patients with hypoplasia and hypomaturation enamel phenotypes. Our *Irf6-*

cKO serves as a viable model in which to study enamel defects, which was previously not possible because of early lethality of *Irf6-null* mice.

Our *Irf6-cKO* model was driven by the *Pitx2-Cre* promoter. *Pitx2* encodes three isoforms: *Pitx2a, Pitx2b,* and *Pitx2c,* which exhibit redundancy in function. In developing teeth, *Pitx2* expression is restricted to the oral epithelium. Its expression remains high throughout the bud and cap stage, and it is found in the enamel knot, undifferentiated cervical loops, and pre-ameloblasts. In the bell stage, *Pitx2* is detected at lower levels in transitional and secretory ameloblasts. This expression pattern overlaps with *Irf6* expression in the tooth; thus, *Pitx2* was an appropriate *Cre* promoter to study the effect of *Irf6* on tooth development. The $Pitx2^{Cre}$ allele has been characterized; the $Pitx2^{Cre}$ allele behaves as a *Pitx2* null allele, in which *Pitx2a, Pitx2b,* and *Pitx2c* are inactive. $Pitx2^{Cre/Cre}$ mice are embryonic lethal, thus our *Irf6-cKO* mice are homozygous for the *Irf6-floxed* allele and heterozygous for the $Pitx2^{Cre}$ allele. In *Pitx2-null* mice, molar development is arrested at the bud stage; however, mice that were heterozygous for the *Pitx2* null allele exhibited normal molar development. Possible effects on enamel and root development were not reported. The effect of *Pitx2* on multiple organs is dose dependent; to determine possible contributions of the *Pitx2-Cre* allele, we analyzed the phenotype of $Pitx2^{Cre/+}$; $Irf6^{fl/+}$ mice as controls. Compared to $Pitx2^{+/+}$; $Irf6^{fl/+}$ mice, the $Pitx2^{Cre/+}$; $Irf6^{fl/+}$ mice did not exhibit significant disruptions to crown or root morphology, although there was a trend for lower, not statistically significant, enamel mineral density of the $Pitx2^{Cre/+}$; $Irf6^{fl/+}$ enamel. Consequently, the $Pitx2^{Cre}$ allele may

have contributed to the lower enamel mineral density, although presence of the *Irf6*^{fl} allele .

Loss of *Irf6* resulted in a delay in enamel maturation, which was apparent in P14, P28, and P84 samples. Histological analysis revealed areas of immature enamel matrix in *Irf6-cKO*, whereas in comparable control sections, the enamel was fully mineralized. When comparing enamel mineral density measurements across P14, P28, and P84 ages, *Irf6-cKO* enamel appeared to lag behind the controls in achieving its final mineral density. This delay in enamel maturation was also visible in *Irf6-cKO* incisors. Additionally, the final mineral density was statistically significantly lower compared to controls, resulting in hypomineralized enamel, which exhibited increased enamel attrition. Micro-CT analysis showed that radiographically, mature *Irf6-cKO* enamel was distinguishable from dentin, suggesting an enamel hypomaturation phenotype versus a hypocalcification phenotype. Enamel formation progresses in several stages: pre-secretory, secretory, and maturation. In the pre-secretory and secretory stages, ameloblast differentiation occurs and deposits an organic enamel matrix layer. In the maturation stage, the organic components of the enamel matrix layer are removed, and mineral deposition occurs. Hypomaturation enamel is often the result of defects in the maturation stage of enamel development. Clinically, hypomaturation enamel exhibits increased attrition, which is consistent with the phenotype observed in *Irf6-cKO* mice.

In order to further define the effect of *Irf6* ablation on enamel structure, SEM was employed. SEM revealed that *Irf6-cKO* mice were able to form enamel prisms accompanied by a seemingly organized rod and interrod structure, suggesting that the initial stages of enamel formation, while delayed, occurred without any major disruptions. This is corroborated by the comparable immature enamel structure observed in *Irf6-cKO* and controls. However, shearing of enamel rods was observed in *Irf6-cKO* mature enamel samples, which would likely not occur if the crystallites were as tightly packed compared to controls. In studies of enamel from patients with hypomaturation enamel, some samples featured prismatic structure accompanied by widened interprismatic gaps. Additionally, organization of the enamel crystals was disrupted, the crystallites were smaller compared to controls, and higher amounts of organic matter were detected. The shearing of enamel rods in *Irf6-cKO* samples may be caused by inefficient removal of organic matrix, thus leading to looser packed enamel rods and weakened enamel structure. This suggest that IRF6 may regulate either removal of the organic matrix or mineral deposition.

In addition to causing enamel defects, *Irf6* ablation in oral epithelium has marked effects on crown and root development. Previous studies demonstrated *Irf6* expression in dental and oral epithelium in embryonic stages, and *Irf6* mutant incisor epithelium invaginated improperly in the bud stage (59). For the first time, we present consequences of Irf6 loss on later stages of tooth development. Subtle morphological differences were detected at P7, and by the time teeth were fully erupted (P28 and

later), marked crown patterning differences were detected. During the bell stage, the inner dental epithelium undergoes folding events, which ultimately determines cuspal position. In *Drosophila*, epithelial folding has been found to be initiated by repositioning of the adherens junctions, i.e. changing polarity, in a Rap1 and α-catenin manner. Rap1, which is also a member of the Rho GTPase family, is believed to regulate Rac1 and RhoA (199, 200). Constitutively active Rap1 is believed to lead to restricted epithelial folding (201). In a similar manner, higher levels of RhoA may lead to alterations in epithelial folding, which can manifest as shallower cusps or loss of cusps as seen in our *Irf6-cKO* samples. Furthermore, one of the causes of taurodontism, which was frequently observed in our *Irf6-cKO* mice is a failure of Hertwig's epithelial root sheath to invaginate at the proper horizontal level (202). The HERS is derived from the inner and outer enamel epithelium and as the HERS migrates inward and apically, it establishes a barrier between the mesenchyme-derived developing periodontium and pulp (125, 127). Folding of the HERS defines the location of the furcation and generates secondary apical foramina (45). Thus, the observed crown and root morphological disturbances may be caused by epithelial polarity directed alterations in epithelial folding.

As investigated in Chapter 3, the IRF6:NME complex has potential roles in the developing facial epithelia. Next, we investigated whether NME also has a role in the tooth. The role of NME has not been investigated in the tooth, and our data suggests that NME is also expressed in teeth, although whether an IRF6:NME interaction exists in the tooth is unknown. In P14 incisor sections, NME2 immunolocalization was altered in

Irf6-cKO samples versus controls.. In P14 control samples, NME2 was distributed throughout the cytoplasm of the ameloblasts (Figure 4.12). In contrast, the Irf6-cKO P14 ameloblasts exhibit lower amounts of NME2 in the cytoplasm, and NME2 appears to aggregate at the distal end of the ameloblasts. In P14 control sections, the ameloblasts are in the transition and maturation stages. The Tomes' processes are no longer as visible, and they are beginning to retreat from the enamel matrix. After the enamel matrix assumes its final thickness, the proximal and distal junctions alter their permeability in preparation for removal of organic components and mineral deposition. NME has roles in regulation of adhesion complexes in epithelia, so NME localization at proximal and distal ends may represent a mechanism in which ameloblasts alter the strength of the junctional complexes. In contrast, the Irf6-cKO P14 ameloblasts appear to be still in the secretory stage; the ameloblasts appear taller, and the Tomes' processes do not appear to have retreated form the developing enamel matrix. At this stage, proteins are actively being secreted, so the distal junctional complex needs to be permeable enough to allow for release of the enamel matrix proteins. NME promotes E-cadherin endocytosis, which ultimately weakens cell-cell contacts. The increased NME may reflect abnormal regulation of permeability at the junctional complexes. Furthermore, the increased localization of NME2 at the distal end of the ameloblasts resembles IRF6 localization in P14 ameloblasts (Figure 4.11). In wild type sections, IRF6 was immunolocalized to the distal end of the ameloblasts, whereas NME2 was evenly distributed throughout the cytoplasm. Loss of IRF6 resulted in altered NME2

localization, suggesting that IRF6 may function to keep NME away from the junctional complexes.

Additionally, as discussed in Chapter 3, reduced NME levels are expected to result in elevated active Rac1 and RhoA levels, which result in disturbances in epithelial adhesion and polarity. In the tooth, Rac1 and RhoA have been detected in the enamel organ, and Rac1 and RhoA expression is higher in differentiated ameloblasts in comparison to non-polarized cells of the inner and outer enamel epithelium (203). Furthermore, RhoGDI (inhibitor of Rho GTPases) is downregulated during ameloblast secretory stages, in which ameloblasts are polarized (204). This suggests that RhoA and Rac1 have roles in the ameloblast polarity. In epithelial cells, RhoA can cause changes in cell shape and polarity via alterations of the actin cytoskeleton (94). F actin is concentrated at proximal and distal ends in ameloblasts, coinciding with the location of the junctional complexes (203). Rac1 moderates E-cadherin cell-cell complexes, and E-cadherin is expressed in inner and outer enamel epithelial cells (205). Following establishment of cusp morphology, differentiated ameloblasts express lower E-cadherin levels (205). Thus, the timing of E-cadherin expression is believed to influence tooth morphogenesis (206). Rac1 is also specifically localized to the distal end of polarizing ameloblasts, further suggesting a role of Rac1 in ameloblast polarity. Our immunohistochemistry showed NME2 concentration at the proximal and distal ends, suggesting that the IRF6:NME interaction may contribute to the observed crown and root morphological disturbances via alterations in Rac1 and RhoA.

Rac1 in polarizing ameloblasts

Rac1 is

Thus, the IRF6:NME interaction may contribute to the observed crown and root morphological disturbances via alterations in Rac1 and RhoA. Further studies are needed to elucidate the role of IRF6 and NME during tooth development and to determine possible downstream effects on adhesion and polarity effector molecules.

Tooth-targeted *Irf6* deletion in mice demonstrated enamel and root patterning defects consistent with CLP patients with *IRF6* mutations. Disturbances in crown morphology, NME expression, and ameloblast polarity suggest that IRF6 may have roles in regulating epithelial polarity in tooth tissues. These results identified a critical and non-redundant role for IRF6 in crown and root formation, suggesting diversity of *IRF6* function in epithelial-derived tissues. Further studies investigating the expression of other proteins associated with enamel disorders, e.g. ameloblastin, enamelin, and matrix metalloproteinase, are needed to help determine the cause of the observed enamel abnormalities.

FIGURES AND TABLES

A

Pitx2$^{+/+}$; *Irf6*$^{fl/+}$ (Control)

B

Pitx2$^{Cre/+}$; *Irf6*$^{fl/fl}$ *(cKO)*

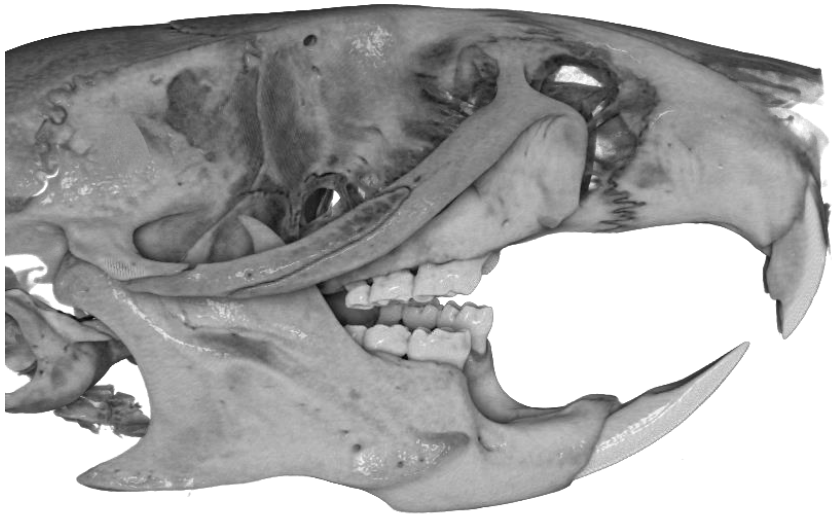

Figure 4.1: *Irf6-cKO* mice survived past birth without any apparent disruptions in mortality. 3D reconstructed skulls from micro-CT scans of six month old control **(A)** and *Irf6-cKO* samples **(B)**. No obvious skeletal differences were detected between controls and *Irf6-cKO* samples.

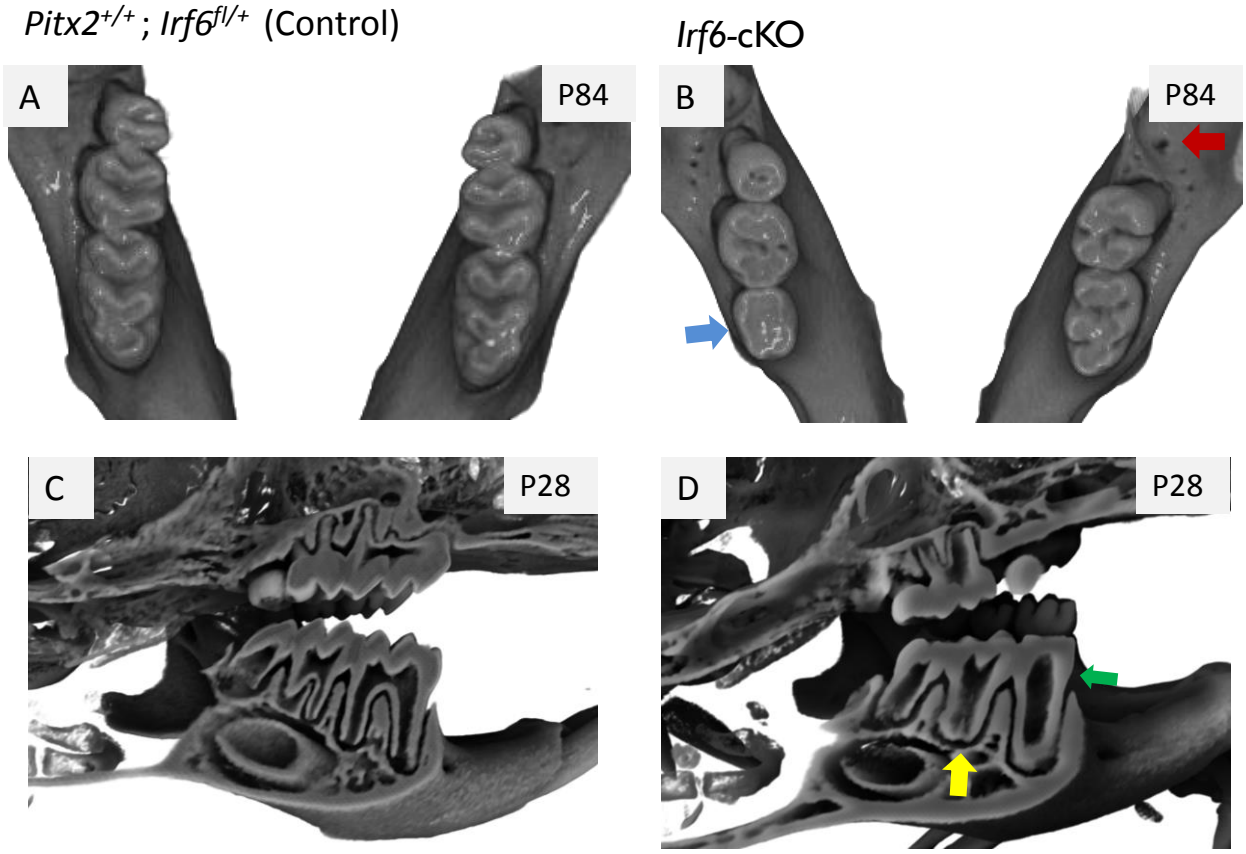

Figure 4.2: Loss of *Irf6* causes defects in crown and root development. (A, B) 3D reconstructions from micro-CT scans showing occurrence of microdontia and loss of normal cusp patterning (blue arrow) as well as hypodontia in P84 *Irf6*-cKO sample **(B)** compared to control sample **(A)**. **(C, D)** Occurrence of microdontia and single peg-shaped root (green arrow) in mandibular first molar and taurodontism in P28 *Irf6*-cKO sample **(D)** compared to control sample **(C)**. Note rapid attrition in *Irf6*-cKO samples **(B, D)**. Other controls (*Pitx2*$^{Cre/+}$*; Irf6*$^{fl/+}$, *Pitx2*$^{+/+}$*; Irf6*$^{fl/fl}$ genotypes) did not exhibit these alterations in crown and root morphology.

	Controls			*Irf6*-cKO
	$Pitx2^{+/+}; Irf6^{fl/+}$	$Pitx2^{Cre/+}; Irf6^{fl/+}$	$Pitx2^{+/+}; Irf6^{fl/fl}$	$Pitx2^{Cre/+}; Irf6^{fl/fl}$
	N=22	N=15	N=19	N=20
Peg shaped molars	0%	0%	0%	25%
Hypodontia	0%	0%	0%	10%
Taurodontism	0%	0%	0%	100%

Table 4.1: Occurrence of crown and root abnormalities observed in control and *Irf6-cKO* samples.

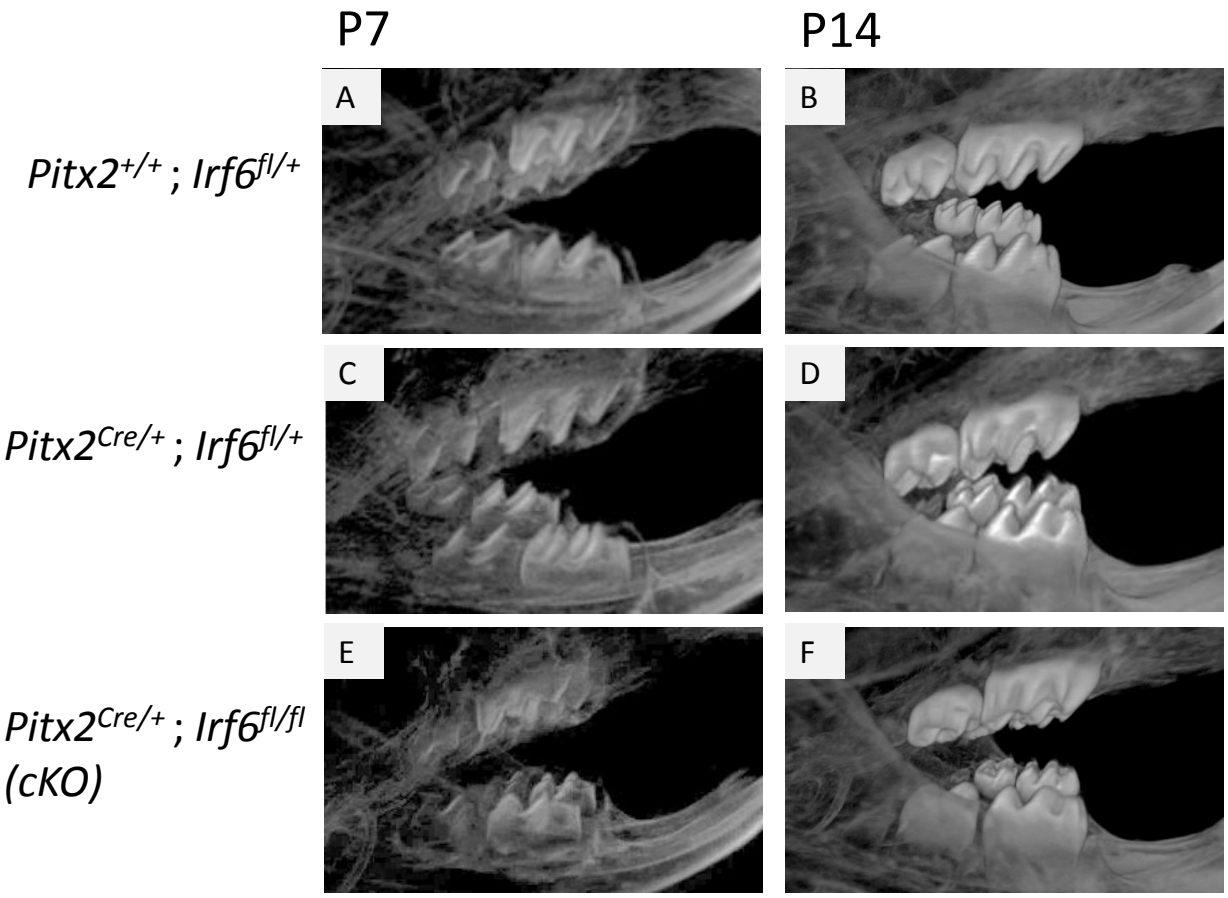

Figure 4.3: Altered crown morphology seen prior to tooth eruption (P7 and P14 samples). Note shallower cusps in *Irf6-cKO* samples (E, F) compared to controls (A, B, C, D).

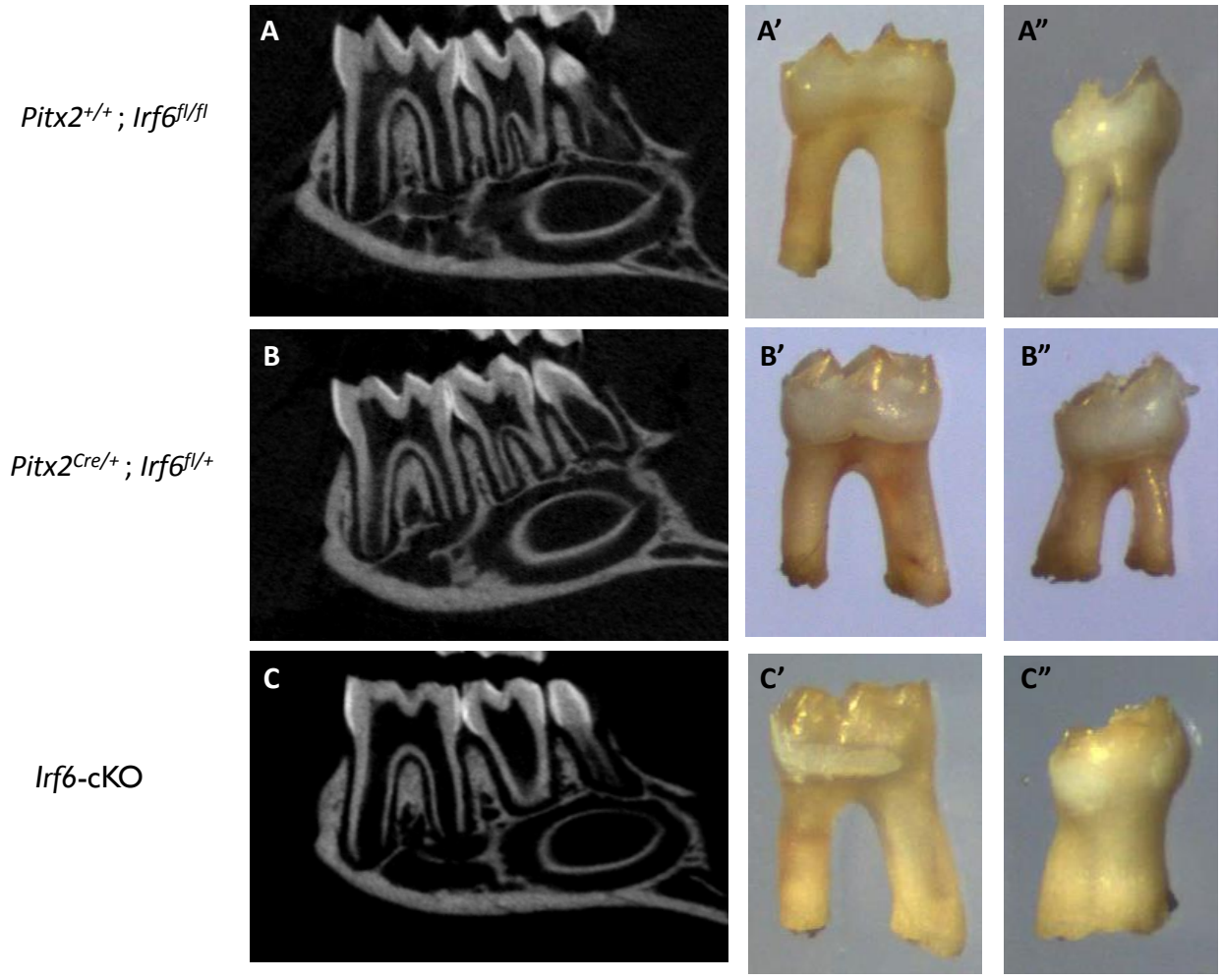

Figure 4.4: Comparison of P28 *Irf6 -cKO* pulp chambers and roots with littermate controls. Taurodontism of mandibular second molars seen in microCT images **(C)** and evident when teeth are removed from the alveolar bone **(C" vs A" and B")**. Mandibular first molars are provided as a comparison **(A', B', C')**.

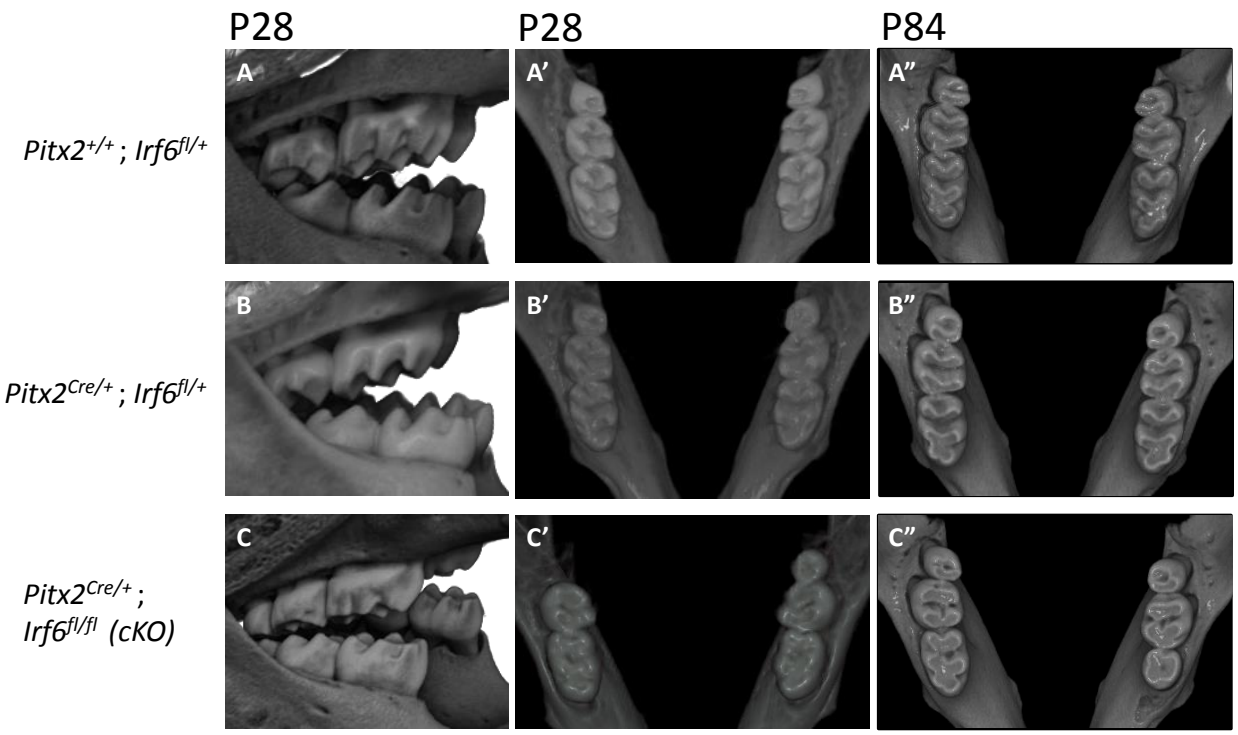

Figure 4.5: Increased enamel attrition observed in *Irf6-cKO* teeth. Following tooth eruption, in P28 and P84 samples, increased enamel wear was observed in *Irf6-cKO* **(C, C', C")** compared to controls **(A, A', A", B, B', B").** Note sheared cusps in *Irf6-cKO* samples (C) and rapid wear from P28 to P84 (C' versus C").

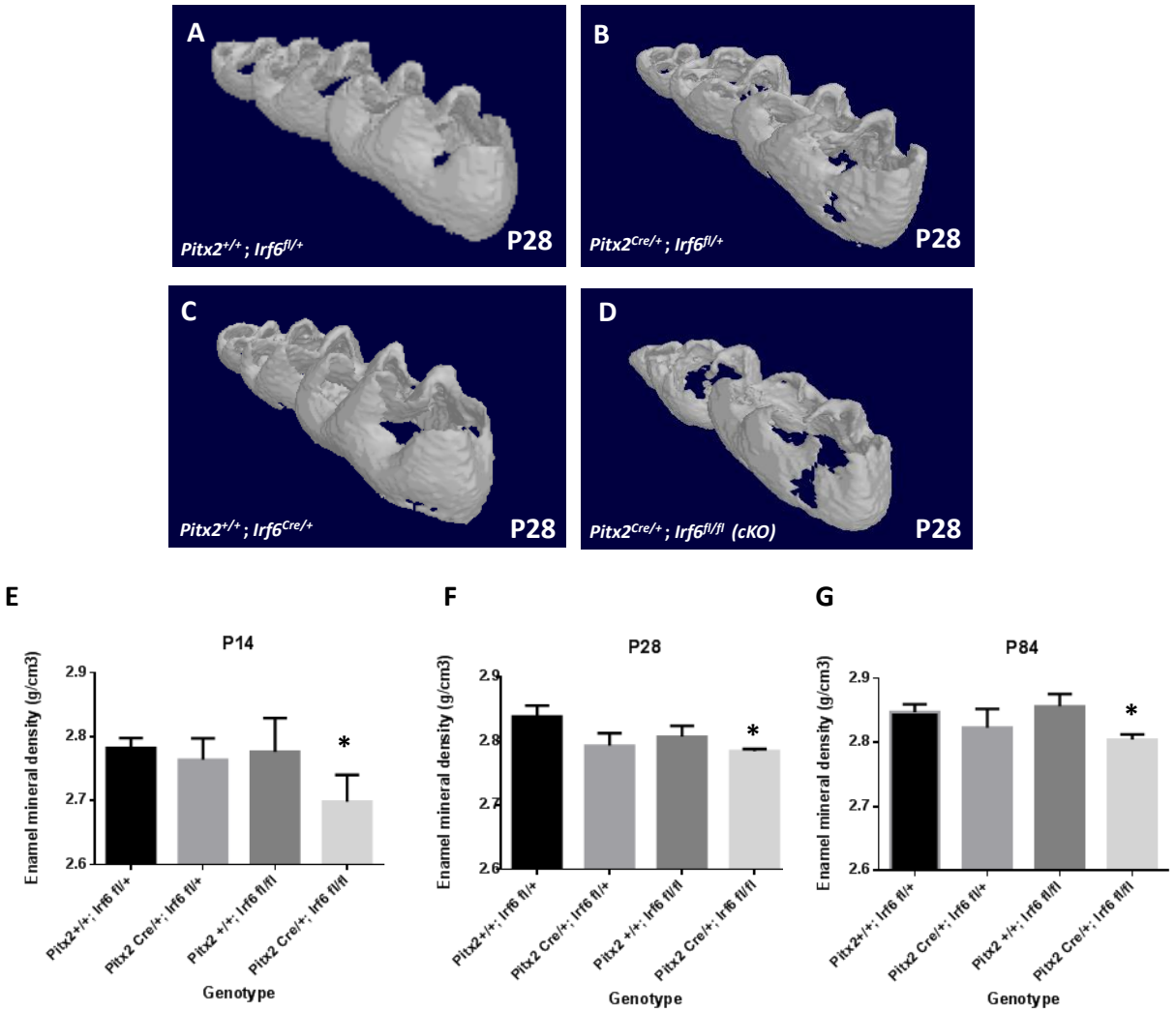

Figure 4.6: Hypomineralized enamel observed in *Irf6-cKO* samples. (A, B, C, D). Threshold for mineralized enamel set for different ages, and lower amounts of mineralized enamel observed in *Irf6-cKO*. P28 samples are shown as examples of enamel thresholding. **(E, F, G)** Among P14, P28, and P84 samples, *Irf6-cKO* enamel had a statistically significant lower enamel mineral density compared to $Pitx2^{+/+}$; $Irf6^{fl/+}$ samples (indicated by asterisks). Statistical significance set at $p<0.05$. For all groups, $3 \leq n \leq 6$.

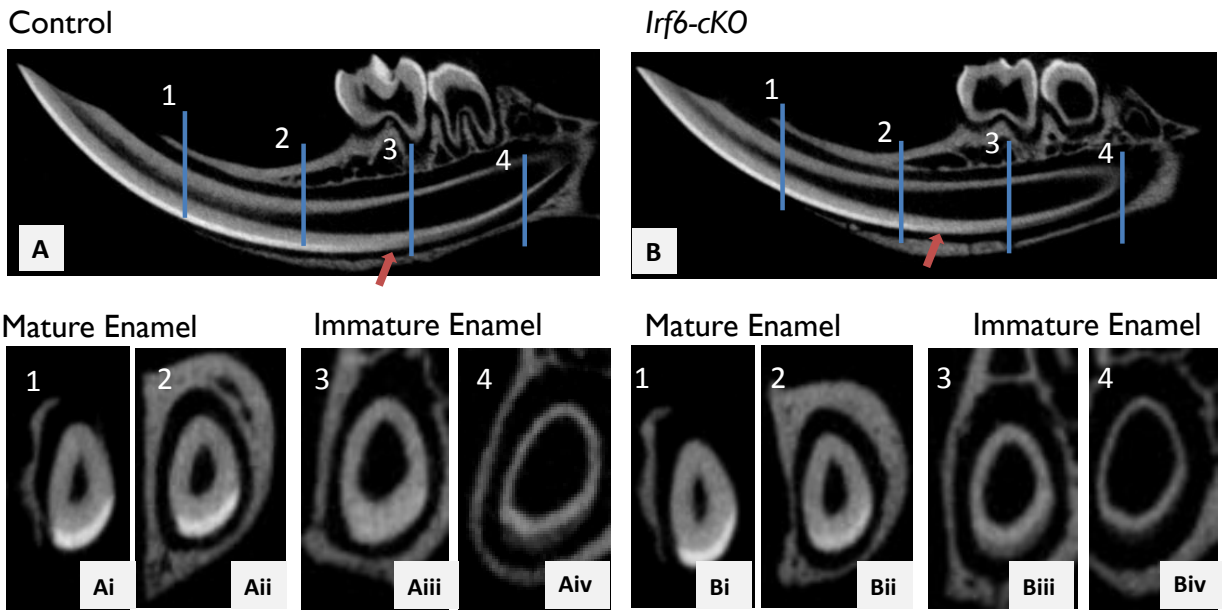

Figure 4.7: Micro-CT analysis of P28 *Irf6*-cKO incisors compared to controls. (A, B) Representative cross sections of the incisors are shown at four landmarks: alveolar crest (Ai, Bi), mental foramen (Aii, Bii), mesial root of mandibular first molar (Aiii, Biii), and mesial root of mandibular second root (Aiv, Biv). Transition between mature and immature enamel located more apically in control versus *Irf6*-cKO (red arrows). Enamel density differences in *Irf6*-cKO samples were visible at molar landmarks with the enamel layer appearing thinner and less bright compared to controls. Controls were either *Pitx2*$^{+/+}$*; Irf6*$^{fl/+,}$ *, Pitx2*$^{Cre/+}$*; Irf6*$^{fl/+}$*, or Pitx2*$^{+/+}$*; Irf6*$^{fl/fl}$ genotypes, and *Irf6*-cKO refers to *Pitx2*$^{Cre/+}$*; Irf6*$^{fl/fl}$ genotype.

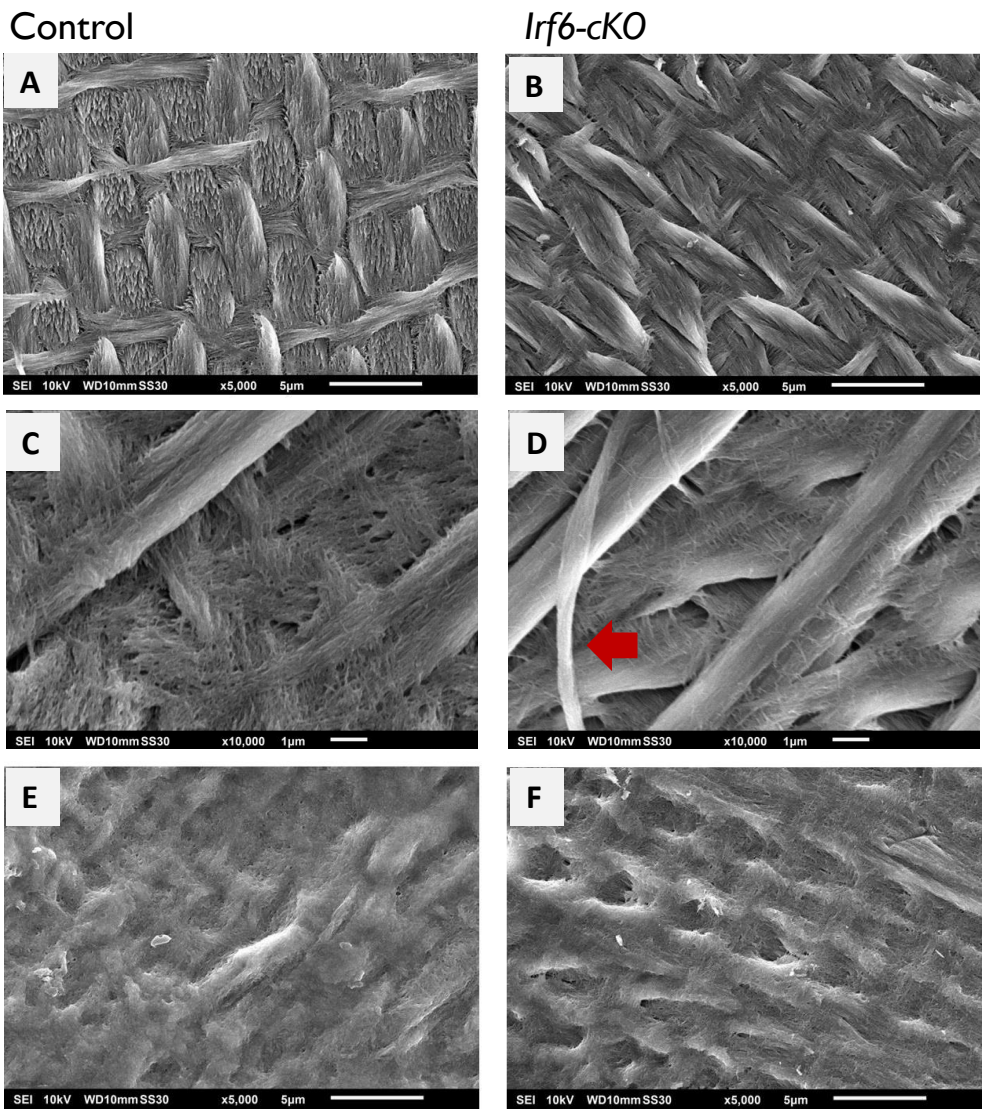

Figure 4.8: SEM analysis of P28 *Irf6*-cKO incisor enamel compared to controls. SEM images of control mature enamel (A, C) and immature enamel (E) were compared with images of *Irf6-cKO* mature enamel (B, D) and immature enamel (F). *Irf6-cKO* mature enamel (B) exhibited comparable prismatic structure compared to controls (A). At a different orientation, shearing of enamel rods observed in *Irf6-cKO* samples (D, red arrow), which was not observed in controls. Immature enamel did not exhibit any appreciable differences between *Irf6-cKO* and control samples.

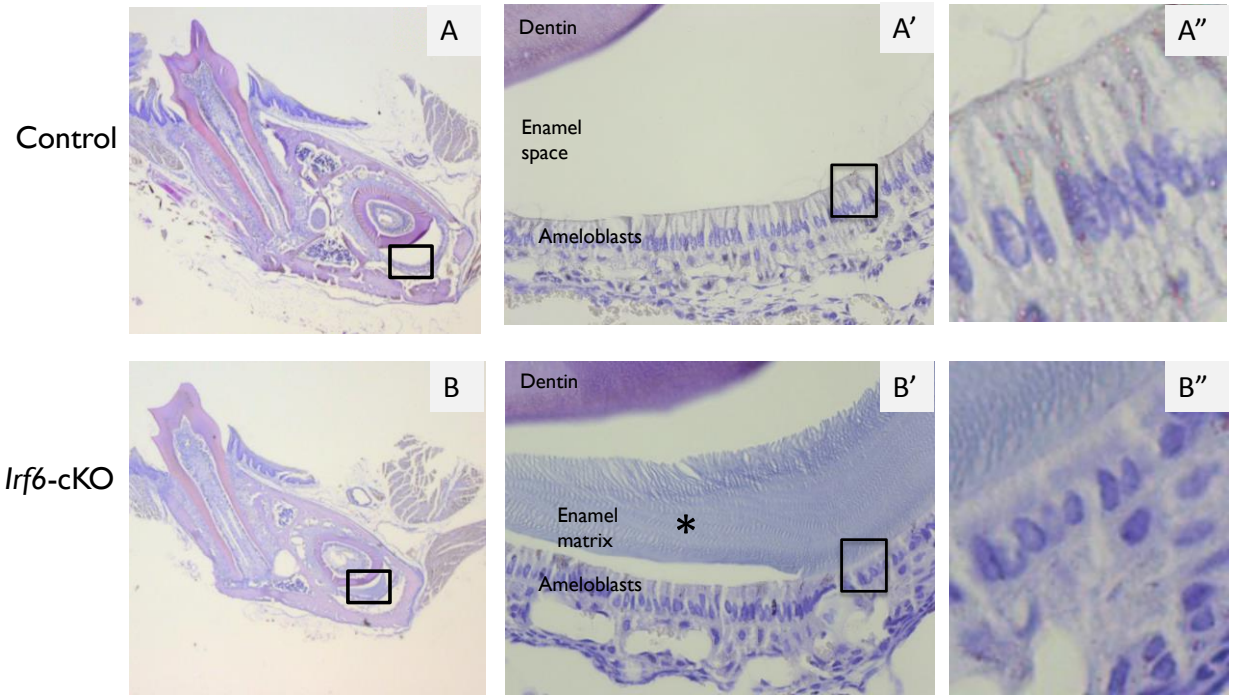

Figure 4.9: Hematoxylin and eosin staining performed on decalcified P28 *Irf6*-cKO and control samples. Enamel space is visibly thinner in *Irf6*-cKO samples compared to controls (B versus A), and immature enamel matrix present in *Irf6*-cKO incisors and absent in comparable control sections (B', asterisk). Ameloblasts of *Irf6*-cKO samples appear irregular and less polarized compared to control samples. Note disturbances in ameloblast morphology and organization in *Irf6*-cKO ameloblasts compared to control ameloblasts (B" versus A").

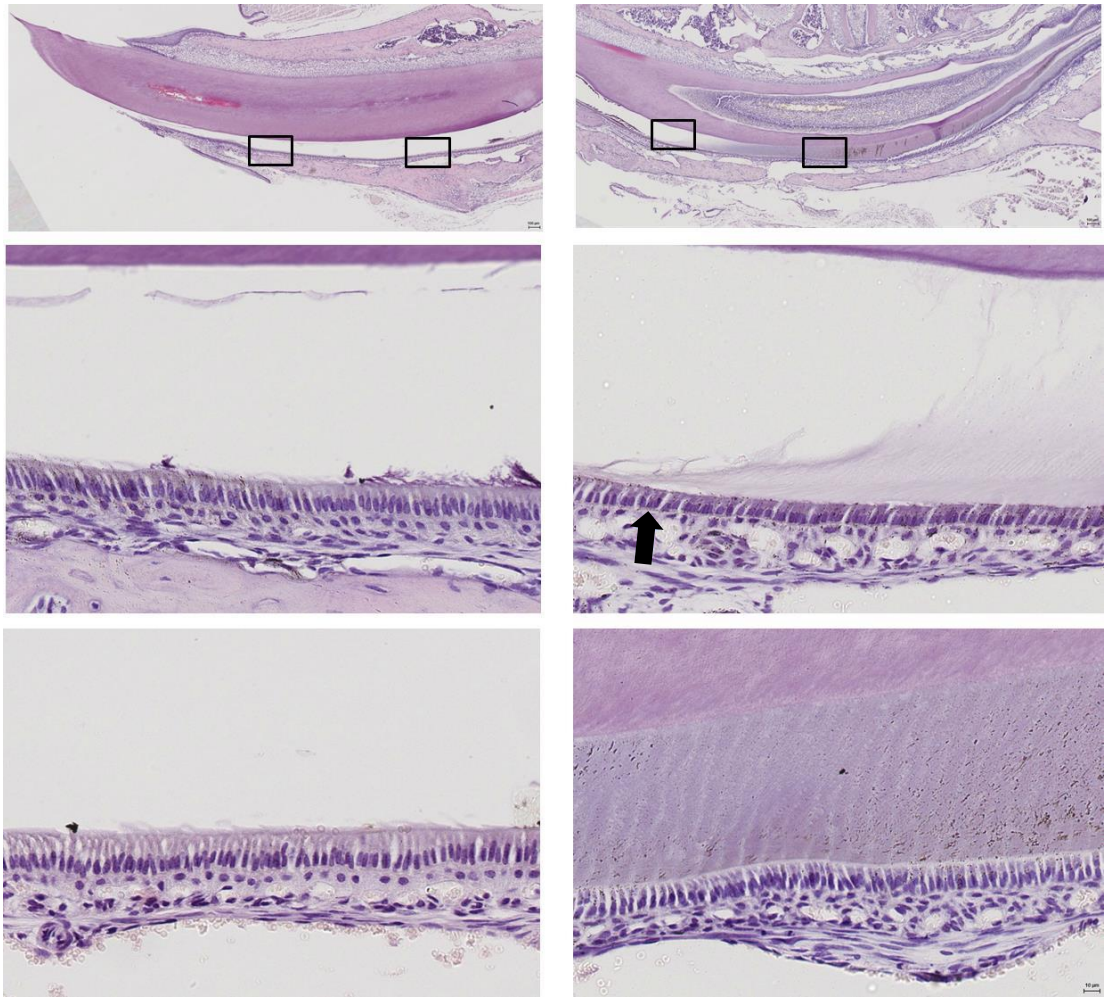

Figure 4.10: Hematoxylin and eosin staining performed on decalcified P28 *Irf6*-cKO and control samples. Sagittal sections of P28 incisors were obtained to examine ameloblasts in different stages. *Irf6-cKO* incisor showed transition between immature enamel and mature enamel (B', arrow). In these regions, *Irf6-cKO* ameloblasts appeared shortened and flattened compared to controls. In regions located more apically and adjacent to unmineralized enamel matrix (B"), *Irf6-cKO* secretory stage ameloblasts were still shorter than control ameloblasts that were closer to maturation stage (B" versus A").

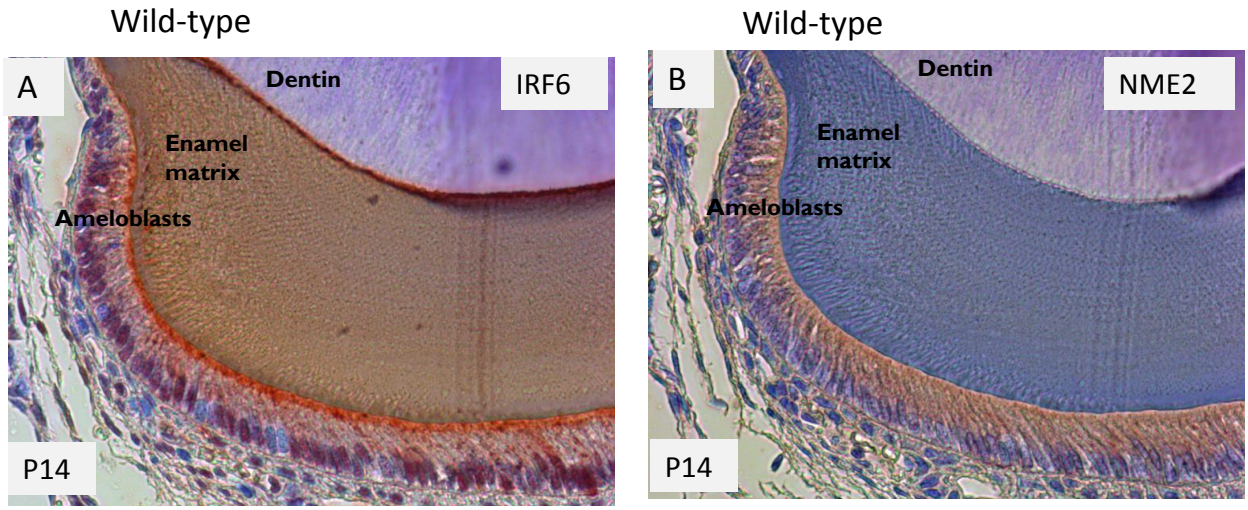

Figure 4.11: Immunolabeling of IRF6 and NME in P14 wild type developing teeth. (A) IRF6 is found in nuclei, cytoplasm, and at the distal end (adjacent to the developing enamel matrix) of ameloblasts. **(B)** NME2 is found in cytoplasm of ameloblasts.

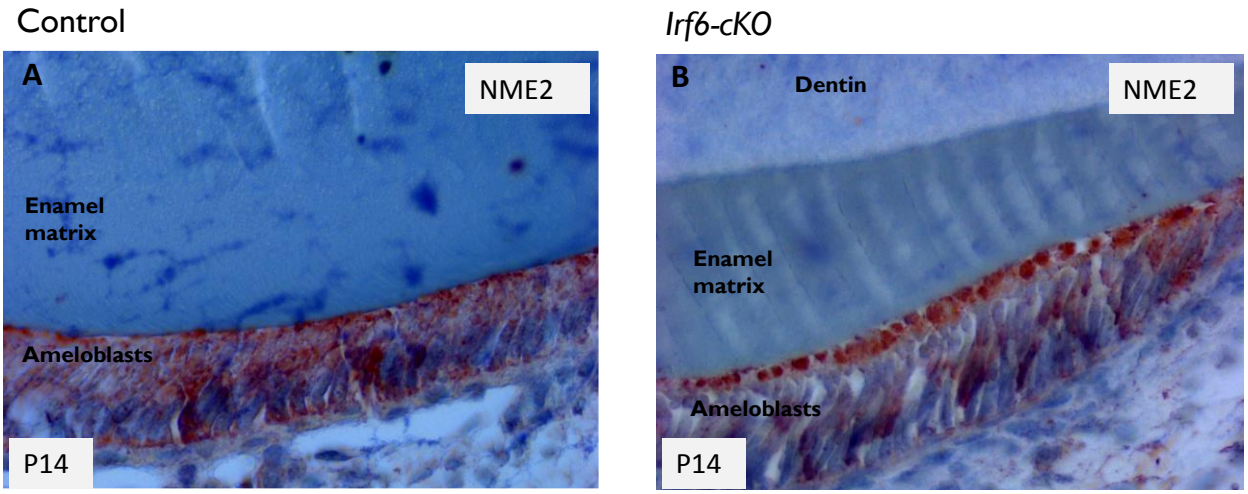

Figure 4.12: Loss of *Irf6* alters NME2 expression. P14 *Irf6-cKO* samples exhibited overall lower amounts of NME2 in ameloblasts, and NME2 appeared to be more concentrated adjacent to the developing enamel matrix in *Irf6-cKO* samples.

Chapter 5: Towards understanding the role of IRF6 in tooth development

INTRODUCTION

Irf6 is expressed in early oral epithelium and has roles in epithelial tooth invagination, and as demonstrated in the previous chapter, loss of *Irf6* results in disruptions to epithelial-derived tooth tissues and cells, including enamel and ameloblasts. Our *Irf6* conditional knockout (*Irf6-cKO*) generated with a *Pitx2*-Cre promoter resulted in disturbances to ameloblast polarity and NME expression. These findings were consistent with our hypothesis that the IRF6:NME complex has a role in epithelial polarity. Because disruptions in p120 catenin and Rac1 lead to loss of ameloblast polarity and severe enamel defects, a similar, more muted effect may be present when *Irf6* is conditionally ablated in oral epithelium (149, 150). However, the phenotype exhibited by the p120 catenin and Rac1 mutants differed from our *Irf6-cKO* enamel in several aspects. For example, the *Irf6-cKO* enamel exhibited hypomineralization, but SEM of mature enamel revealed formation of an organized prismatic structure, which was not present in the p120 catenin and Rac1 mutants (149, 150). Additionally, loss of *Irf6* results in alterations in crown and root morphology, which were also not reported in p120 catenin and Rac1 mutants. Thus, additional studies on enamel development in *Irf6-cKO* mice are required in order to understand *Irf6* function during tooth development.

During amelogenesis, or enamel development, ameloblasts, which form enamel and are derived from the oral epithelium, undergo several morphological and functional stages:

presecretory, secretory, transition, and maturation. In the presecretory stage, following odontoblast differentiation and predentin deposition, ameloblasts differentiate and begin enamel deposition. As ameloblasts progress toward the secretory stage, they elongate into tall, columnar cells, develop Tomes' processes, and secrete enamel matrix proteins, including amelogenin (AMEL), ameloblastin (AMBN), enamelin (ENAM), and matrix metalloproteinase (MMP20). During this stage, the ameloblasts move in a sliding pattern relative to one another, altering the strength of adherens junctions between ameloblasts. At the end of the secretory stage, the Tomes' process is lost as the enamel reaches its full thickness. In the transition stage, the ameloblasts lose their columnar shape and begin the transition between ruffle and smooth-ended cells. In the maturation stage, the ameloblasts secrete enamel proteinases to remove enamel matrix proteins as well as transport ions to enhance mineral accretion. As the protein matrix is removed, the enamel crystals grow wider and larger as mineral is deposited. If the matrix proteins are not removed, mineral deposition is inhibited and can lead to enamel defects.

Amelogenin (*AMEL*), enamelin (*ENAM*), kallikrein-4 (*KLK4*), and matrix metalloproteinase (*MMP20*) are often implicated in amelogenesis imperfecta. Amelogenesis imperfecta (AI) refers to a collection of inherited enamel disorders, which are classified by stage of enamel formation affected. *AMEL* mutations cause a spectrum of enamel defects, which range from hypoplastic to hypocalcified forms. AI has four main categories: hypoplastic, hypocalcification, hypomaturation, and hypomaturation-

hypoplastic with taurodontism. Hypoplastic enamel refers to enamel that is thinner with normal mineralization, and it typically results from defects in the secretory stage. Clinically, hypoplastic enamel is radiographically distinguishable from dentin, appears translucent, and often features pitting and grooves. *ENAM* mutations have been found in hypoplastic AI cases, whereas *MMP20* and *KLK4* mutations tend to be associated with hypocalcified and hypomature enamel. Accordingly, hypocalcified enamel results from defects in enamel maturation. Hypocalcified enamel is of normal thickness, appears more radiolucent compared to dentin, has a chalky appearance, and wears rapidly. Hypomature enamel also results from defects in enamel maturation, and it is radiographically indistinguishable from dentin. Clinically, hypomature enamel has a mottled appearance and wears faster than normal enamel. Hypomaturation-hypoplastic enamel with taurodontism also includes taurodontic teeth, which feature enlarged, apically displaced pulp chambers, loss of cervical constriction, and apical displacement/loss of furcation. Other dental abnormalities associated with amelogenesis imperfecta include microdontia, root resorption, short roots, tooth agenesis, and aberrations in crown morphology. Thus, enamel matrix proteins may contribute to the tooth phenotype observed in *Irf6-cKO* mice.

In this chapter, we aimed to identify stages of tooth development affected by loss of *Irf6.* Bell stages of crown development were selected in order to examine the developing enamel matrix and secretory stage ameloblasts (postnatal days 4 and 7 in mice), and postnatal days 13 and 14 were selected for study of root development and

maturation stage ameloblasts. Gene and protein expression of enamel matrix proteins were evaluated in *Irf6-cKO* samples versus controls.

RESULTS

Loss of *Irf6* causes alterations in crown morphology and enamel defects

As discussed in Chapter 4, *Irf6-cKO* mice exhibited striking crown morphological disturbances. Mandibular first molars featured crown shapes of varying sizes and loss of cusp patterning (Figure 5.1). These ranged from a reduced crown shape retaining normal cusp patterning (Figure 5.1, black arrow) to complete loss of cusp patterning (Figure 5.1, red arrow). In all samples examined, disturbances in crown morphology of mandibular first molars were observed unilaterally, i.e. disturbances on one side were not mirrored on the contralateral side. Mandibular second molars exhibited subtle changes in cusp, ridge, and groove patterns; for example, deeper grooves were occasionally observed (Figure 5.1, blue arrow).

Irf6-cKO mice exhibited hypomineralized enamel, which was accompanied by increased enamel attrition. As shown in Chapter 4, *Irf6-cKO* enamel exhibited reduced enamel mineral density, although mature enamel was radiographically distinguishable from dentin (Figure 5.2, D and D'). Enamel defects were detected in the continuously erupting mandibular incisor. In ages P24 to P84, cross sections were obtained from regions apical to the mesial root of the mandibular first molar. The murine incisor is

continuously erupting, thus these sections represent different stages of enamel mineralization, and delays in enamel maturation were observed. Enamel was thinner and more radiolucent when compared to controls, particularly around maturation stages, i.e. P28 (enamel outlined in Figure 5.2, C' versus C). In comparison, the mandibular first molar, in which enamel development was complete, differences between control and *Irf6-cKO* enamel were more subtle (D' versus D).

Comparison of Irf6-cKO ameloblasts with controls

In mice, the mandibular first molar is in the bell stage during P4 and P7 ages. Thus, these ages were selected for examination of the ameloblasts during enamel matrix deposition. In P4, the ameloblasts have already differentiated and are in the secretory stage. They appear as tall, columnar cells with the nuclei oriented away from the developing enamel matrix. In control and *Irf6-cKO* samples, the secretory ameloblasts exhibited easily observable polarity, and no apparent differences were detected between *Irf6-cKO* and controls (Figure 5.3).

In P7, the ameloblasts are actively secreting enamel matrix, and the enamel layer is visibly thicker compared to P4. Compared to ameloblasts that are located near the future cementoenamel junction (CEJ) of the tooth (Figure 5.4, B', white arrow), ameloblasts that differentiated earlier and are located more occlusally exhibited mild disturbances in organization and polarity (Figure 5.4, B', black arrow). P7 *Irf6-cKO*

incisors also exhibited a delay in enamel formation as observed by the thin dentin layer (asterisks) and absence of the enamel layer (Figure 5.4, B", asterisks)

In P14, enamel matrix deposition is complete in mandibular first molars, and in demineralized sections, the enamel is represented by an empty space. Ameloblasts are still present, and they have reached the maturation stage. In the control sample, the ameloblasts have shortened but remain polarized (Figure 5.5, A'). In contrast, the *Irf6-cKO* ameloblasts appear less organized, and increased spacing was observed in between ameloblasts (Figure 5.5, B'). In corresponding P14 incisor sections, enamel formation was delayed in *Irf6-cKO* samples (Figure 5.5). Consistent with earlier microCT observations, the enamel layer was thinner, and the ameloblasts appear to be in the secretory stage, whereas in the control sample, the ameloblasts had already shortened and were approaching maturation stages (Figure 5.5, B" versus A").

Loss of *Irf6* causes root alterations

In addition to crown and enamel defects, root alterations were noted. Histological sections of P14 HERS revealed that the *Irf6-cKO* HERS appeared shorter compared to controls (Figure 5.6 B' versus A'). As discussed in Chapter 4, taurodontic mandibular second molars were noted. Coronal microCT sections from cervical and midroot regions of the mandibular molar roots were obtained at P28 and P84. At the cervical region (occlusal of the bifurcation between mesial and distal roots), root morphology was comparable between all genotypes. In the midroot sections (apical to the bifurcation),

which showed sections through the mesial and distal roots, *Irf6-cKO* mandibular second molars lacked separation between mesial and distal roots. Instead, they exhibited C-shaped roots (Figure 5.7, D' and Figure 5.9, D', red arrow). *Irf6-cKO* mandibular first molars, which exhibited separation between mesial and distal roots, also exhibited a statistically significant reduction in separation between mesial and distal roots (Figure 5.8). A mild decrease in separation between mesial and distal roots, although not statistically significant, was observed in *Pitx2*$^{Cre/+}$*; Irf6*$^{fl/fl}$ samples. When *Irf6-ckO* mandibular first molars exhibited a single root, a single canal was observed (Figure 5.9, D, blue arrow), showing complete loss of separate mesial and distal roots and canals.

Knockdown of IRF6 in ameloblast-like cells

To test the effects of *Irf6* knockdown in an *in vitro* model, siRNAs specific for IRF6 were used on LS8 cells, an ameloblast-like cell line (Figure 5.9). IRF6 expression was first verified in LS8 cells using qpCR. Although low, IRF6 levels were detectable. Using siRNAs for IRF6 (Life Technologies; Carlsbad, California), IRF6 was silenced in LS8 cells. Reverse transcriptase (RT) and qPCR were performed to evaluate percent of IRF6 knockdown. Cells that exhibited >60% knockdown (compared to the scrambled negative control and cells that received only lipofectamine) of IRF6 were considered adequately silenced. Expression of enamel matrix proteins (amelogenin, ameloblastin, enamelin, kallikrein-4, and matrix metalloproteinase-20) was evaluated using qPCR. No difference was detected in amelogenin, (*Amel*) ameloblastin (*Ambn*), enamelin (*Enam*),

kallikrein-4 (*Klk4*), and matrix metalloproteinase-20 (*Mmp20*). Expression of these enamel matrix proteins was low, suggesting that the LS8 cells used in this study represented a largely undifferentiated state. This suggests that in undifferentiated cells, because of its low expression and its lack of effect on enamel matrix proteins, IRF6 likely has a minimal role.

IRF6 and the expression of genes involved in enamel and dentin formation

To determine the effects of IRF6 on expression of genes involved in enamel and dentin formation, *Irf6* molars were harvested at P4 and P13. The population of P4 ameloblasts were believed to be largely in the secretory stage, whereas ameloblasts in the P13 stage were believed to primarily represent maturation stages. To represent ameloblasts in all stages, enamel organs of P13 incisors were harvested. RT-PCR and qPCR were performed with RNA harvested from P4 and P13 samples. To verify that *Irf6* expression was sufficiently reduced in *Irf6-cKO* samples, *Irf6* mRNA expression was checked using *Gapdh* as a reference gene. *Irf6* was statistically significantly reduced in P4 and P13 samples (Figure 5.10A; Figure 5.11A; Figure 5.12A, $p<0.05$ for molars and $p<0.10$ for enamel organs). Gene expression of enamel matrix proteins (*Amel, Enam, Ambn, Mmp20, Klk4*) was evaluated using qPCR. P4 molars exhibited an enamel matrix protein expression profile characteristic of secretory stage ameloblasts: high levels of *Amel* and *Enam* as well as higher levels of *Mmp20* compared to *Klk4*. Of these enamel matrix proteins, loss of *Irf6* did not result in a demonstrable effect (Figure 5.9A). In P4 samples, genes involved in dentin development were also evaluated (tissue non-specific alkaline

phosphatase, dentin matrix protein 1, and osterix). Tissue non-specific alkaline phosphatase (*Tnap*) and dentin matrix protein 1 (*Dmp1*) did not exhibit an effect in response to *Irf6* loss. Osterix (*Osx*) exhibited a statistically significant decrease in response to loss of *Irf6*. Subsequently, *Wnt3a*, *Wnt10b,* and transforming growth factor-beta (*Tgf-β*) were evaluated, and *Wnt10b* also exhibited a statistically significant decrease (Figure 5.10B). ($p<0.05$)

In comparison to P4 molars, P13 molars exhibited an enamel matrix gene expression profile consistent with ameloblasts in maturation stages: *Amel*, *Enam*, and *Ambn* gene expression levels were considerably lower compared to P4 levels, and *Klk4* expression was approximately five fold higher compared to *Mmp20* (Figure 5.10A). Similar to P4 molars, none of the enamel matrix proteins exhibited an appreciable gene expression effect in response to *Irf6* loss. Although *Wnt10b* and *Osx* levels were comparable between P4 and P13 molars, *Irf6* loss did not result in downregulation of *Wnt10b* or *Osx* in P13 molars (Figure 5.11B).

P13 enamel organs exhibited a gene expression profile characteristic of a mixed population of ameloblasts (Figure 5.12A). High levels of *Amel* (characteristic of secretory stage ameloblasts) and high levels of *Klk4* (characteristic of maturation stage ameloblasts) were detected. Irf6 loss did not exhibit a statistically significant effect on the expression of enamel matrix proteins, although *Klk4* appears to exhibit a slight

decrease in Irf6-cKO samples. No difference was detected in *Wnt10b* and *Osx* expression between *Irf6-cKO* and control enamel organs (Figure 5.12B).

Loss of IRF6 causes alterations in enamel matrix proteins

Amelogenin (AMEL) was detected in secretory stage ameloblasts adjacent to the developing enamel matrix of incisors and molars in *Irf6-cKO* and control samples. AMEL expression was comparable between *Irf6-cKO* and control samples at P4 (Figure 5.13). In *Irf6-cKO* P14 incisors, AMEL was detected at higher levels in ameloblasts compared to controls. In *Irf6-cKO* P28 incisors, AMEL was detected in the ameloblasts as well as in the immature enamel matrix, which in corresponding control sections where the enamel was fully mineralized, AMEL was not detected.

KLK4 was detected in maturation stage ameloblasts adjacent to the immature enamel matrix in P14 ameloblasts. In comparable *Irf6-cKO* sections, KLK4 was expressed at much lower levels compared to controls (Figure 5.14)

DISCUSSION

As described in the previous chapter and this chapter, loss of *Irf6* results in disturbances in crown and root morphology, enamel hypomineralization, and ameloblast polarity. Here, we attempt to further define the role of *Irf6* in tooth development.

Irf6 mandibular molars exhibited a range of crown variations, including complete loss of normal cusp patterning. During tooth development, cusp patterning begins with the emergence of the secondary enamel knots (207-209). Similar to the primary enamel knot, secondary enamel knots are epithelium derived and function as signaling centers. Components of the *fibroblast growth factor (Fgf), bone morphogenetic protein (Bmp), Ectodysplasin A (Eda)*, *Sonic hedgehog (Shh)*, and *Wnt* pathways are expressed in enamel knots. Whereas the primary enamel knot develops at the top of the tooth bud in the late bud stage and is found in all teeth, secondary enamel knots are formed in the bell stage and are only found in teeth with multiple cusps (premolars and molars). Notably, *Irf6* P4 molars exhibited decreased *Wnt10b* mRNA expression. *Wnt10b* is expressed in dental epithelium and enamel knots, and disrupting Wnt/beta-catenin signaling during the bell stage leads to flattened, smaller and irregular cusps (210-212). Additionally, in the enamel knot, *Wnt* signaling also activates *Eda,* which also has roles in regulation of tooth shape, size, and number. The *Tabby* mouse, a murine homolog for patients with anhidrotic ectodermal dysplasia and features an *Eda* mutation, exhibits smaller teeth and reduced molar cusps (213, 214). Thus, interference with signaling in the enamel knot may result in downstream effects on multiple pathways, which may lead to the aberrant cusp morphology observed in *Irf6-cKO* mice.

The *Irf6* influence on *Wnt* transcription may also be manifested in the abnormal root morphology observed in *Irf6-cKO* samples. Disruptions in *Wnt/β-catenin* signaling can lead to tooth root defects, including shorter or absence of tooth roots (210).

Additionally, *Wnt10b* has a similar expression pattern to *Wnt10a* in oral epithelium and enamel knots, and *Wnt10a-null* mice exhibit blunted cusps as well as taurodontic mandibular molars (212, 215) . Root defects are often accompanied by defects in Hertwig's Epithelial Root Sheath (HERS), which is formed from the fusion of the inner and outer enamel epithelium (45). In the bell stage, *Wnt10b* has been detected in the outer enamel epithelium, suggesting it may contribute to the formation of HERS (216). During root development, cells comprising the HERS divide as HERS simultaneously migrates apically. Furcation development is believed to be dependent on HERS folding, and taurodontism is believed to be caused by a failure of or aberrant folding of the HERS (45). Comparison of *Irf6-cKO* and control HERS suggested that although the *Irf6-cKO* HERS appears intact, it may not have elongated properly (Figure 5.6). Consequently, furcation development is disrupted, and separation of the mesial and distal roots is lost.

Similar to crown development, root development is also dependent on epithelial-mesenchymal interactions. The HERS is derived from the enamel epithelium, and following its development, is believed to induce odontoblast differentiation in the root. Studies of dentin markers such as *Osterix* (*Osx*) indicate that odontoblast differentiation is spatially and temporally regulated (217). Conditional knockouts for *Osx* using either the *Collagen Ia* or *Osteocalcin* promoter revealed root dentin phenotypes, but not crown dentin phenotypes (217). *Osx* conditional knockouts exhibited reduced separation between mesial and distal roots, which was also exhibited in our *Irf6-cKO* mice. Additionally, P4 *Irf6-cKO* molars exhibited reduced *Osx* expression, suggesting

that *Osx* is a contributing factor to the altered root morphology observed in *Irf6-cKO* mice. *Osx* has not been detected in the HERS, nor has it been detected in enamel epithelium, although WNT has been detected in the HERS (218). *Osx* regulates *Wnt* signaling; thus, there is a possibility that *Irf6* effects on *Osx* expression occurs via epithelial-mesenchymal crosstalk (219).

In examining stages of enamel development, *If6-cKO* mice exhibited a delay in enamel maturation, and the ultimate enamel mineral density was lower compared to controls. In the earlier stages of ameloblast development, i.e. presecretory and early secretory, *Irf6-cKO* ameloblasts were comparable to controls. However, as the ameloblasts neared the maturation stage, they appeared more disorganized and shorter compared to controls. This suggests that *Irf6* has a role in later stages of enamel development. Furthermore, in an undifferentiated ameloblast-like cell line (LS8 cells), *Irf6* was detected at very low levels and did not cause any changes in mRNA expression of enamel matrix proteins. In P4 and P13 molars, *Irf6* ablation did not cause any statistically significant changes in the enamel matrix proteins, although at the protein level, changes in AMEL and KLK4 were detected. For example, *Irf6-cKO* P14 and P28 samples exhibited elevated AMEL levels in ameloblasts compared to controls. Furthermore, in P14 samples, this was accompanied by a decrease in KLK4 expression. Mutations in *AMEL* and *KLK4* have been found in individuals with amelogenesis imperfecta, suggesting that the enamel defects may be caused by abnormal expression of enamel matrix proteins (220). Individuals with *AMEL* mutations exhibit a range of

enamel phenotypes, which range from hypoplastic to hypomature or severely hypocalcified forms. *KLK4* mutations are frequently associated with defects in enamel maturation, which is consistent with the enamel phenotype reported in *Irf6-cKO* mice. KLK4 cleaves AMEL at several different sites during the late secretory and maturation stages of enamel development (129, 221, 222). *Klk4-null* secretory stage enamel is indistinguishable from wild-type enamel, whereas in later stages, residual enamel proteins were detected in *Klk4-null* samples. After the enamel has reached its final thickness (by the end of the secretory stage), removal of enamel proteins is critical toward mineral deposition. Residual proteins inhibit proper enamel crystallite growth and mineralization; improper cleavage of enamel proteins leads to smaller enamel crystallites and increased spacing between crystallites (132). Consequently, the final enamel structure is compromised, which may lead to the hypomineralized phenotype observed in the *Irf6-cKO* mice.

We have shown that loss of *Irf6* causes defects in crown, root, and enamel formation. This suggests that *Irf6* may have several roles in the tooth development and maturation. Via interactions with components of the *Wnt/β-catenin* pathway, *Irf6* may participate in cusp patterning or HERS folding. Furthermore, *Irf6* appears to have roles in enamel maturation; by influencing the expression of enamel matrix proteins such as AMEL and KLK4, *Irf6* can affect final enamel structure. These findings contribute toward the understanding of the role of *Irf6* in tooth development as well as tooth abnormalities associated with epithelial disorders.

FIGURES

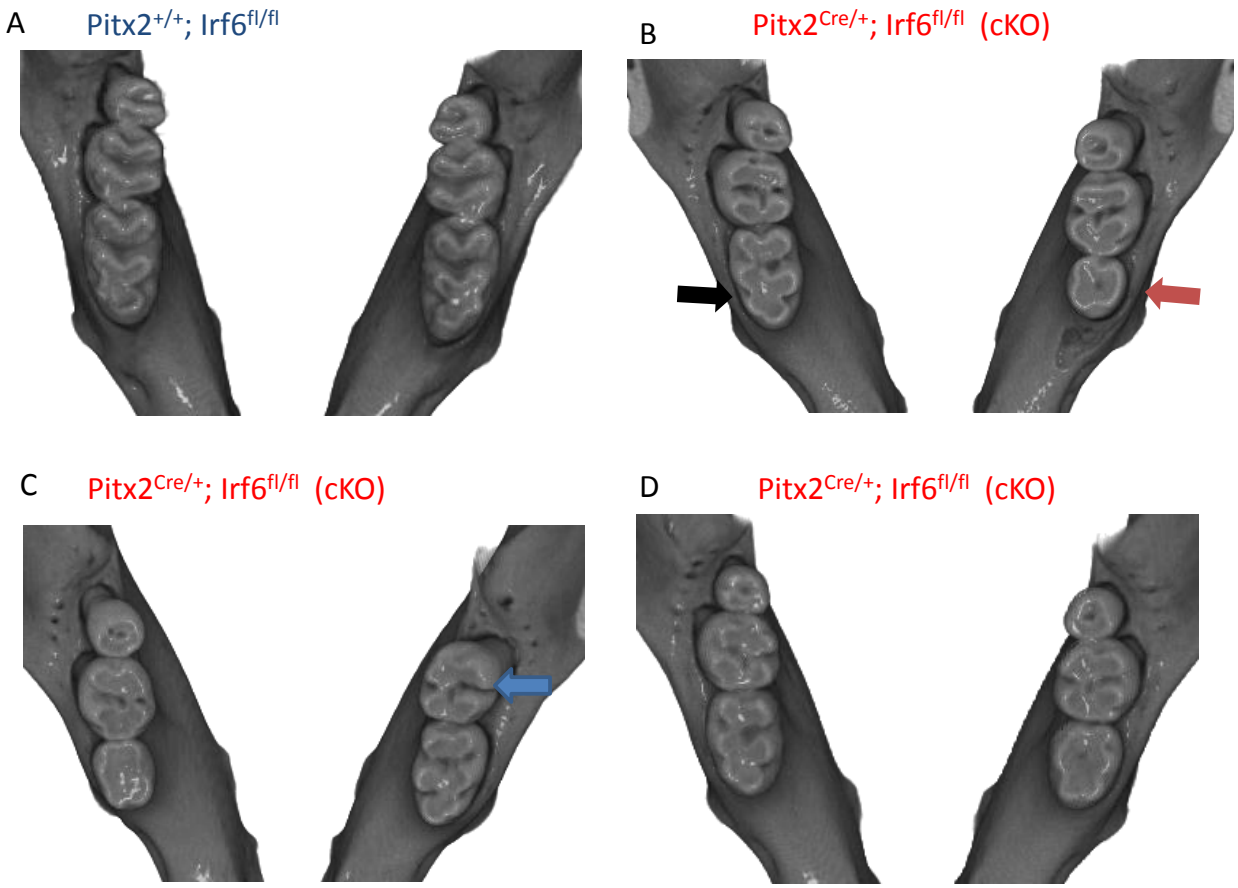

Figure 5.1: Variations in crown morphology observed in P84 *Irf6-cKO* samples.

Compared to the controls (A), *Irf6-cKO* (B, C, D) mice exhibited a variety of crown shapes, including reduced crown size with normal cusp patterning (B, black arrow), complete loss of cusp patterning (B, red arrow). Mandibular second molars also exhibited altered crown patterning, including deeper grooves (blue arrow)

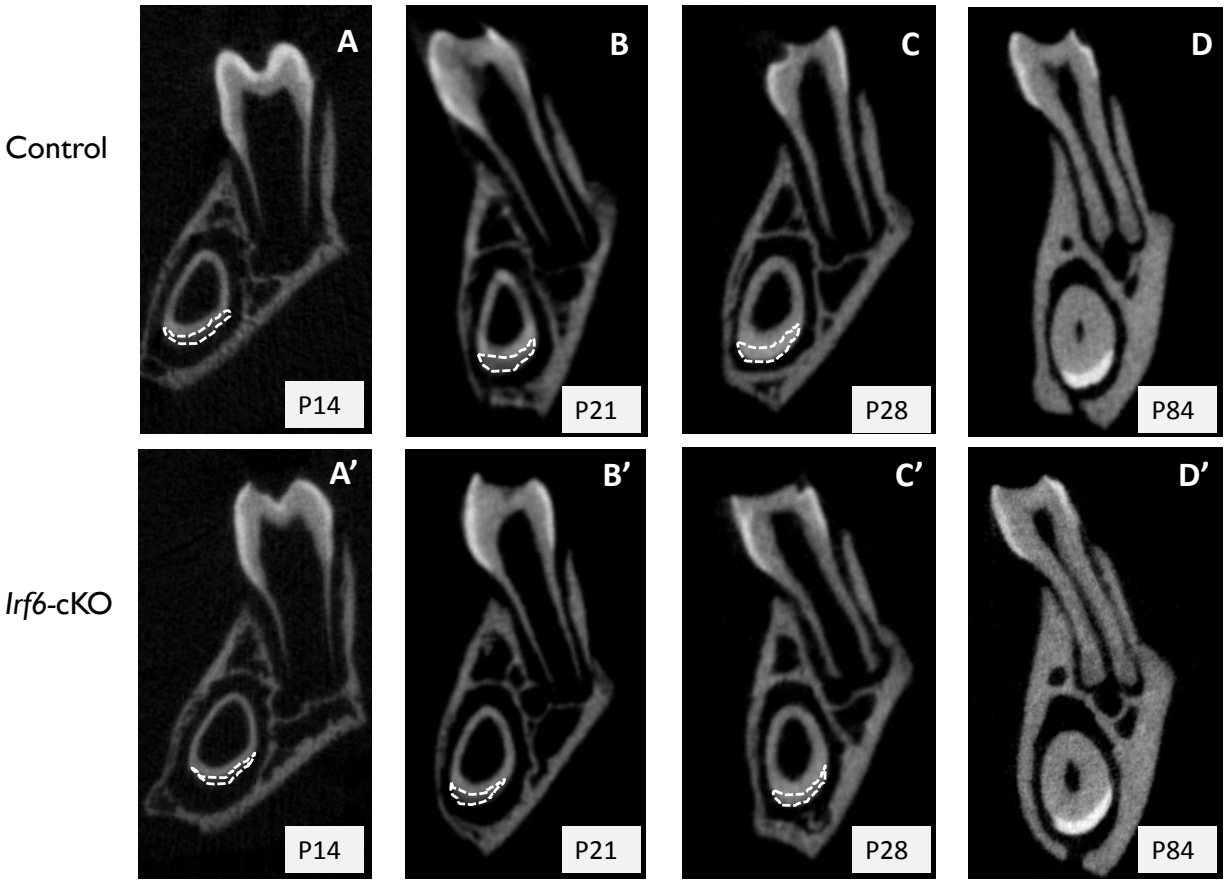

Figure 5.2: Enamel maturation delay observed in *Irf6-cKO* samples. In P14 and P21 samples, *Irf6-cKO* mice exhibited thinner enamel (enamel outlined in white) compared to controls (B', C' versus B, C). In P28 samples, *Irf6-cKO* samples exhibited thinner enamel, and enamel was clearly more radiolucent compared to controls (C' versus C). By P84, when the enamel is fully mineralized, the differences in enamel radiolucency were more subtle (D' versus D).

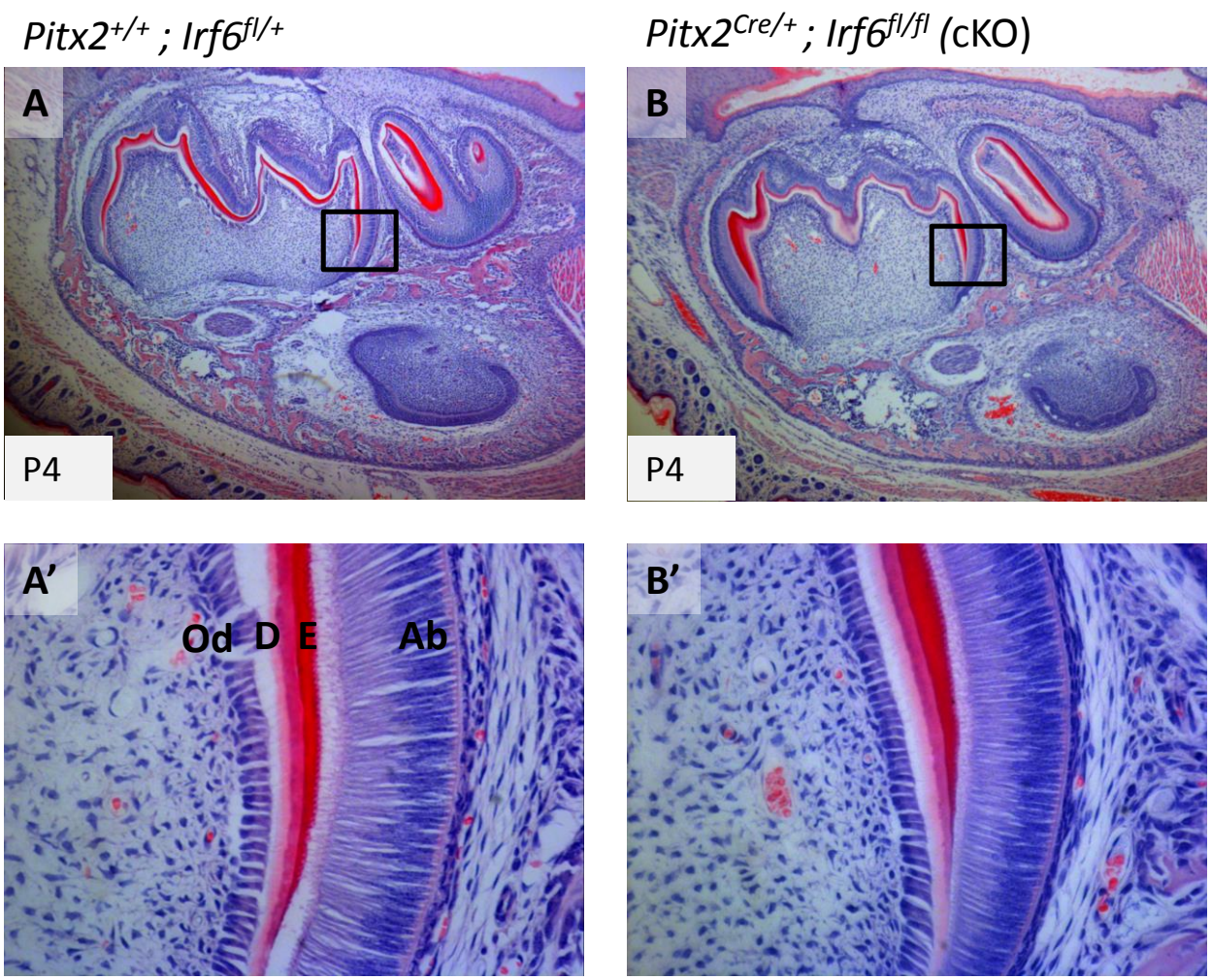

Figure 5.3: *Irf6-cKO* P4 samples exhibit polarized ameloblasts comparable to controls.

Od=odontoblasts, D=dentin, E=enamel, Ab=ameloblasts. Secretory ameloblasts in mandibular first molars are polarized in *Irf6-cKO* and control (*Pitx2*$^{+/+}$ *; Irf6*$^{fl/+}$) samples (A', B').

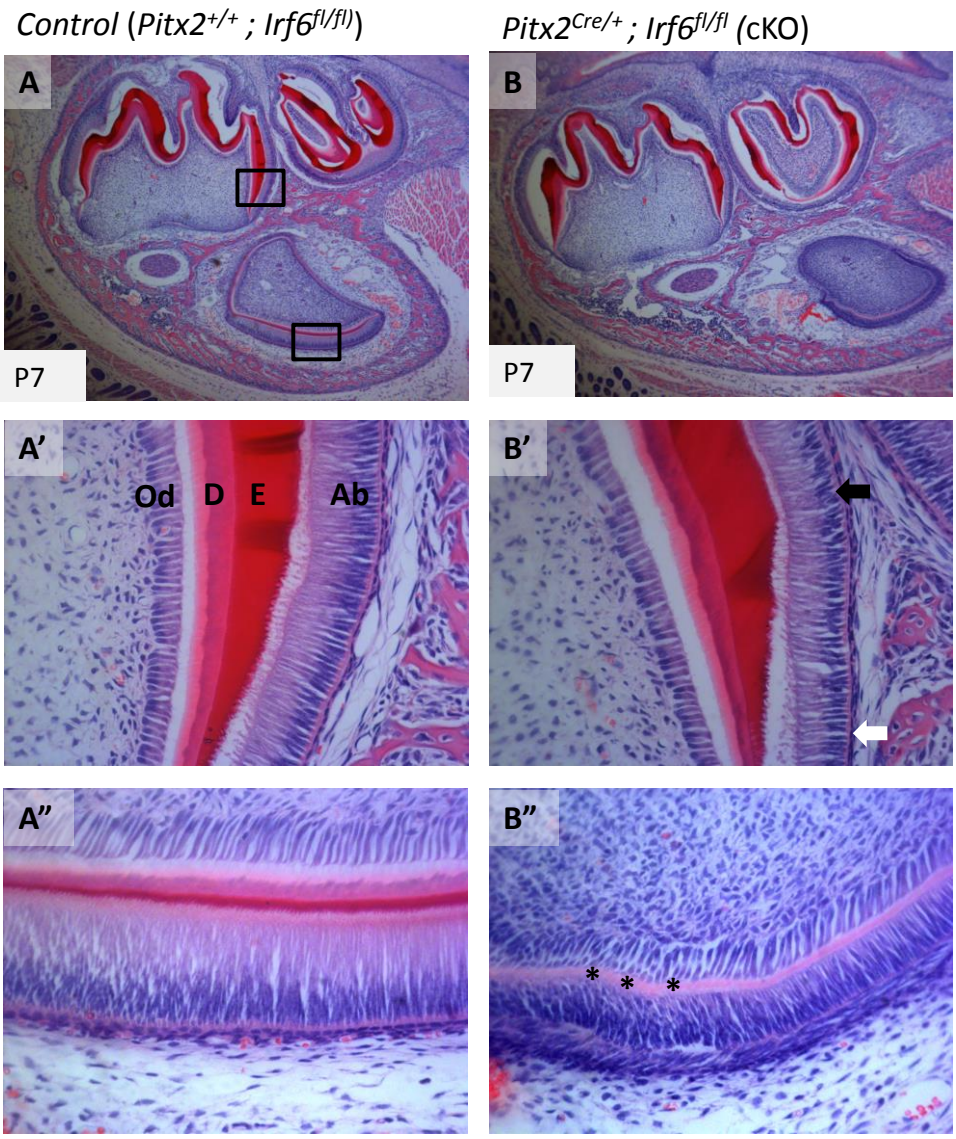

Figure 5.4: P7 *Irf6-cKO* samples exhibit disturbances in polarity and enamel formation. Od=odontoblasts, D=dentin, E=enamel, Ab=ameloblasts. In *Irf6-cKO* P7 mandibular first molars, ameloblasts that differentiated earlier and located more occlusally exhibited slight disturbances in organization and polarity (black arrow) compared to ameloblasts near the future cementoenamel junction of the tooth (whiter arrow). *Irf6-cKO* P7 incisors also exhibited a delay in enamel formation as observed by the thin dentin layer (asterisks) and absence of the enamel layer (B" compared to A").

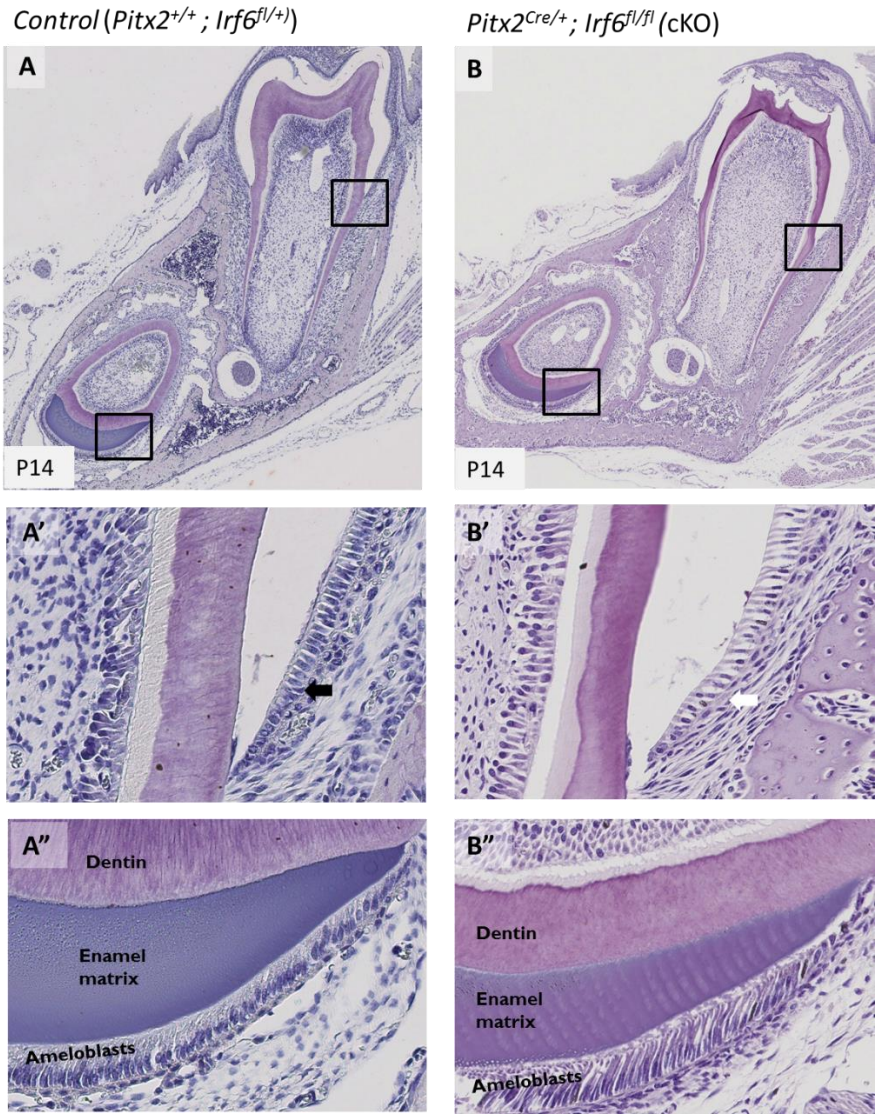

Figure 5.5: P14 *Irf6-cKO* samples exhibit disturbances in ameloblast organization and enamel formation. Ameloblasts are in the maturation stages. In the control sample (A'), ameloblasts have shortened, but remain polarized (black arrow). *Irf6-cKO* ameloblasts appeared less organized and increased spacing was observed between ameloblasts (Figure 5.5, B'). In incisor sections, enamel layer was thinner (B" versus A"). Ameloblasts in control samples appear to have shortened are are approaching

maturation stages (A”), whereas in *Irf6-cKO* samples, the ameloblasts appear to still be in secretory stages (B”).

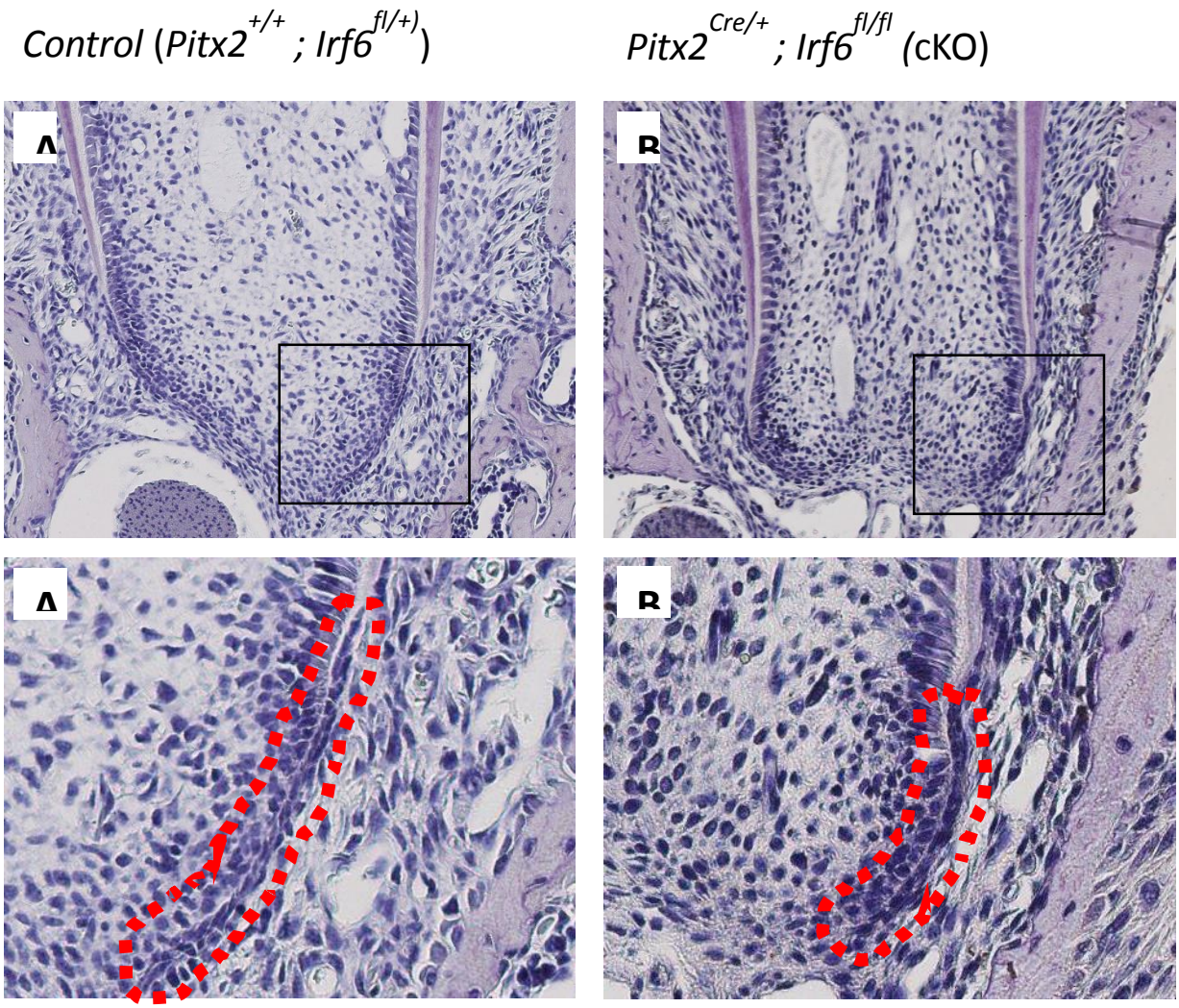

Figure 5.6: HERS appears shortened in *Irf6-cKO* P14 samples compared to controls.

HERS is outlined in red, and the HERS appears shorter in the *Irf6-cKO* samples versus controls (B' versus A').

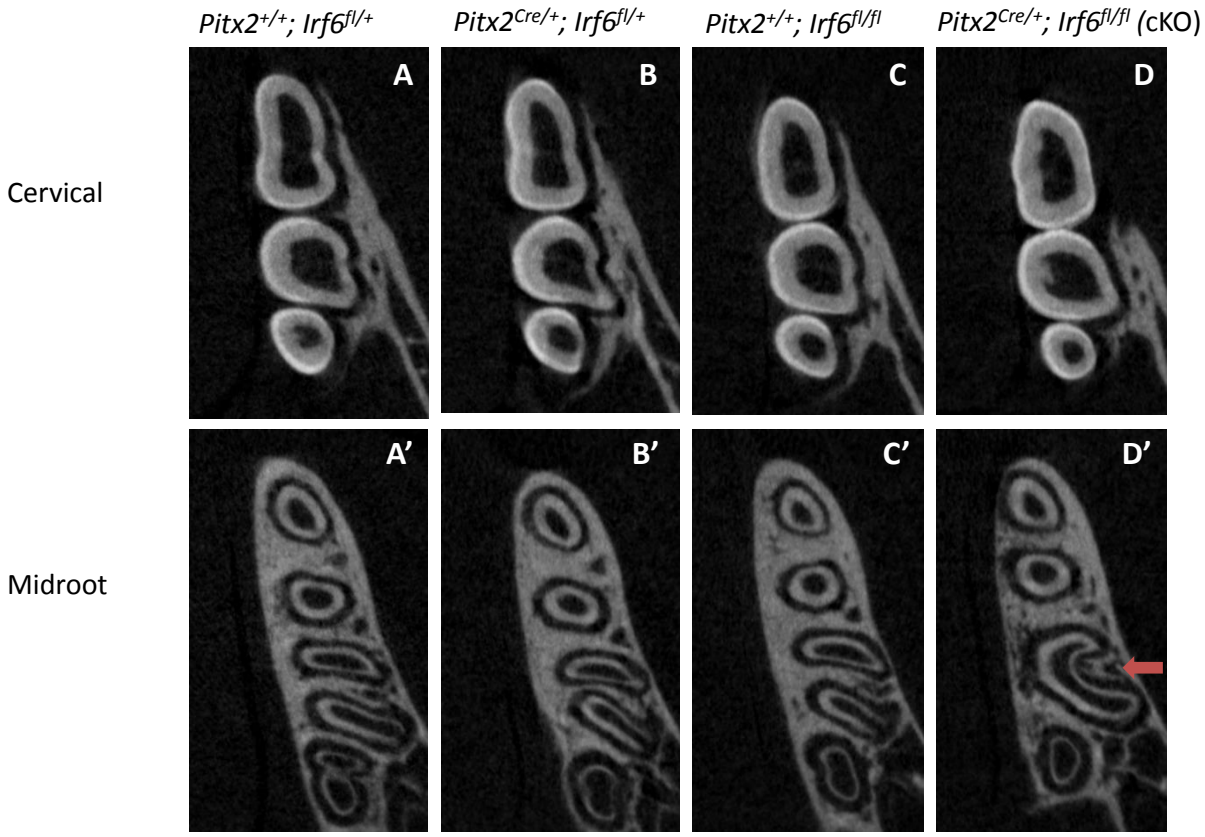

Figure 5.7: C shaped roots observed in *Irf6-cKO* P28 mandibular second molars.

Micro-CT coronal slices obtained at cervical and midroot regions. Note C-shaped mandibular second molar (D' red arrow). None of the other genotypes exhibited C-shaped mandibular second molar roots.

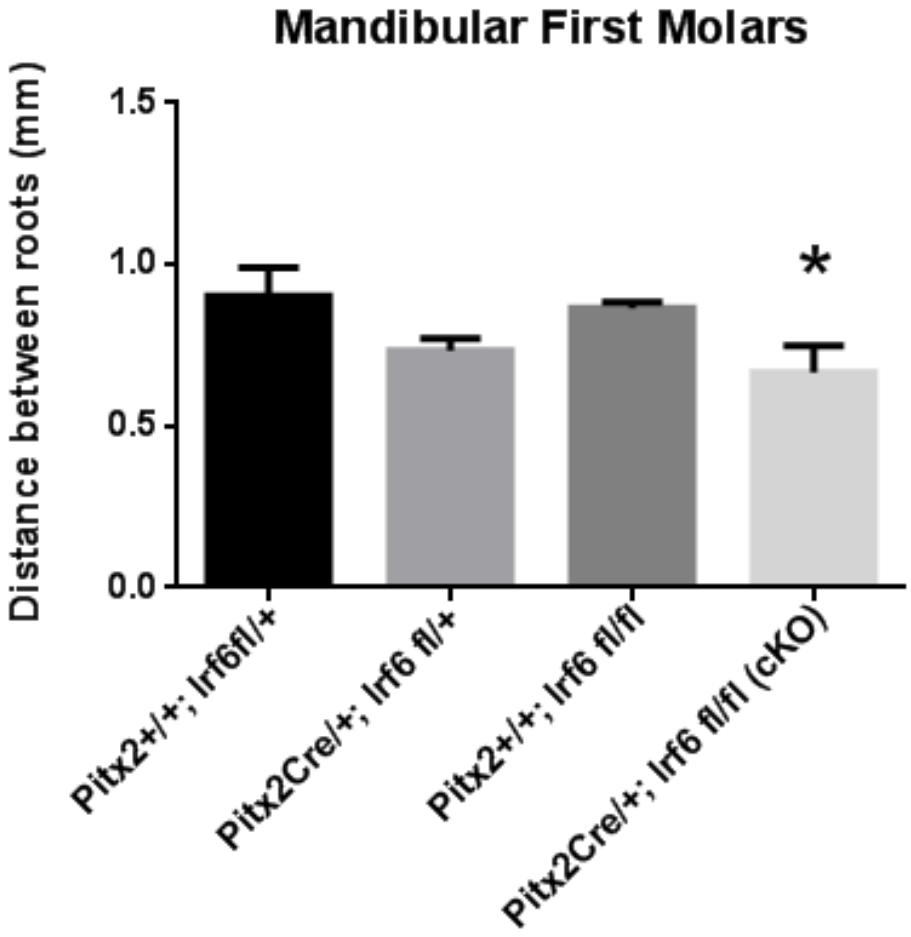

Figure 5.8: Reduced separation between mesial and distal roots observed in *Irf6-cKO* samples. Distance between center of mesial and center of distal root measured in mandibular first molars. Statistically significant difference observed. $P<0.05$.

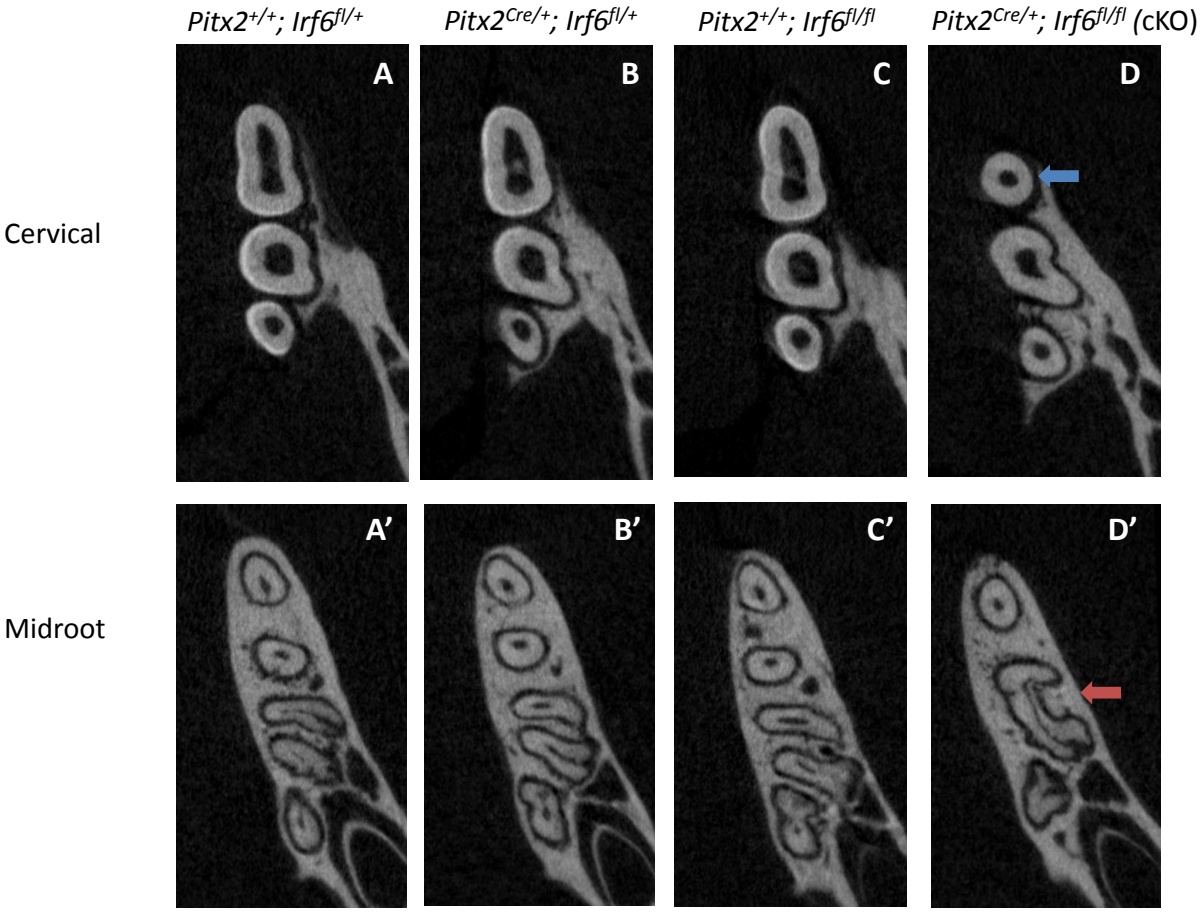

Figure 5.9: Root morphological alterations observed in *Irf6-cKO* P84 mandibular molars. Micro-CT coronal slices obtained at cervical and midroot regions. Note single-rooted mandibular first molar (D, blue arrow) and C-shaped mandibular second molar (D' red arrow). None of the other genotypes exhibited C-shaped mandibular second molar roots.

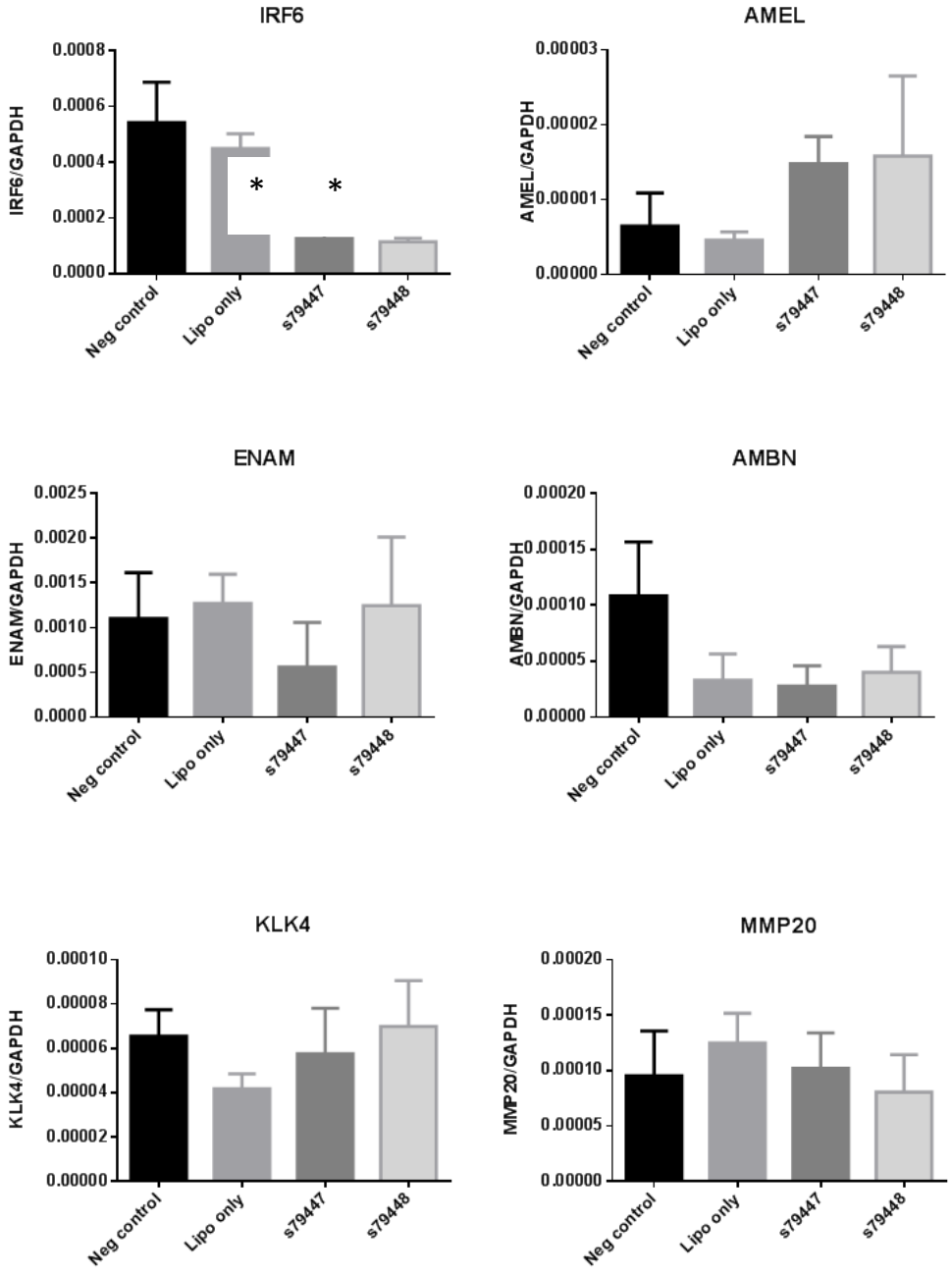

Figure 5.10: Knockdown of *Irf6* in LS8 cells. *Irf6* is detected in LS8 cells at low levels, and IRF6 knockdown does not cause changes in mRNA expression of enamel matrix proteins in LS8 cells. *Gapdh* used as a reference.

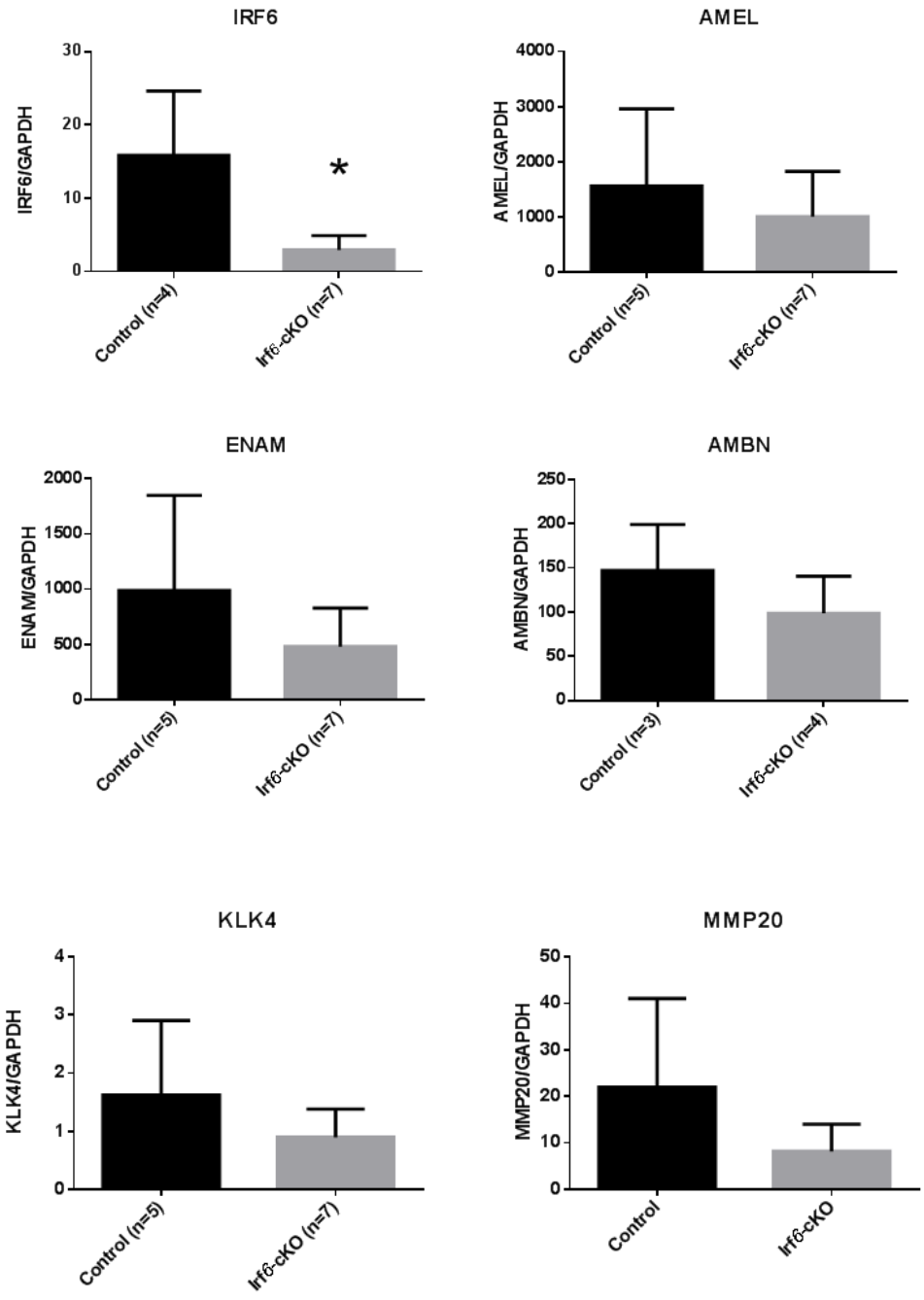

Figure 5.11: Loss of IRF6 in P4 molars does not cause changes in mRNA expression of enamel matrix proteins. Relative expression of *Amel, Enam, Ambn*, *Klk4,* and *Mmp20* did not exhibit a statistical difference compared to controls. *Gapdh* used as a reference. *: statistical significance at $p<0.05$

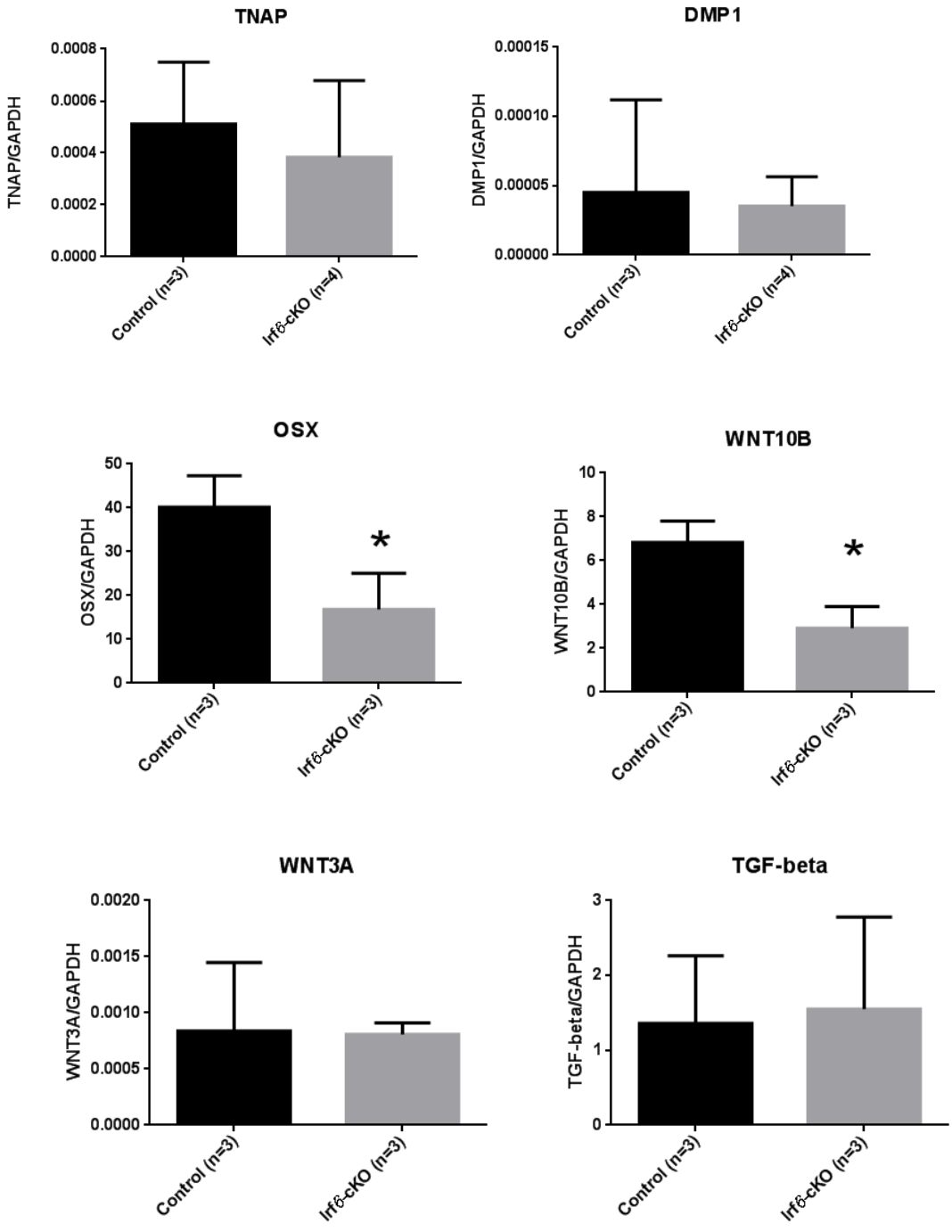

Figure 5.12: Loss of IRF6 in P4 molars causes changes in mRNA expression of osterix and Wnt10B. *Osx* and *Wnt10b* appear to be downregulated in *Irf6-cKO* P4 mandibular molars. Relative expression of *Tnap, Dmp1, Wnt3a,* and *Tgfβ* did not exhibit a statistical

difference compared to controls. *Gapdh* used as a reference. *: statistical significance at $p<0.05$

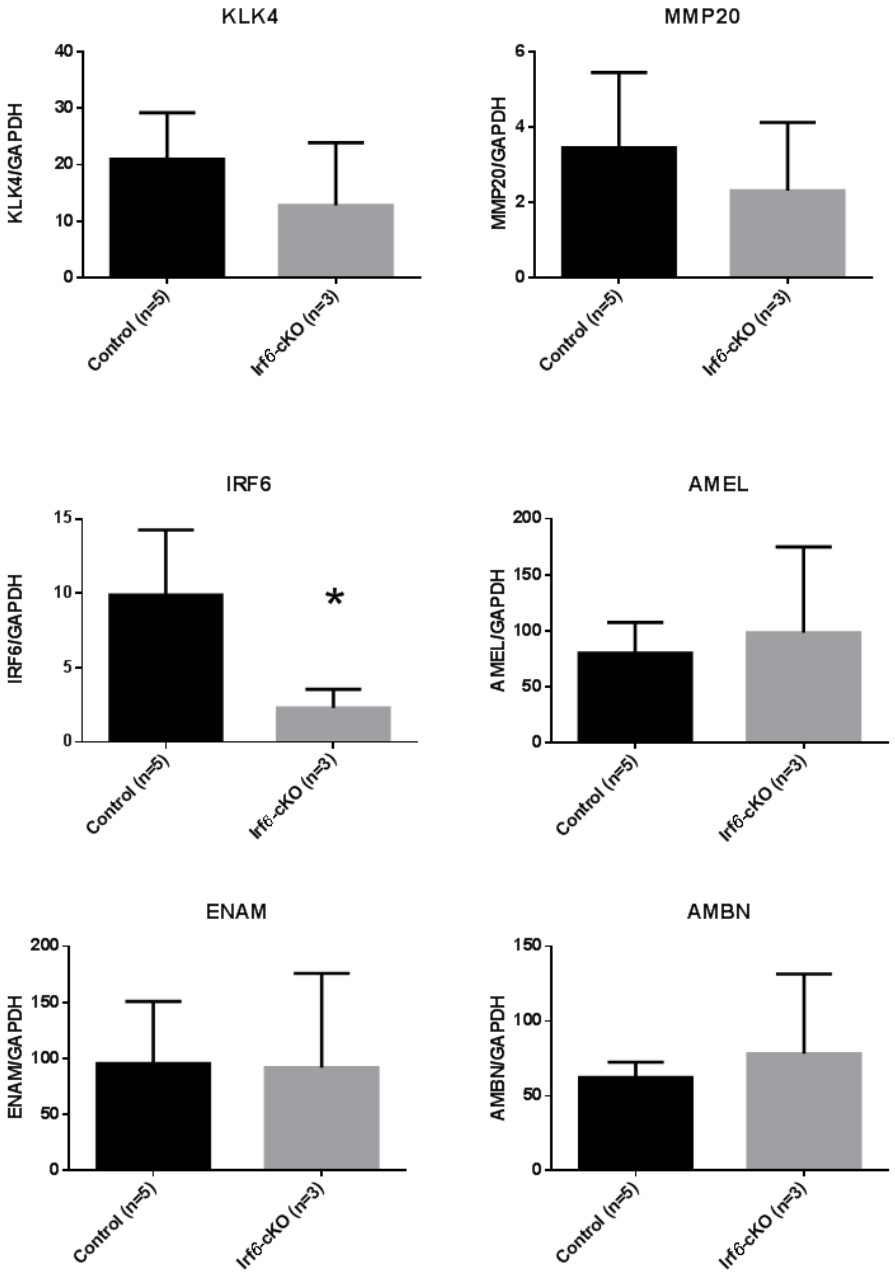

Figure 5.13: Loss of IRF6 in P13 molars does not cause changes in mRNA expression of enamel matrix proteins. Relative expression of *Amel, Enam, Ambn*, *Klk4,* and *Mmp20* did not exhibit a statistical difference compared to controls. *Gapdh* used as a reference.

*: statistical significance at $p<0.05$

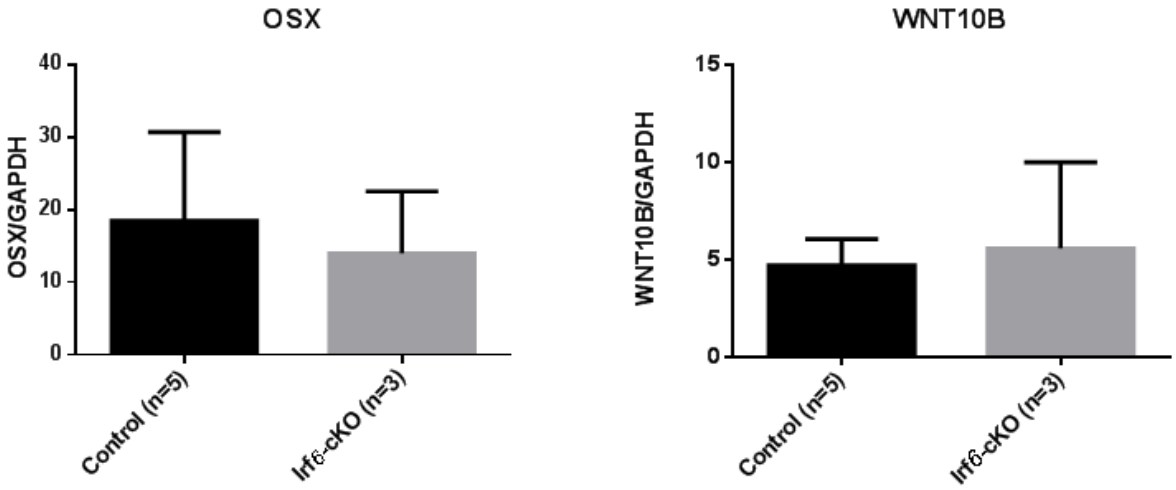

Figure 5.14: Loss of IRF6 in P13 molars does not cause changes in mRNA expression of Osterix and Wnt10B *Gapdh* used as a reference. *: statistical significance at $p<0.05$

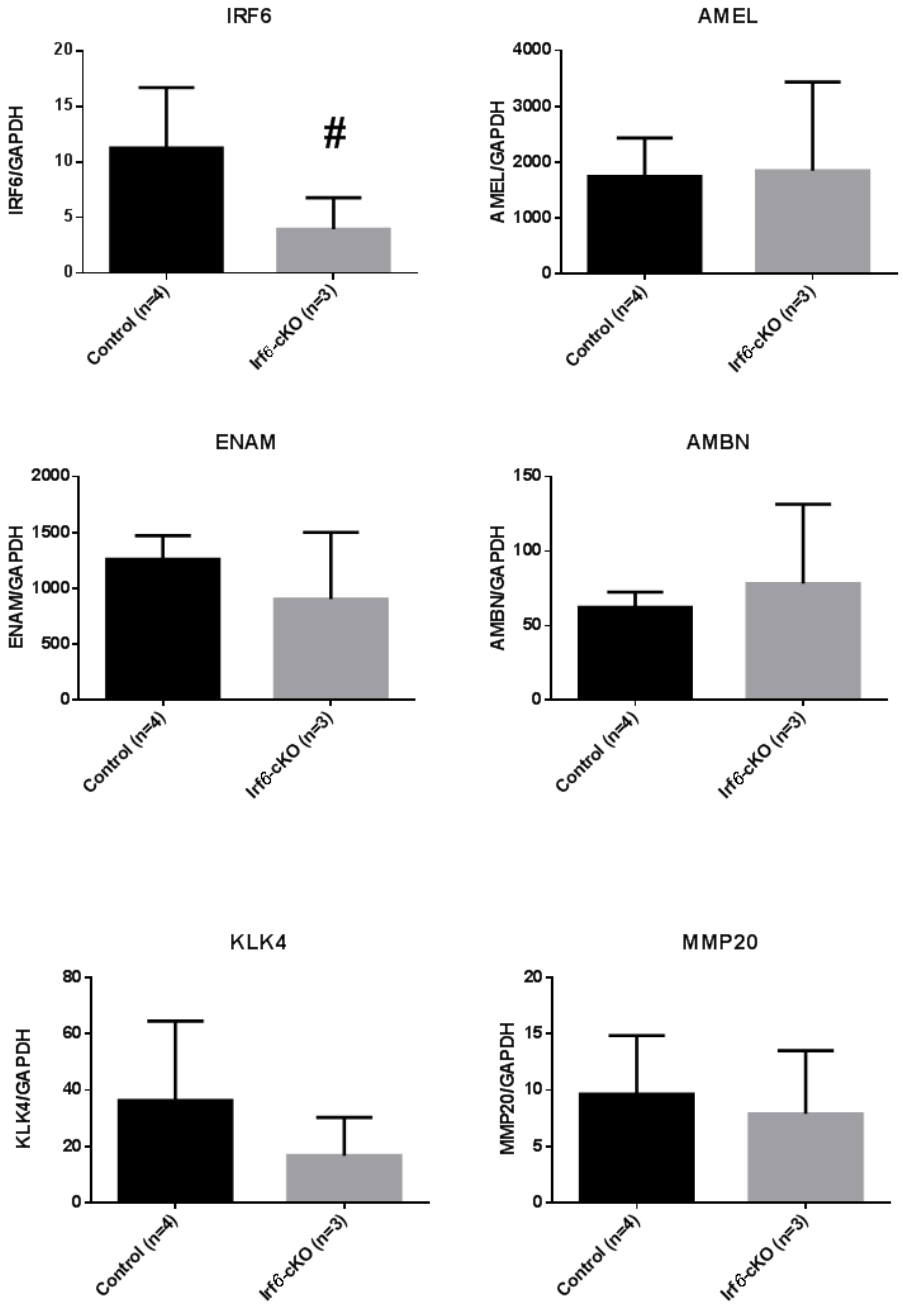

Figure 5.15: Loss of IRF6 in P13 enamel organs does not cause changes in mRNA expression of enamel matrix proteins. Relative expression of *Amel, Enam, Ambn*, *Klk4,* and *Mmp20* did not exhibit a statistical difference compared to controls. *Gapdh* used as a reference. #: statistical significance at $p<0.10$

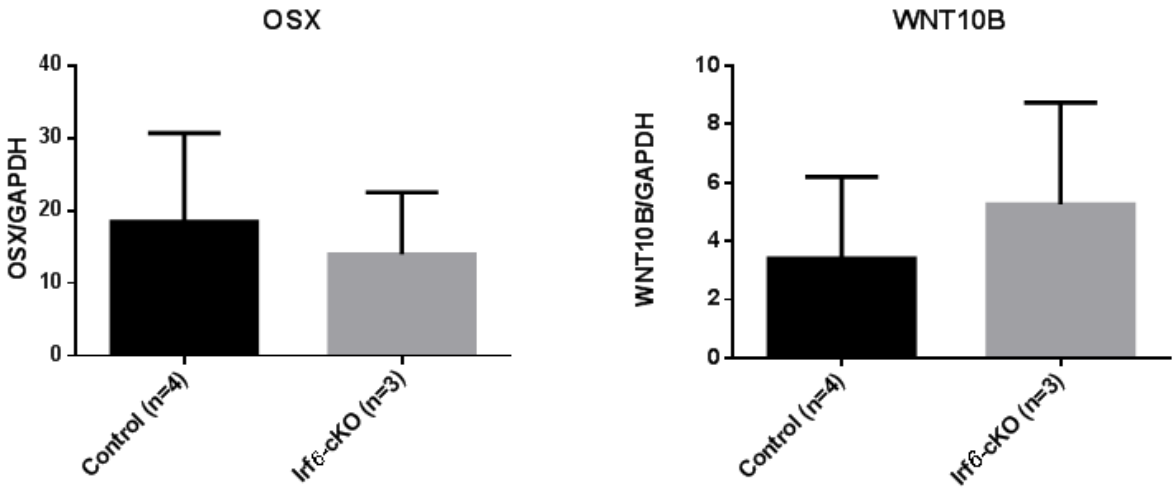

Figure 5.16: Loss of IRF6 in P13 enamel organs does not cause changes in mRNA expression of osterix and Wnt10B. *Gapdh* used as a reference. #: statistical significance at $p<0.10$

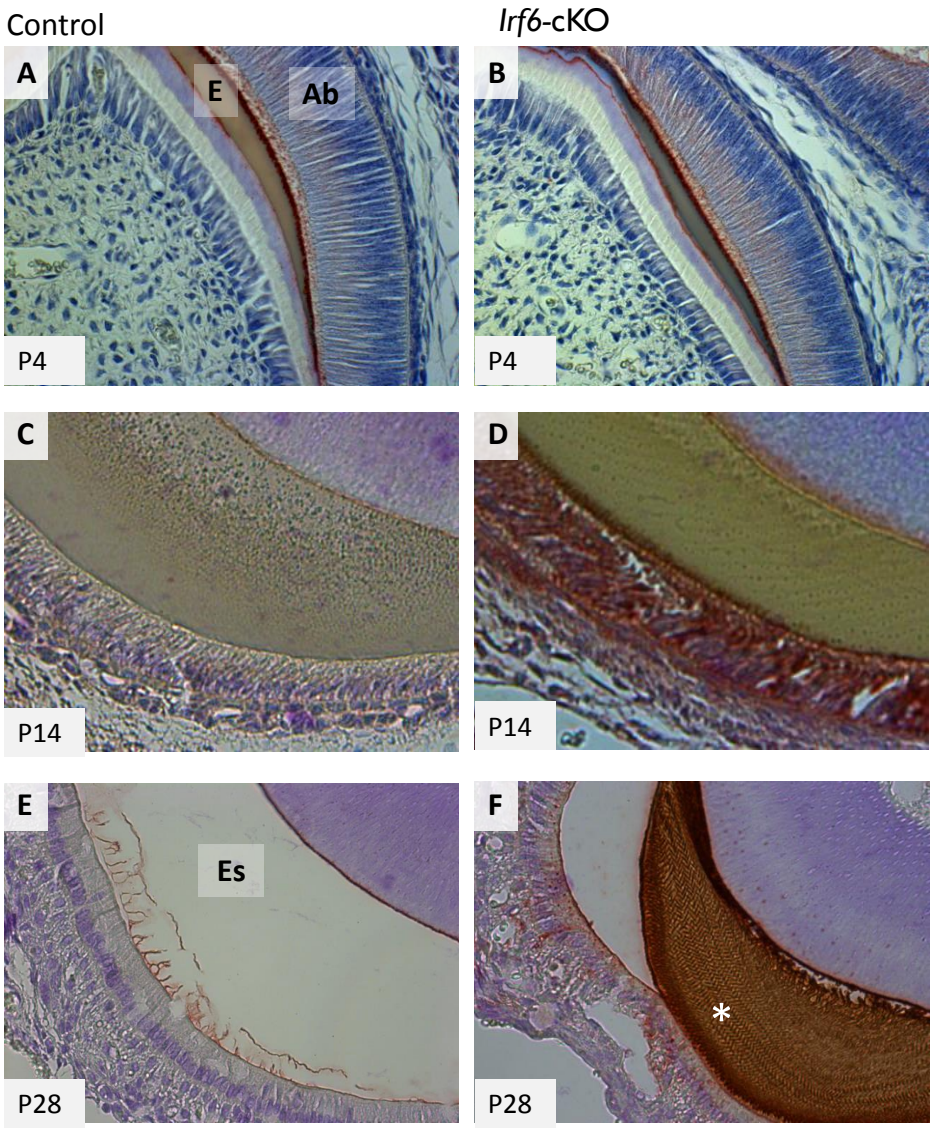

Figure 5.17: Loss of *Irf6* alters AMEL expression. Abbreviations: Ab=ameloblasts, E=enamel, Es=enamel space **(A, B)** P4 *Irf6*-cKO mandibular first molars exhibit amelogenin immunostaining in secretory ameloblasts and developing enamel matrix. **(C, D, E, F)** P14 and P28 *Irf6*-cKO incisors exhibit higher AMEL levels in secretory ameloblasts compared to controls (D versus C). AMEL was also detected in immature enamel matrix in P28 *Irf6*-cKO samples (F, asterisk), which was not present in controls (E).

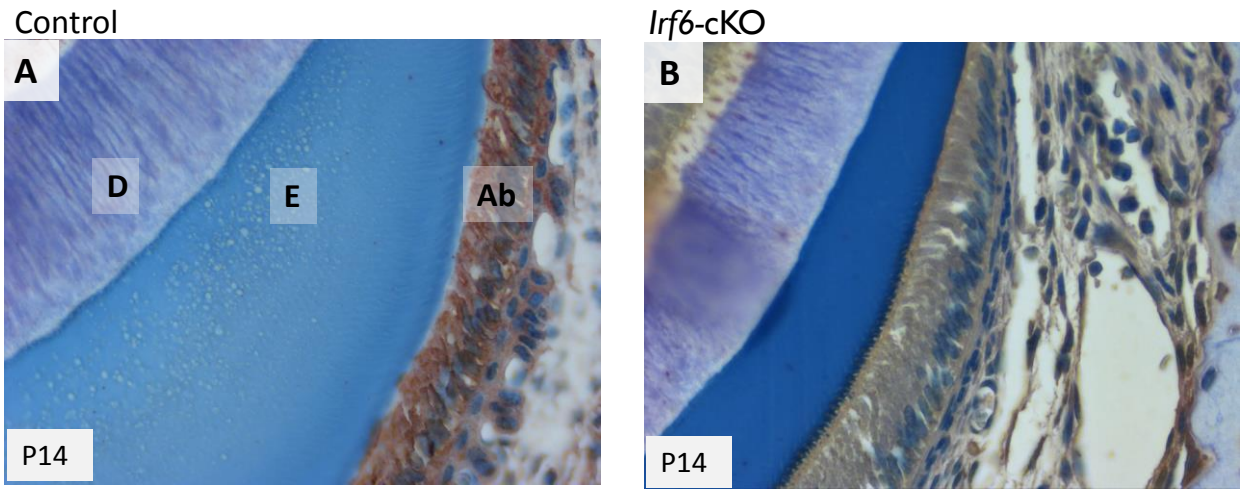

Figure 5.18: Loss of *Irf6* alters KLK4 expression. Abbreviations: D=dentin, Ab=ameloblasts, E=enamel P14 *Irf6*-cKO incisors exhibit lower KLK4 levels in ameloblasts compared to controls (B versus A).

Chapter 6: Discussion

IRF6 has cytoplasmic and nuclear roles

In the original IRF6 yeast two hybrid screen, several binding partners were identified, and NME2 attracted the most interest because of its known roles in epithelium. Via the same protein sequences that bind NME2, we found that IRF6 also binds to NME1.

The NME complex has been deemed a crucial factor in the establishment of epithelial polarity. Via interactions with other cytoplasmic proteins such as TIAM1 and LBC, both guanine exchange factors, the NME complex had the ability to influence the expression of GTPases Rac1 and RhoA (Figure 6.1). In our studies, HEK293T cells ectopically expressing a mutation in which the IRF6:NME interaction is disrupted, exhibited higher levels of Rac1 and RhoA compared to cells ectopically expressing a wild-type IRF6. Irf6 deficient keratinocytes also express higher RhoA levels (191). This suggests that the IRF6:NME complex affects the expression of Rho GTPases, which can cause alterations in epithelial polarity (Figure 6.2). Loss of polarity leads to alterations in E-cadherin distribution and reorganization of the actin cytoskeleton, which likely promotes proliferation (Figure 6.2). Irf6 null mice and chicks in which IRF6 expression is ablated exhibit reduced E-cadherin, altered epithelial shape, and a hyperproliferative epidermis (73, 74, 164). Therefore, these effects may be consequences of Rac1 or RhoA mediated rearrangement of the actin cytoskeleton and alteration of E-cadherin dynamics (e.g. promoting E-cadherin removal from the membrane).

Furthermore, NME is implicated in other pathways involving GTPases. For example, NME directly inhibits Ras GTPase signaling (82, 223). Active Ras stimulates the formation of the Raf/MEK/ERK complex, which is anchored by the kinase suppressor of Ras (KSR) (82). NME forms a complex with KSR and RGS19, a Gα Interacting Protein, which prevents the Raf/MEK/ERK complex from forming (82). Whether or not the IRF6:NME interaction is needed for this inhibition is unknown (Figure 6.3). When nuclear translocation of the Raf/MEK/ERK complex is inhibited, Raf/MEK/ERK is unable to activate its transcriptional targets. Whether the IRF6:NME complex has a role in Ras signaling or formation of the RGS19/KSR/NME complex is currently unknown. However, similar to IRF6 loss, loss of Rgs19 causes delayed palatal fusion (84) (Figure 6.4). Because RGS19 is expected to upregulate NME1/2; loss of RGS19 is expected to result in downregulation of *NME1/2* transcription, which would likely lower cytoplasmic NME1/NME2 (82). This downregulation may inhibit formation of the IRF6:NME complex, subsequently contributing to disruptions in epithelial fusion .

Additionally, formation of the IRF6:NME complex may be regulated by IRF6's phosphorylation status. Similar to other IRFs, serine phosphorylation likely mediates IRF6 protein-protein interactions. When three conserved serines (S413, S418, and S424) were mutated to alanines (abolishing the phosphorylation sites), IRF6:NME binding was lost. Despite NME's known function as a nuclear diphosphate kinase, abolishing the

kinase activity of NME does not alter its interaction with IRF6 (74). Thus, NME does not appear to be responsible for IRF6 phosphorylation. Recent studies have identified Receptor-interacting protein kinase 4 (RIPK4) as a candidate (Figure 6.5); ablation of S413 and S424 serine sites prevents RIPK4 activation of IRF6 (114). Nuclear localization of IRF6 was lowered when HEK293T cells were transfected with S413-418-424AAA constructs, indicating that serine phosphorylation may also regulate IRF6 nuclear translocation and subsequent regulation of transcriptional targets. Further supporting the importance of serine phosphorylation, a kinase-dead RIPK4 does not interact with IRF6 and does not promote nuclear translocation (114).

In the nucleus, IRF6 has known transcriptional targets, including GRHL3 and OVO-like 1 (OVOL1) (62, 182). GRHL3 has roles in keratinocyte differentiation and establishment of the oral periderm; in the absence of *IRF6*, *GRHL3* expression is downregulated. OVOL1 also promotes keratinocyte differentiation, and *IRF6* knockdown results in *OVOL1* downregulation. When IRF6 was silenced in HEK293T cells, the resultant decrease in NME1/NME2 suggests that IRF6 may regulate transcription of NME1/NME2 in addition to acting as a binding partner. Given NME's role in establishing epithelial polarity, transcriptional activation of *NME* is likely to promote epithelial cell differentiation (Figure 6.2). When IRF6 function is lost, transcription of these differentiation factors is downregulated, proliferation increases, and epithelial cells are less differentiated (Figure 6.2). This is corroborated by reports of lower levels of IRF6 expression in less

differentiated squamous cell carcinomas (SCC) compared to more differentiated forms of SCC.

IRF6 has diverse functions, which include nuclear and cytoplasmic roles. Here, we presented data suggesting that the IRF6:NME complex contributes to epithelial polarity. We have found that disruption of the IRF6:NME complex disrupted normal IRF6 protein-protein interactions and elevated active levels of Rac1 and RhoA. Furthermore, IRF6 nuclear translocation and the IRF6:NME interaction appeared to be mediated by serine phosphorylation. Because of NME's diverse functions, the IRF6:NME complex has the potential to impact many processes crucial for proper epithelial function.

IRF6 function and its contribution epithelial function and CLP

Our studies demonstrated that IRF6 mutations found in individuals with CLP and VWS had the ability to disrupt the IRF6:NME complex. Additionally, variants in NME1/NME2 found in individuals with CLP disrupted the IRF6:NME complex. This suggests specificity of the IRF6:NME interaction and contribution toward the formation of CLP. The NME complex has multiple functions in the epithelia, including mediating active GTPase (Rac1, RhoA, and Ras) levels and E-cadherin endocytosis. These processes contribute toward fusion of facial primordia and palatogenesis.

Mutations that disrupted the IRF6:NME complex also resulted in elevated levels of Rac1 and RhoA. Notably, Irf6 deficient keratinocytes exhibit lower levels of Arhgap29 and Arhgap29 has been identified as a downstream target of Irf6 (83, 97). ARHGAP29 promotes inactivation of GTPases, particularly RhoA (97). ARHGAP is also predicted to be associated with nonsyndromic forms of CLP (224-226). These variants were predicted to have a negative effect on ARHGAP29 function, suggesting that at least in some cases of CLP, elevated levels of active RhoA are present. RhoA also has roles in keratinocyte differentiation; RhoA stimulation of its downstream target Rho-associated, coiled-coil containing protein kinase II (ROCK II) promotes differentiation (99). When ROCK II activity is inhibited, cell proliferation is upregulated (99). ROCK inhibitors disrupt palatal fusion, and TGFβ3, which is expressed in the MEE, is also believed to regulate RhoA/ROCK activity, further suggesting the importance of RhoA in palatogenesis (67, 100). Thus, we suggest that the IRF6:NME complex participates in the regulation of RhoA, and disruption of IRF6:NME leads to aberrant levels of active RhoA, which interfere with proper epithelial function.

IRF6 clearly has roles in development and maintenance of epithelia. When IRF6 function is disrupted, dysregulation of epithelial cell-cell adhesion is observed. For example, IRF6 mutations cause VWS and PPS, which feature epidermal adhesions as well as orofacial clefts. *Irf6-null* mice exhibit a dramatic epithelial phenotype, including a hyperproliferative epidermis coupled with an absence of granular and cornified layers

(73). Epidermal adhesions were also noted between the tail and hindlimbs as well as in the oral cavity, and it was theorized that the absence of the granular and cornified layers caused the ectopic adhesions. One of the main components of cell-cell adhesive complexes is E-cadherin; alterations in E-cadherin cell-cell adhesion complexes have consequences on cell proliferation, cell shape, and cytoskeletal architecture (88, 183). One of the mediators of E-cadherin endocytosis is adaptor protein complex 2 (AP-2) (186, 187). AP-2 translocation to the cell membrane is mediated by ADP-ribosylation factor 6 (ARF6), which also recruits NME1 during adherens junctions disassembly (188, 189). In chick epithelia, *Irf6* knockdown causes redistribution of E-cadherin; E-cadherin appeared patchy and irregular at the plasma membrane, suggesting that the IRF6:NME complex may mediate E-cadherin endocytosis. Loss of IRF6 may promote NME1 recruitment to the cell membrane and subsequent upregulation of E-cadherin endocytosis. Consequently, the dissolution of these E-cadherin cell-cell adhesions result in loss of polarity and increased epithelial proliferation. This may account for the hyperproliferation of the epithelia as seen in *Irf6* mutants.

Additionally, mutations in *IRF6* transcription targets result in epithelial characteristics that resemble VWS epithelial abnormalities. For example, *GRHL3* mutations are associated with some cases of VWS, and similar to *Irf6* mutants, *Grhl3-null* mice lack oral periderm (61, 227). The periderm has crucial roles in fusion of facial processes and palatogenesis. Periderm development and removal is carefully timed; the periderm

prevents premature fusion, and its removal must be coordinated with the joining of two facial processes (50). *Irf6* expression in the periderm is specific; prior to periderm development, the morphology of *Irf6* epithelia is comparable to controls (61). We presented data suggesting that similar to other IRFs, IRF6 translocation is regulated by serine phosphorylation. Loss of serine phosphorylation prevents nuclear translocation and thus, transcriptional targets such as *GRHL3* would not be activated. *GRHL3* is also a promoter of cell differentiation in epithelial cells, so downregulation of *GRHL3* would likely lead to increased cell proliferation. Thus, timing of serine phosphorylation may influence cell differentiation in the epithelia. If the serine phosphorylation is ablated, epithelial cell differentiation would be downregulated. *IRF6* is also believed to regulate *RIPK4* expression, and RIPK4 is believed to phosphorylate IRF6, so loss of either is likely to result in a similar phenotype (114, 228). Notably, RIPK4 mutations have been found in individuals with PPS (176-178). Furthermore, *Ripk4-null* mice feature a similar phenotype to *Irf6-null* mice; both feature a hyperproliferative epidermis and loss of epidermal differentiation (179, 180). Therefore, IRF6's role as a transcription factor and its effects on downstream targets likely regulates critical events in palatogenesis and epithelial maintenance.

Furthermore, wound healing is impaired in these individuals; compared to other patients, VWS patients have a higher occurrence of complications following surgical

procedures. The severity of these complications also tends to be higher in VWS patients, suggesting that IRF6 has roles beyond facial development.

Epithelial polarity and tooth development

In Chapter 3, we described the results of studies showing that the IRF6:NME interaction has potentially diverse roles, including a role in establishing epithelial polarity. Thus, as tall, columnar cells in which polarity is tied to function, ameloblasts were of considerable interest. *Irf6-cKO* ameloblasts exhibited disruptions in morphology, polarity, and organization, indicating that *Irf6* has roles in ameloblast function.

In Chapter 3, we found that disruption of the IRF6:NME complex elevated active levels of Rac1 and RhoA; based on known functions of Rac1 and RhoA, these disturbances are likely to disrupt epithelial polarity. Prior to the studies described here, the role of NME has not been investigated in the tooth, and we show that NME is expressed in ameloblasts, although whether an IRF6:NME interaction exists in the tooth is unknown. Immunohistochemistry showed redistribution of NME in *Irf6-cKO* samples, suggesting that IRF6 regulates NME expression. In P14 control samples, NME2 was distributed throughout the cytoplasm of the ameloblasts. In contrast, the *Irf6-cKO* P14 ameloblasts exhibit lower amounts of NME2 in the cytoplasm, and NME2 appears to aggregate at the distal end of the ameloblasts. NME has roles in regulation of adhesion complexes in epithelia, so NME localization at proximal and distal ends may represent a mechanism in

which ameloblasts alter the strength of the junctional complexes. The increased NME may reflect abnormal regulation of permeability at the distal junctional complexes. Thus, the IRF6:NME interaction may contribute to the observed ameloblast disturbances via downstream elevated Rac1 and RhoA expression. Previous studies have implicated Rac1 and RhoA in tooth development (150, 152, 229). A conditional knockout *Rac1* mouse (driven by the *Keratin 14* promoter) exhibited hypoplastic enamel and subsurface hypomineralization, and mice expressing a dominant negative *RhoA* exhibited hypolastic enamel with subsurface defects (150, 152). Rac1 and RhoA are expressed by ameloblasts during the differentiation and secretory stages of amelogenesis (203). Increased levels of Rac1 and RhoA activity are also correlated with increased amelogenin expression, and amelogenin knockouts express higher levels of RhoGDI, an inhibitor of Rac1 and RhoA (203, 204, 230). Therefore, in addition to disrupting ameloblast polarity, overexpression of Rac1/RhoA may account for the elevated levels of AMEL observed in *Irf6-cKO* samples (Figure 6.6).

Disruptions in epithelial polarity also may be manifested in aberrations in epithelium invagination. Previous studies demonstrated *Irf6* expression in dental and oral epithelium in embryonic stages, and *Irf6* mutant incisor epithelium invaginated improperly in the bud stage (59). Improper invagination may lead to arrest of tooth development, resulting in hypodontia as observed in VWS patients and *Irf6-cKO* mice. In later stages, for instance, the bell stage, the inner dental epithelium undergoes folding

events, which ultimately determines cuspal position (45). Alterations in epithelial folding can manifest as shallower cusps or loss of cusps as seen in *Irf6-cKO* samples. Disruptions in epithelial folding are not restricted to the crown. The inner and outer enamel epithelium fuse to form the Hertwig's epithelial root sheath (HERS), which largely directs root formation (45, 126). One of the causes of taurodontism, which was observed in all *Irf6-cKO* mice is a failure of HERS to invaginate at the proper horizontal level (202). Consequently, the observed crown and root morphological disturbances may be caused by epithelial polarity directed disruptions in epithelial folding.

IRF6 is critical towards advancing enamel to maturation stages

Loss of *Irf6* resulted in a delay in enamel maturation, which was apparent in P14, P28, and P84 incisors and molars. Histological analysis revealed areas of immature enamel matrix in *Irf6-cKO*, whereas in comparable control sections, the enamel was fully mineralized. When comparing enamel mineral density measurements across P14, P28, and P84 ages, *Irf6-cKO* enamel lagged behind the controls in achieving its final mineral density. Additionally, the final enamel mineral density was lower compared to controls. SEM revealed that *Irf6-cKO* mice were able to form enamel prisms accompanied by a seemingly organized rod and interrod structure, suggesting that the initial stages of enamel formation occurred without any major disruptions.

In the earlier stages of ameloblast development, i.e. presecretory and early secretory, *Irf6-cKO* ameloblasts were comparable to controls. However, as the ameloblasts neared the maturation stage, they appeared more disorganized and shorter compared to controls. This suggests that *Irf6* has a role in later stages of enamel development. *Irf6-cKO* P14 and P28 samples exhibited elevated AMEL levels in ameloblasts compared to controls. Furthermore, in P14 samples, this was accompanied by a decrease in KLK4 expression. These changes in *AMEL* and *KLK4* are consistent with an enamel maturation stage defect. *KLK4* mutations are frequently associated with defects in enamel maturation, which is consistent with the enamel phenotype reported in our *Irf6-cKO* mice (Figure 6.6). KLK4 cleaves AMEL at several different sites during the late secretory and maturation stages of enamel development (221, 222). *Klk4-null* secretory stage enamel is indistinguishable from wild-type enamel, whereas in later stages, residual enamel proteins were detected in *Klk4-null* samples (221). The elevated AMEL observed in the P14 samples may also indicate inadequate removal of enamel matrix proteins. Residual proteins inhibit proper enamel crystallite growth and mineralization; improper cleavage of enamel proteins leads to smaller enamel crystallites and increased spacing between crystallites, which may account for the shearing of the enamel rods and the accelerated enamel attrition (Figure 6.6).

IRF6 and Signaling Pathways Involved in Tooth Development

Tooth development is dependent on epithelial-mesenchymal reciprocal signaling, and our data suggests that *IRF6* participates in WNT signaling pathways. Notably, *Irf6* P4 molars exhibited decreased *Wnt10b* mRNA expression. *Wnt10b* is expressed in dental epithelium and enamel knots, and disrupting Wnt/beta-catenin signaling during the bell stage leads to flattened, smaller and irregular cusps (210). Interference with signaling in the enamel knot may result in downstream effects on multiple pathways, which may lead to the aberrant cusp morphology observed in *Irf6-cKO* mice.

Additionally, disruptions in *Wnt/β-catenin* signaling can lead to tooth root defects, including shorter or absence of tooth roots, and *Wnt10a-null* mice exhibit taurodontic mandibular molars as well as blunted cusps (215, 231). Similar to crown development, root development is also dependent on epithelial-mesenchymal interactions. The WNT pathway is implicated in root development. A conditional knockout for β-catenin (driven by the *Osteocalcin* promoter) does not form roots, and Syndecan-1, a Wnt/β-catenin signaling enhancer, is found in the HERS (231, 232). HERS is derived from the enamel epithelium, and is known to induce odontoblast differentiation by epithelial-mesenchymal interactions in the root. *Osterix (OSX),* which is expressed in root odontoblasts, was downregulated in *Irf6-cKO* P4 molars. *Osx* regulates *Wnt* signaling; thus, there is a possibility an *Irf6* effect on *Osx* expression could occur via epithelial-mesenchymal crosstalk (219).

The manner in which *IRF6* participates in WNT signaling is unknown, although RIPK4 and RhoA have been implicated. RIPK4 has been shown to activate canonical WNT signaling via phosphorylation of Dishevelled 2 (DVL2). In turn, DVL2 promotes the nuclear transport of β-catenin (by inhibiting proteosomal degradation of β-catenin), which activates Wnt transcriptional targets (233). IRF6 has been found to transcriptionally regulate *RIPK4*; via RIPK4, IRF6 may influence WNT pathways (Figure 6.7). Furthermore, mice expressing dominant negative RhoA exhibited upregulation of Wnt3a and β-catenin, suggesting that RhoA can influence the canonical WNT pathway as well (230). Via alterations in RhoA expression, IRF6 may also impact WNT signaling (Figure 6.7). In the absence of IRF6, active RhoA increases, leading to downregulation of WNT and WNT targets (Figure 6.8).

Conclusion

Three specific aims were targeted toward elucidating *Irf6* function in epithelial polarity and developing teeth. Using *in vitro* and *in vivo* methods, we have investigated the impact of the IRF6:NME complex on polarity effector molecules and the consequences of *Irf6* ablation on ameloblast polarity. In finding IRF6 VWS mutations that disrupted the IRF6:NME complex and altered Rac1 and RhoA activation, we provided insight into the pathways in which IRF6 contributes to CLP. A conditional murine model in which *Irf6* was ablated in developing tooth buds was developed, and our model demonstrated

enamel, crown, and root defects (Table 6.1). Based on our observations, *Irf6* may have several roles in the tooth. Via interactions with components of the *Wnt/β-catenin* pathway, *Irf6* may participate in cusp patterning or HERS folding. Furthermore, alterations in *Rac1* and *RhoA* activation (as demonstrated by our *in vitro* studies when the IRF6:NME complex is disrupted) are likely to contribute to cusp patterning. *Irf6* also appears to have roles in enamel maturation; by influencing the expression of enamel matrix proteins such as AMEL and KLK4, *Irf6* can affect final enamel structure. Overall, our findings contributed toward the understanding of the role of *Irf6* in CLP, as well as tooth abnormalities associated with epithelial disorders.

FIGURES AND TABLES

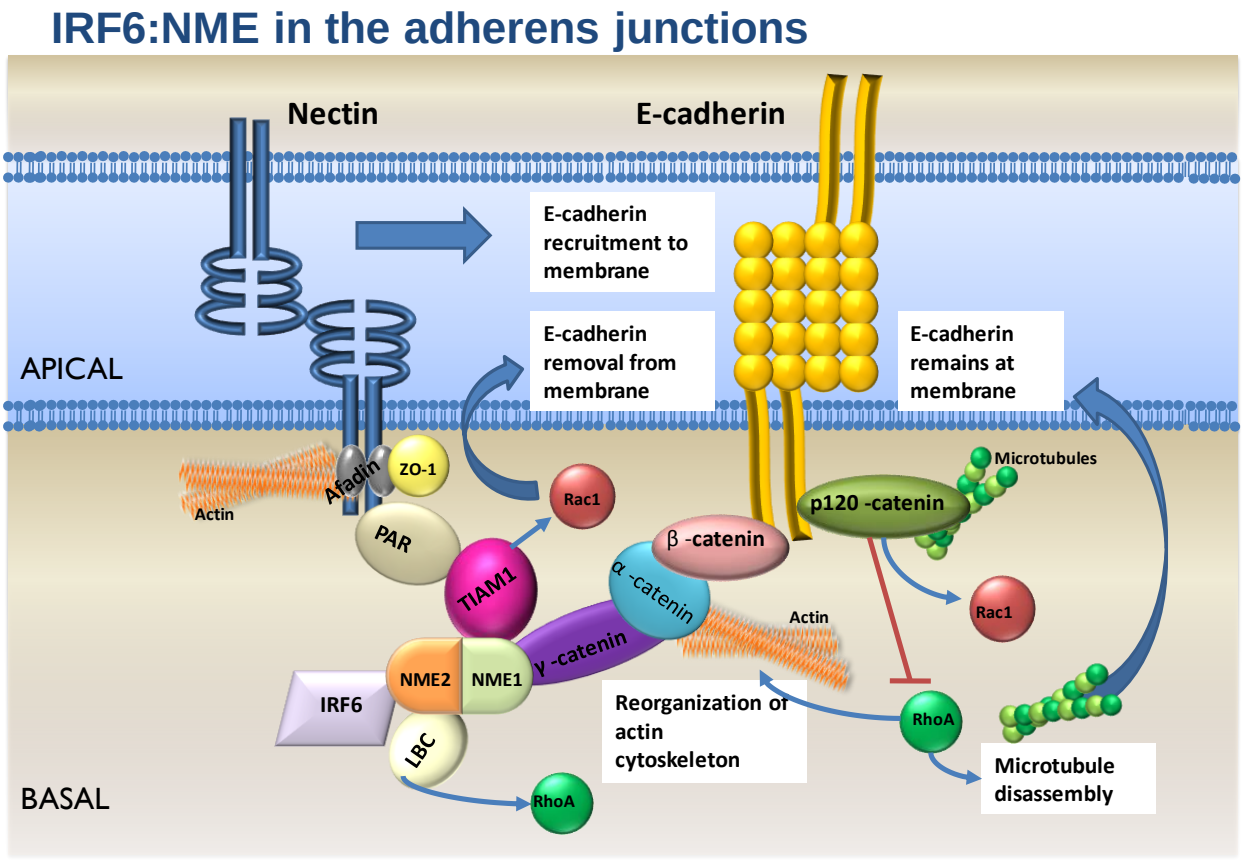

Figure 6.1: Schematic of contributors to epithelial polarity in adherens junctions.

Although the cell adhesion molecules Nectin and E-cadherin do not interact directly, they are connected via interactions with other proteins. Via an interaction with NME, IRF6 has the potential to impact expression of Rac1/RhoA, E-cadherin dynamics, and reorganization of the actin cytoskeleton.

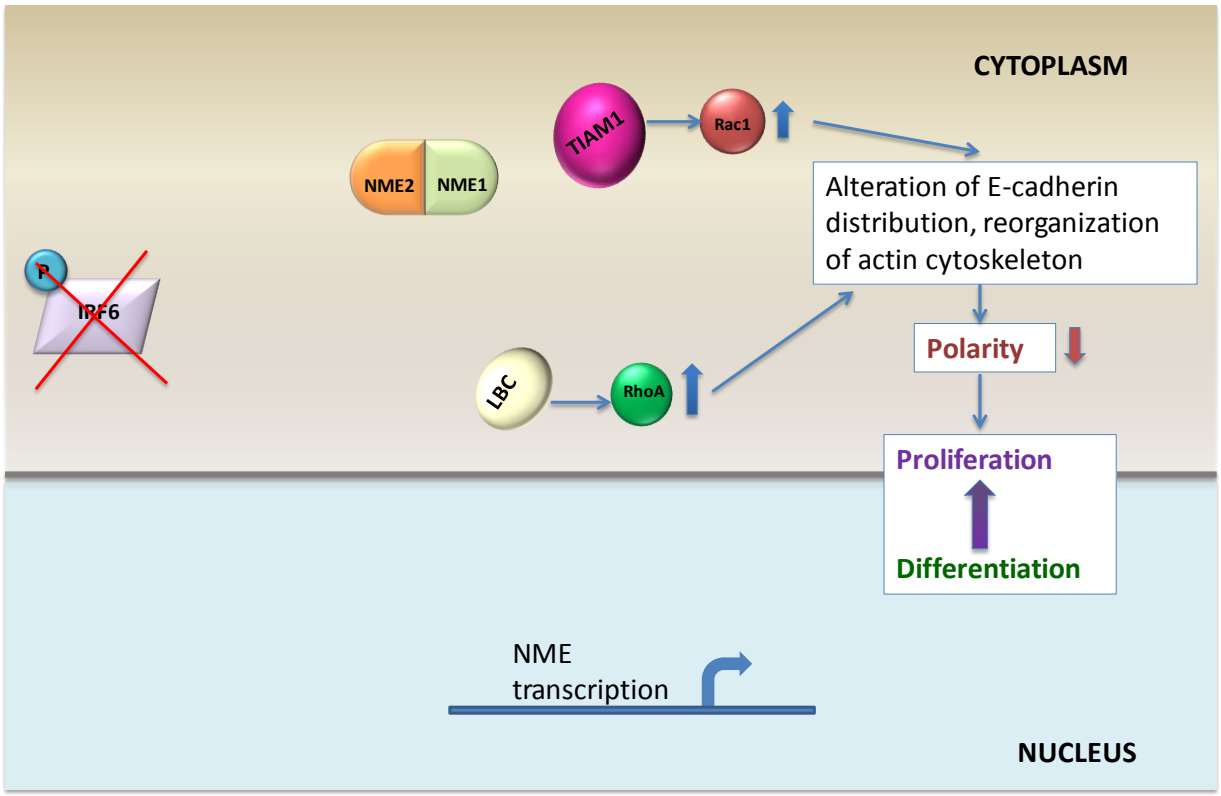

Figure 6.2: Schematic for hypothesized effects when IRF6 is lost. In the absence of IRF6, the IRF6:NME complex does not form, and LBC/TIAM1 inhibition is lost. Active Rac1 and RhoA levels increase, leading to loss of polarity and increased proliferation.

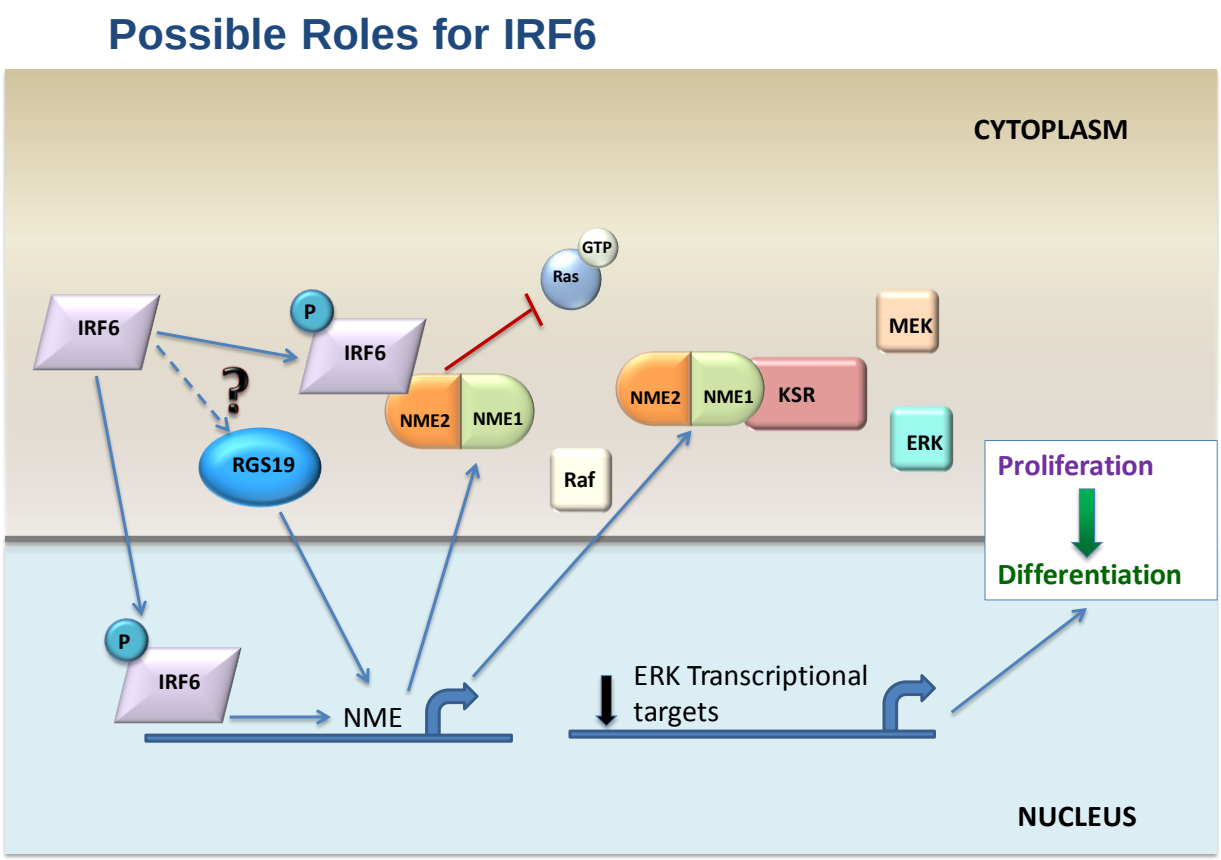

Figure 6.3: Schematic for hypothesized role for the IRF6:NME complex. RGS19 is known to regulate *NME* transcription, and NME inhibts *Ras* activation (which normally promotes transcription of ERK targets). NME also binds to KSR, and this interaction inhibits the activation of ERK transcriptional targets. Whether or not IRF6 interacts with RGS19 is unknown.

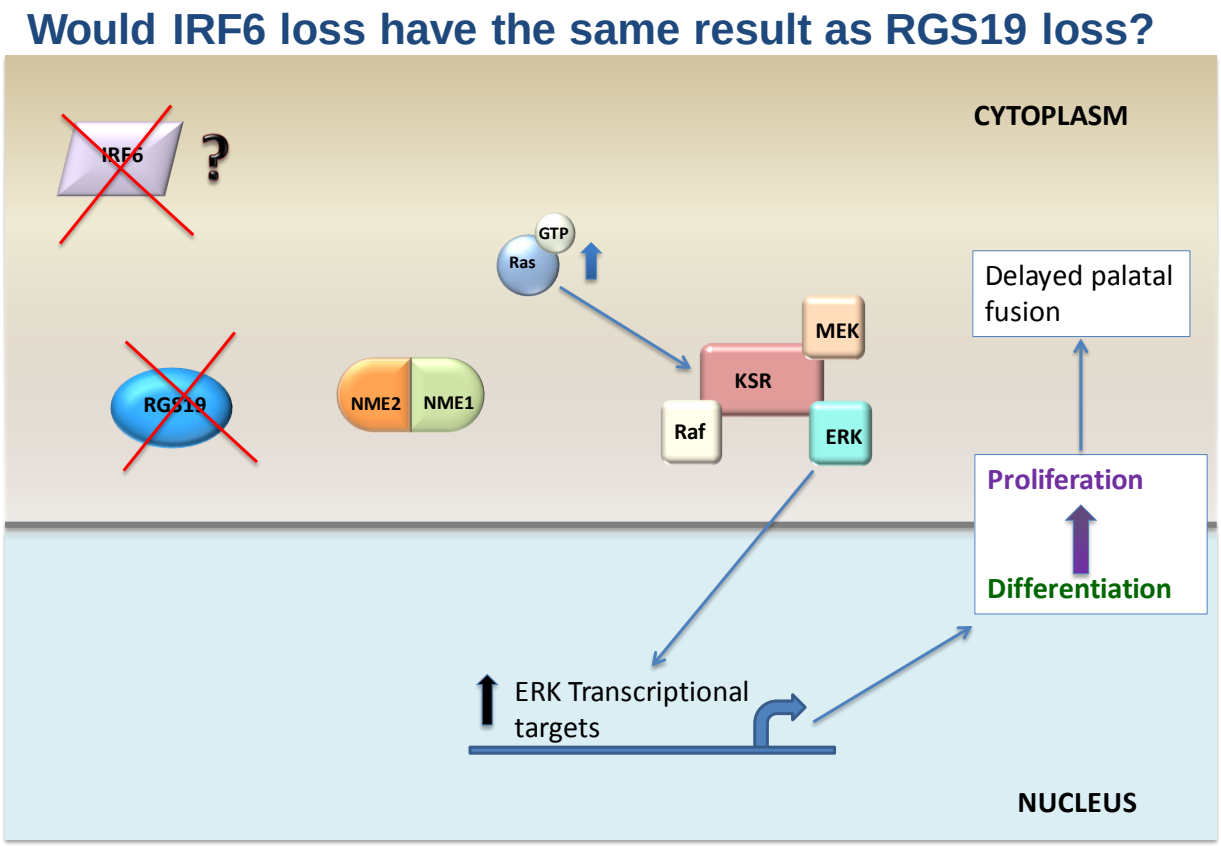

Figure 6.4: Studies have shown that RGS19 leads to delayed palatal fusion. Loss of RGS19 leads to activation of Ras signaling, which leads to formation of the Raf/MEK/ERK complex and transcription of ERK targets. RGS19 mutants exhibit an increase in proliferation and delayed palatal fusion, which has been reported in *Irf6* mutants. However, the relationship between IRF6 and RGS19 is unknown.

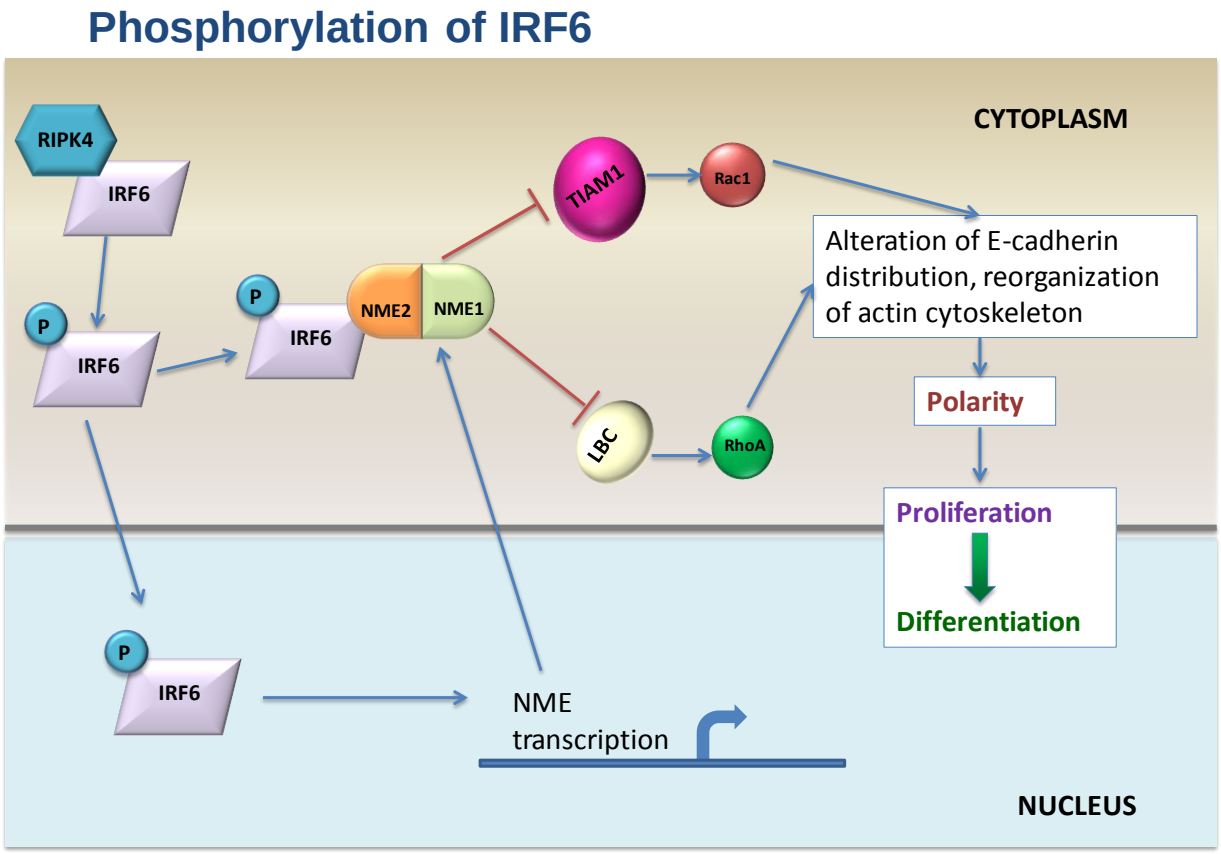

Figure 6.5: Schematic for hypothesized role for the IRF6:NME complex. RIPK4 is believed to phosphorylate IRF6, promoting nuclear translocation. In addition to acting as a protein-protein interactor for NME1/NME2, IRF6 may also regulate *NME* transcription. Based on our results, the IRF6:NME interaction is needed for LBC/TIAM1 inhibition. The resultant changes in RhoA/Rac1 lead to alterations in E-cadherin distribution and the actin cytoskeleton, which alter epithelial polarity. IRF6 has roles in keratinocyte differentiation; thus, wild-type IRF6 is predicted to promote differentiation.

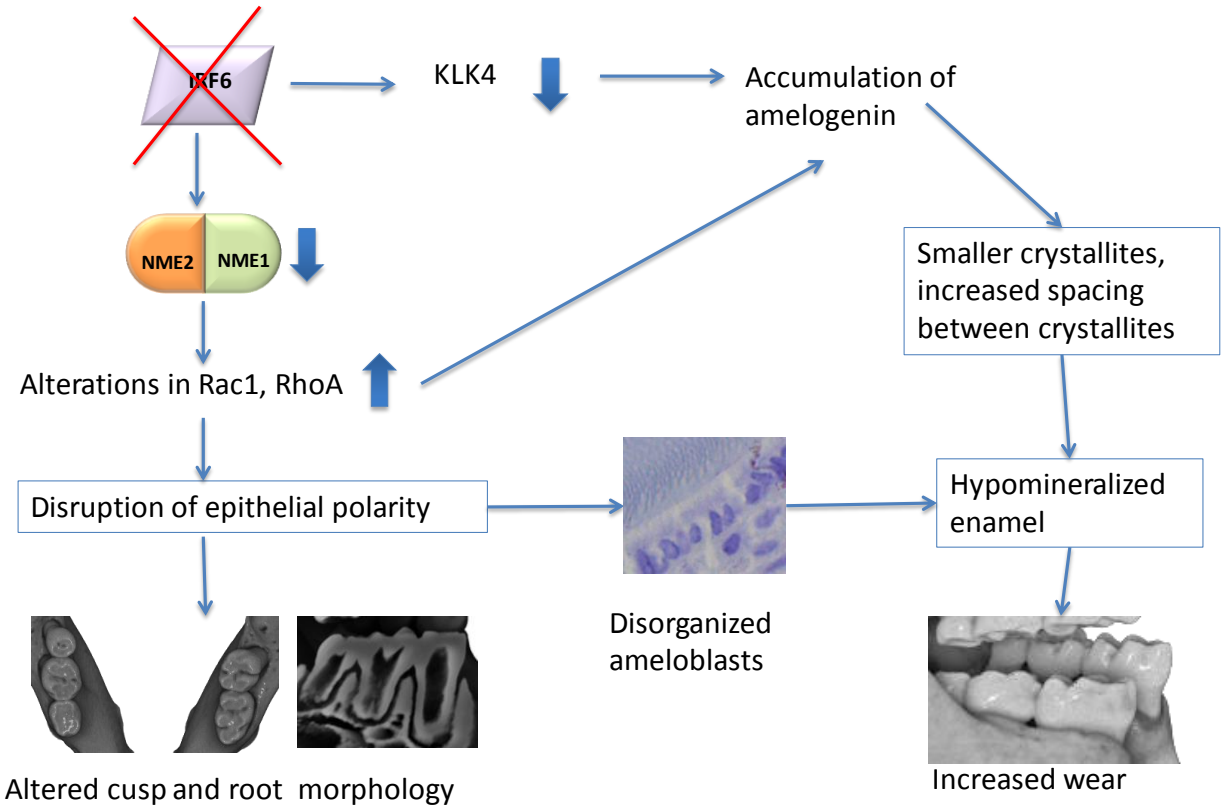

Figure 6.6: Alterations in epithelial polarity and disturbances in enamel matrix proteins may account for defects in crown/root morphology, ameloblast polarity, and enamel.

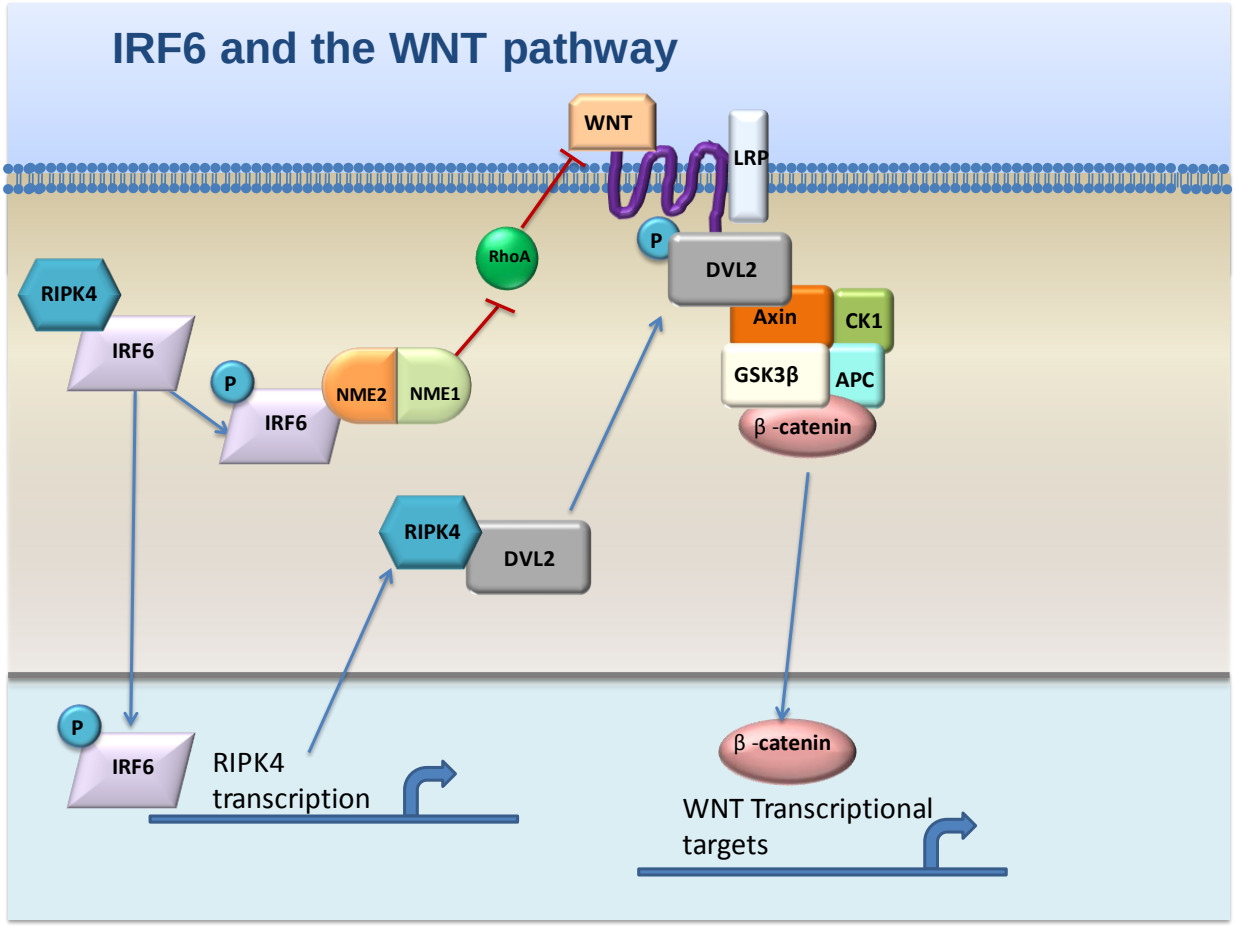

Figure 6.7: Possible roles for IRF6 in the WNT pathway. IRF6 may participate in the WNT pathway via transcriptional regulation of RIPK4 or inhibition of RhoA (through the IRF6:NME interaction). RIPK4 phosphorylates DVL2, which promotes β-catenin dissociation from the Axin/CK1/GSK3β/APC complex and subsequent β-catenin activation of WNT transcriptional targets. RhoA has been reported to inhibit WNT signaling.

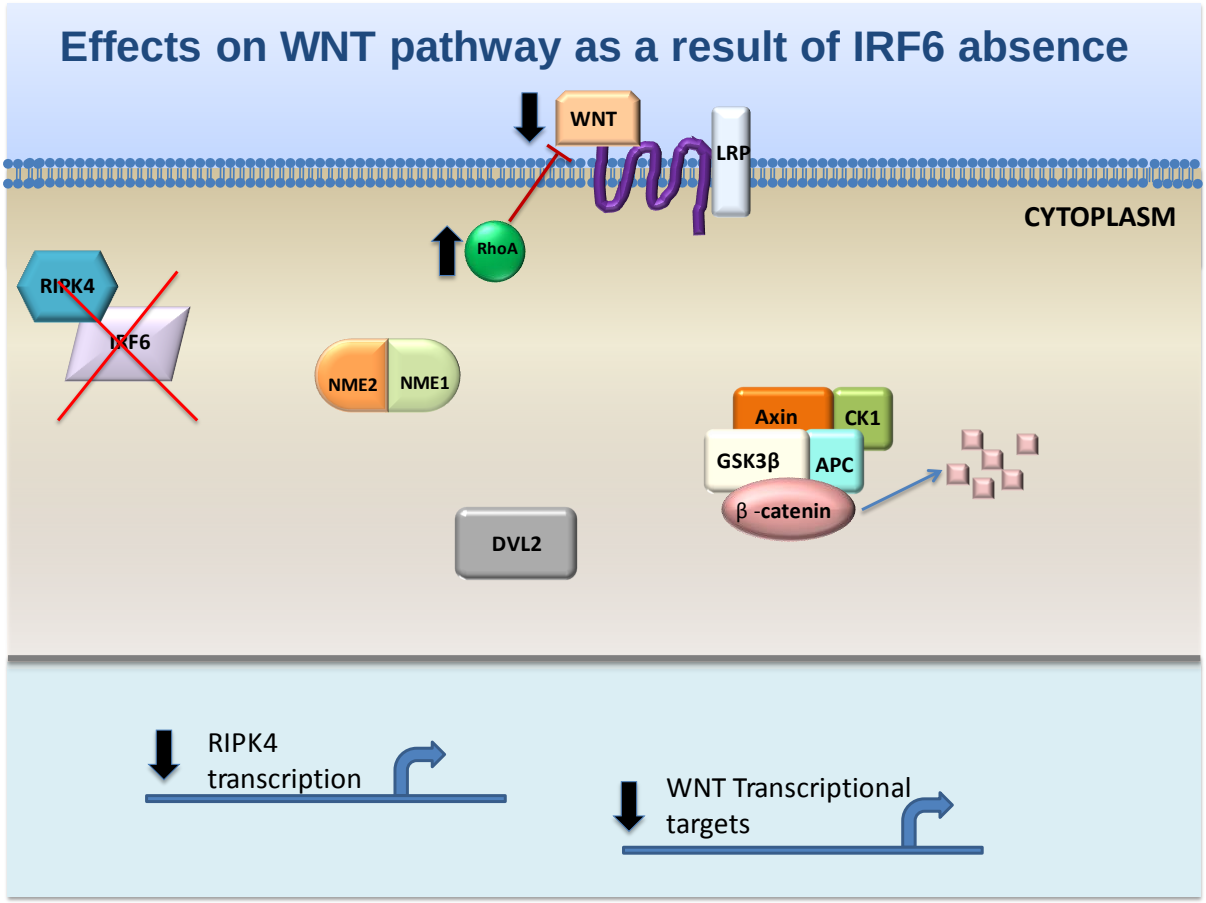

Figure 6.8: Effects on WNT pathway as a result of IRF6 loss. In the absence of IRF6, *RIPK4* transcription is downregulated, and the IRF6:NME complex is not formed. Consequently, DVL2 is not phosphorylated, the Axin/CK1/GSK3β/APC complex degrades β-catenin, and transcription of WNT targets is downregulated. Furthermore, RhoA increases, and WNT signaling is inhibited.

Tooth abnormalities observed in *Irf6-cKO* mice		
Defect	**Possible Contributing Factors**	**Connections to IRF6**
Aberrant crown morphology, including loss of cusp patterning	Wnt10a	Wnt10a null molars exhibit blunted cusps similar to *Irf6-cKO* molars, Wnt10 and Wnt10b have a similar expression pattern in teeth
	Wnt10b	Decrease in *Wnt10b* mRNA in *Irf6-cKO* P4 molars
	Eda pathway	Wnt signaling activates Eda, Eda mutations result in reduced molar cusps
Altered root morphology, including taurodontism	IRF6 mutations	VWS patients with IRF6 mutations exhibit taurodontism
	Osterix	Decrease in *Osx* mRNA in *Irf6-cKO* P4 molars
	Wnt10a	Wnt10a null molars exhibit taurodontic mandibular molars similar to *Irf6-cKO* mandibular molars
	Wnt pathways, e.g. Wnt/beta-catenin signaling	Disruptions in Wnt/beta-catenin signaling leads to short roots
	HERS factors	HERS in *Irf6-cKO* mice appears shorter compared to controls Wnt signaling may have roles in HERS folding and elongation
Hypomineralized enamel, increased enamel attrition	Amelogenin	AMEL expressed at higher levels in P14 and P28 *Irf6-cKO* incisors
	Kallikrein 4	KLK4 expressed at lower levels in P14 and P28 *Irf6-cKO* incisors
Hypodontia	IRF6 mutations	VWS patients with IRF6 mutations exhibit taurodontism
	Wnt10a	Patients with Wnt10a mutations exhibit tooth agenesis
Altered ameloblast polarity	NME	IRF6 forms a complex with NME, *Irf6-cKO* ameloblasts exhibit altered NME distribution
	Rac1	HEK293T cells overexpressing IRF6 mutations

Table 6.1: Summary of tooth defects observed in *Irf6-cKO* mice.

REFERENCES

1. Murray, J. (2000) Meeting Report. . In *WHO Meeting: International Collaborative Research on Craniofacial Anomalies* Geneva, Switzerland

2. Murray, J. C. (2002) Gene/environment causes of cleft lip and/or palate. *Clin Genet* **61**, 248-256

3. Robert J. Gorlin, M. Michael Cohen, and Hennekam, R. C. M. (2001) *Syndromes of the head and neck*, Oxford University Press, New York

4. Vanderas, A. P. (1987) Incidence of cleft lip, cleft palate, and cleft lip and palate among races: a review. *The Cleft palate journal* **24**, 216-225

5. Kondo, S., Schutte, B. C., Richardson, R. J., Bjork, B. C., Knight, A. S., Watanabe, Y., Howard, E., de Lima, R. L., Daack-Hirsch, S., Sander, A., McDonald-McGinn, D. M., Zackai, E. H., Lammer, E. J., Aylsworth, A. S., Ardinger, H. H., Lidral, A. C., Pober, B. R., Moreno, L., Arcos-Burgos, M., Valencia, C., Houdayer, C., Bahuau, M., Moretti-Ferreira, D., Richieri-Costa, A., Dixon, M. J., and Murray, J. C. (2002) Mutations in IRF6 cause Van der Woude and popliteal pterygium syndromes. *Nature genetics* **32**, 285-289

6. Ghassibe, M., Revencu, N., Bayet, B., Gillerot, Y., Vanwijck, R., Verellen-Dumoulin, C., and Vikkula, M. (2003) Gene symbol: IRF6. Disease: Van der Woude syndrome. *Human genetics* **113**, 558

7. Kayano, S., Kure, S., Suzuki, Y., Kanno, K., Aoki, Y., Kondo, S., Schutte, B. C., Murray, J. C., Yamada, A., and Matsubara, Y. (2003) Novel IRF6 mutations in Japanese patients with Van der Woude syndrome: two missense mutations (R45Q and P396S) and a 17-kb deletion. *Journal of human genetics* **48**, 622-628

8. Kim, Y., Park, J. Y., Lee, T. J., and Yoo, H. W. (2003) Identification of two novel mutations of IRF6 in Korean families affected with Van der Woude syndrome. *International journal of molecular medicine* **12**, 465-468

9. Shotelersuk, V., Srichomthong, C., Yoshiura, K., and Niikawa, N. (2003) A novel mutation, 1234del(C), of the IRF6 in a Thai family with Van der Woude syndrome. *International journal of molecular medicine* **11**, 505-507

10. Wang, X., Liu, J., Zhang, H., Xiao, M., Li, J., Yang, C., Lin, X., Wu, Z., Hu, L., and Kong, X. (2003) Novel mutations in the IRF6 gene for Van der Woude syndrome. *Human genetics* **113**, 382-386

11. Chakravarti, A. (2004) Finding needles in haystacks--IRF6 gene variants in isolated cleft lip or cleft palate. *N Engl J Med* **351**, 822-824

12. Gatta, V., Scarciolla, O., Cupaioli, M., Palka, C., Chiesa, P. L., and Stuppia, L. (2004) A novel mutation of the IRF6 gene in an Italian family with Van der Woude syndrome. *Mutat Res* **547**, 49-53

13. Ghassibe, M., Revencu, N., Bayet, B., Gillerot, Y., Vanwijck, R., Verellen-Dumoulin, C., and Vikkula, M. (2004) Six families with van der Woude and/or popliteal pterygium syndrome: all with a mutation in the IRF6 gene. *Journal of medical genetics* **41**, e15

14. Matsuzawa, N., Yoshiura, K., Machida, J., Nakamura, T., Niimi, T., Furukawa, H., Toyoda, T., Natsume, N., Shimozato, K., and Niikawa, N. (2004) Two missense mutations in the IRF6 gene in two Japanese families with Van der Woude syndrome. *Oral surgery, oral medicine, oral pathology, oral radiology, and endodontics* **98**, 414-417

15. Zucchero, T. M., Cooper, M. E., Maher, B. S., Daack-Hirsch, S., Nepomuceno, B., Ribeiro, L., Caprau, D., Christensen, K., Suzuki, Y., Machida, J., Natsume, N., Yoshiura, K., Vieira, A. R., Orioli, I. M., Castilla, E. E., Moreno, L., Arcos-Burgos, M., Lidral, A. C., Field, L. L., Liu, Y. E., Ray, A., Goldstein, T. H., Schultz, R. E., Shi, M., Johnson, M. K., Kondo, S., Schutte, B. C., Marazita, M. L., and Murray, J. C. (2004) Interferon regulatory factor 6 (IRF6) gene variants and the risk of isolated cleft lip or palate. *N Engl J Med* **351**, 769-780

16. Peyrard-Janvid, M., Pegelow, M., Koillinen, H., Larsson, C., Fransson, I., Rautio, J., Hukki, J., Larson, O., Karsten, A. L., and Kere, J. (2005) Novel and de novo mutations of the IRF6 gene detected in patients with Van der Woude or popliteal pterygium syndrome. *Eur J Hum Genet* **13**, 1261-1267

17. Wang, X. F., Xiao, M. Z., Shi, J. N., Zhang, H. B., Hu, L. D., and Kong, X. Y. (2005) [IRF6 gene mutation analysis in a van Der Woude syndrome family in Henan province]. *Shanghai Kou Qiang Yi Xue* **14**, 234-237

18. Du, X., Tang, W., Tian, W., Li, S., Li, X., Liu, L., Zheng, X., Chen, X., Lin, Y., and Tang, Y. (2006) Novel IRF6 mutations in Chinese patients with Van der Woude syndrome. *J Dent Res* **85**, 937-940

19. Du, X. Y., Tang, W., Tian, W. D., Li, X. Y., Liu, L., and Zheng, X. H. (2006) [Identification of three novel mutations of IRF6 in Chinese families with Van der Woude syndrome]. *Zhonghua Yi Xue Yi Chuan Xue Za Zhi* **23**, 82-83

20. Matsuzawa, N., Shimozato, K., Natsume, N., Niikawa, N., and Yoshiura, K. (2006) A novel missense mutation in Van der Woude syndrome: usefulness of fingernail DNA for genetic analysis. *J Dent Res* **85**, 1143-1146

21. Brosch, S., Baur, M., Blin, N., Reinert, S., and Pfister, M. (2007) A novel IRF6 nonsense mutation (Y67X) in a German family with Van der Woude syndrome. *International journal of molecular medicine* **20**, 85-89

22. Birnbaum, S., Reutter, H., Lauster, C., Scheer, M., Schmidt, G., Saffar, M., Martini, M., Hemprich, A., Henschke, H., Kramer, F. J., and Mangold, E. (2008) Mutation screening in the IRF6-gene in patients with apparently nonsyndromic orofacial clefts and a positive family history suggestive of autosomal-dominant inheritance. *American journal of medical genetics* **146A**, 787-790

23. de Medeiros, F., Hansen, L., Mawlad, E., Eiberg, H., Asklund, C., Tommerup, N., and Jakobsen, L. P. (2008) A novel mutation in IRF6 resulting in VWS-PPS spectrum disorder with renal aplasia. *American journal of medical genetics* **146A**, 1605-1608

24. Paranaiba, L. M., Martelli-Junior, H., Oliveira Swerts, M. S., Line, S. R., and Coletta, R. D. (2008) Novel mutations in the IRF6 gene in Brazilian families with Van der Woude syndrome. *International journal of molecular medicine* **22**, 507-511

25. Tan, E. C., Lim, E. C., Yap, S. H., Lee, S. T., Cheng, J., Por, Y. C., and Yeow, V. (2008) Identification of IRF6 gene variants in three families with Van der Woude syndrome. *International journal of molecular medicine* **21**, 747-751

26. Birnbaum, S., Ludwig, K. U., Reutter, H., Herms, S., de Assis, N. A., Diaz-Lacava, A., Barth, S., Lauster, C., Schmidt, G., Scheer, M., Saffar, M., Martini, M., Reich, R. H., Schiefke, F., Hemprich, A., Potzsch, S., Potzsch, B., Wienker, T. F., Hoffmann, P., Knapp, M., Kramer, F. J., Nothen, M. M., and Mangold, E. (2009) IRF6 gene variants in Central European patients with non-syndromic cleft lip with or without cleft palate. *Eur J Oral Sci* **117**, 766-769

27. Jehee, F. S., Burin, B. A., Rocha, K. M., Zechi-Ceide, R., Bueno, D. F., Brito, L., Souza, J., Leal, G. F., Richieri-Costa, A., Alonso, N., Otto, P. A., and Passos-Bueno, M. R. (2009) Novel mutations in IRF6 in nonsyndromic cleft lip with or without cleft palate: when should IRF6 mutational screening be done? *American journal of medical genetics* **149A**, 1319-1322

28. Little, H. J., Rorick, N. K., Su, L. I., Baldock, C., Malhotra, S., Jowitt, T., Gakhar, L., Subramanian, R., Schutte, B. C., Dixon, M. J., and Shore, P. (2009) Missense mutations that cause Van der Woude syndrome and popliteal pterygium

syndrome affect the DNA-binding and transcriptional activation functions of IRF6. *Human molecular genetics* **18**, 535-545

29. Matsuzawa, N., Kondo, S., Shimozato, K., Nagao, T., Nakano, M., Tsuda, M., Hirano, A., Niikawa, N., and Yoshiura, K. (2010) Two missense mutations of the IRF6 gene in two Japanese families with popliteal pterygium syndrome. *American journal of medical genetics* **152A**, 2262-2267

30. Rutledge, K. D., Barger, C., Grant, J. H., and Robin, N. H. (2010) IRF6 mutations in mixed isolated familial clefting. *American journal of medical genetics* **152A**, 3107-3109

31. Scioletti, A. P., Brancati, F., Gatta, V., Antonucci, I., Peissel, B., Pizzuti, A., Mortellaro, C., Tete, S., Gherlone, E., Palka, G., and Stuppia, L. (2010) Two novel mutations affecting splicing in the IRF6 gene associated with van der Woude syndrome. *The Journal of craniofacial surgery* **21**, 1654-1656

32. Birkeland, A. C., Larrabee, Y., Kent, D. T., Flores, C., Su, G. H., Lee, J. H., and Haddad, J., Jr. (2011) Novel IRF6 mutations in Honduran Van der Woude syndrome patients. *Mol Med Report* **4**, 237-241

33. Salahshourifar, I., Wan Sulaiman, W. A., Halim, A. S., and Zilfalil, B. A. (2012) Mutation screening of IRF6 among families with non-syndromic oral clefts and identification of two novel variants: Review of the literature. *Eur J Med Genet* **55**, 389-393

34. Burdick, A. B. (1986) Genetic epidemiology and control of genetic expression in van der Woude syndrome. *J Craniofac Genet Dev Biol Suppl* **2**, 99-105

35. Cox, T. C. (2004) Taking it to the max: the genetic and developmental mechanisms coordinating midfacial morphogenesis and dysmorphology. *Clin Genet* **65**, 163-176

36. Sun, D., Baur, S., and Hay, E. D. (2000) Epithelial-mesenchymal transformation is the mechanism for fusion of the craniofacial primordia involved in morphogenesis of the chicken lip. *Dev Biol* **228**, 337-349

37. Nanci, A. (2003) Chapter 3. Embryology of the Head, Face, and Oral Cavity In *Ten Cate's Oral Histology: Development, Structure, and Function* (Nanci, A., ed), Mosby, St. Louis

38. Jiang, R., Bush, J. O., and Lidral, A. C. (2006) Development of the upper lip: morphogenetic and molecular mechanisms. *Dev Dyn* **235**, 1152-1166

39. Friedman, O., Wang, T. D., and Milczuk, H. A. (2010) Cleft Lip and Palate. In *Cummings Otolarynology Head & Neck Surgery* (Flint, P. W., Haughey, B. H.,

Lund, V. J., Niparko, J. K., Richardson, M. A., Robbins, K. T., and Thomas, J. R., eds) pp. 2659-2675, Mosby, Philadelphia, PA

40. Dyleski, R. A., and Crockett, D. A. (2006) Cleft Lip and Palate: Evaluation and Treatment of Primary Deformity In *Head & Neck Surgery--Otolarynology* (Bailey, B. J., Johnson, J. T., and Newlands, S. D., eds), Lippincott Williams & Wilkins

41. Lorot-Marchand, A., Guerreschi, P., Pellerin, P., Martinot, V., Gbaguidi, C. C., Neiva, C., Devauchelle, B., Frochisse, C., Poli-Merol, M. L., and Francois-Fiquet, C. (2015) Frequency and socio-psychological impact of taunting in school-age patients with cleft lip-palate surgical repair. *Int J Pediatr Otorhinolaryngol*

42. Ramstad, T., Ottem, E., and Shaw, W. C. (1995) Psychosocial adjustment in Norwegian adults who had undergone standardised treatment of complete cleft lip and palate. II. Self-reported problems and concerns with appearance. *Scand J Plast Reconstr Surg Hand Surg* **29**, 329-336

43. Sousa, A. D., Devare, S., and Ghanshani, J. (2009) Psychological issues in cleft lip and cleft palate. *J Indian Assoc Pediatr Surg* **14**, 55-58

44. Petrackova, I., Zach, J., Borsky, J., Cerny, M., Hacklova, R., Tvrdek, M., and Janota, J. (2015) Early and late operation of cleft lip and intelligence quotient and psychosocial development in 3-7 years. *Early Hum Dev* **91**, 149-152

45. Nanci, A. (2008) *Ten Cate's Oral Histology: Development, Structure, and Function*, Mosby Elsevier, St. Louis

46. Sadler, T. (2006) *Langman's Medical Embryology*, Lippincott, Williams & Wilkins, Philadelphia

47. Depew, M. J., and Compagnucci, C. (2008) Tweaking the hinge and caps: testing a model of the organization of jaws. *J Exp Zool B Mol Dev Evol* **310**, 315-335

48. Fuchs, E., and Raghavan, S. (2002) Getting under the skin of epidermal morphogenesis. *Nature reviews* **3**, 199-209

49. M'Boneko, V., and Merker, H. J. (1988) Development and morphology of the periderm of mouse embryos (days 9-12 of gestation). *Acta Anat (Basel)* **133**, 325-336

50. Richardson, R. J., Hammond, N. L., Coulombe, P. A., Saloranta, C., Nousiainen, H. O., Salonen, R., Berry, A., Hanley, N., Headon, D., Karikoski, R., and Dixon, M. J. (2014) Periderm prevents pathological epithelial adhesions during embryogenesis. *The Journal of clinical investigation* **124**, 3891-3900

51. Fitchett, J. E., and Hay, E. D. (1989) Medial edge epithelium transforms to mesenchyme after embryonic palatal shelves fuse. *Dev Biol* **131**, 455-474

52. Martinez-Alvarez, C., Tudela, C., Perez-Miguelsanz, J., O'Kane, S., Puerta, J., and Ferguson, M. W. (2000) Medial edge epithelial cell fate during palatal fusion. *Dev Biol* **220**, 343-357

53. Martinez-Alvarez, C., Bonelli, R., Tudela, C., Gato, A., Mena, J., O'Kane, S., and Ferguson, M. W. (2000) Bulging medial edge epithelial cells and palatal fusion. *Int J Dev Biol* **44**, 331-335

54. Nawshad, A. (2008) Palatal seam disintegration: to die or not to die? that is no longer the question. *Dev Dyn* **237**, 2643-2656

55. Dudas, M., Li, W. Y., Kim, J., Yang, A., and Kaartinen, V. (2007) Palatal fusion - where do the midline cells go? A review on cleft palate, a major human birth defect. *Acta histochemica* **109**, 1-14

56. Kurosaka, H., Iulianella, A., Williams, T., and Trainor, P. A. (2014) Disrupting hedgehog and WNT signaling interactions promotes cleft lip pathogenesis. *The Journal of clinical investigation* **124**, 1660-1671

57. Cano, A., Perez-Moreno, M. A., Rodrigo, I., Locascio, A., Blanco, M. J., del Barrio, M. G., Portillo, F., and Nieto, M. A. (2000) The transcription factor snail controls epithelial-mesenchymal transitions by repressing E-cadherin expression. *Nat Cell Biol* **2**, 76-83

58. Frebourg, T., Oliveira, C., Hochain, P., Karam, R., Manouvrier, S., Graziadio, C., Vekemans, M., Hartmann, A., Baert-Desurmont, S., Alexandre, C., Lejeune Dumoulin, S., Marroni, C., Martin, C., Castedo, S., Lovett, M., Winston, J., Machado, J. C., Attie, T., Jabs, E. W., Cai, J., Pellerin, P., Triboulet, J. P., Scotte, M., Le Pessot, F., Hedouin, A., Carneiro, F., Blayau, M., and Seruca, R. (2006) Cleft lip/palate and CDH1/E-cadherin mutations in families with hereditary diffuse gastric cancer. *Journal of medical genetics* **43**, 138-142

59. Blackburn, J., Ohazama, A., Kawasaki, K., Otsuka-Tanaka, Y., Liu, B., Honda, K., Rountree, R. B., Hu, Y., Kawasaki, M., Birchmeier, W., Schmidt-Ullrich, R., Kinoshita, A., Schutte, B. C., Hammond, N. L., Dixon, M. J., and Sharpe, P. T. (2012) The role of Irf6 in tooth epithelial invagination. *Dev Biol* **365**, 61-70

60. Knight, A. S., Schutte, B. C., Jiang, R., and Dixon, M. J. (2006) Developmental expression analysis of the mouse and chick orthologues of IRF6: the gene mutated in Van der Woude syndrome. *Dev Dyn* **235**, 1441-1447

61. Richardson, R. J., Dixon, J., Jiang, R., and Dixon, M. J. (2009) Integration of IRF6 and Jagged2 signalling is essential for controlling palatal adhesion and fusion competence. *Human molecular genetics* **18**, 2632-2642

62. de la Garza, G., Schleiffarth, J. R., Dunnwald, M., Mankad, A., Weirather, J. L., Bonde, G., Butcher, S., Mansour, T. A., Kousa, Y. A., Fukazawa, C. F., Houston, D. W., Manak, J. R., Schutte, B. C., Wagner, D. S., and Cornell, R. A. (2013) Interferon regulatory factor 6 promotes differentiation of the periderm by activating expression of Grainyhead-like 3. *J Invest Dermatol* **133**, 68-77

63. Bush, J. O., and Jiang, R. (2012) Palatogenesis: morphogenetic and molecular mechanisms of secondary palate development. *Development* **139**, 231-243

64. Heldin, C. H., Miyazono, K., and ten Dijke, P. (1997) TGF-beta signalling from cell membrane to nucleus through SMAD proteins. *Nature* **390**, 465-471

65. Massague, J. (1998) TGF-beta signal transduction. *Annu Rev Biochem* **67**, 753-791

66. Pelton, R. W., Dickinson, M. E., Moses, H. L., and Hogan, B. L. (1990) In situ hybridization analysis of TGF beta 3 RNA expression during mouse development: comparative studies with TGF beta 1 and beta 2. *Development* **110**, 609-620

67. Fitzpatrick, D. R., Denhez, F., Kondaiah, P., and Akhurst, R. J. (1990) Differential expression of TGF beta isoforms in murine palatogenesis. *Development* **109**, 585-595

68. Iwata, J., Suzuki, A., Pelikan, R. C., Ho, T. V., Sanchez-Lara, P. A., Urata, M., Dixon, M. J., and Chai, Y. (2013) Smad4-Irf6 genetic interaction and TGFbeta-mediated IRF6 signaling cascade are crucial for palatal fusion in mice. *Development* **140**, 1220-1230

69. Xu, X., Han, J., Ito, Y., Bringas, P., Jr., Urata, M. M., and Chai, Y. (2006) Cell autonomous requirement for Tgfbr2 in the disappearance of medial edge epithelium during palatal fusion. *Dev Biol* **297**, 238-248

70. Carroll, T. J., Park, J. S., Hayashi, S., Majumdar, A., and McMahon, A. P. (2005) Wnt9b plays a central role in the regulation of mesenchymal to epithelial transitions underlying organogenesis of the mammalian urogenital system. *Developmental cell* **9**, 283-292

71. Thomason, H. A., Zhou, H., Kouwenhoven, E. N., Dotto, G. P., Restivo, G., Nguyen, B. C., Little, H., Dixon, M. J., van Bokhoven, H., and Dixon, J. (2010) Cooperation between the transcription factors p63 and IRF6 is essential to prevent cleft palate in mice. *The Journal of clinical investigation* **120**, 1561-1569

72. Ferretti, E., Li, B., Zewdu, R., Wells, V., Hebert, J. M., Karner, C., Anderson, M. J., Williams, T., Dixon, J., Dixon, M. J., Depew, M. J., and Selleri, L. (2011) A Conserved Pbx-Wnt-p63-Irf6 Regulatory Module Controls Face Morphogenesis by Promoting Epithelial Apoptosis. *Developmental cell* **21**, 627-641

73. Ingraham, C. R., Kinoshita, A., Kondo, S., Yang, B., Sajan, S., Trout, K. J., Malik, M. I., Dunnwald, M., Goudy, S. L., Lovett, M., Murray, J. C., and Schutte, B. C. (2006) Abnormal skin, limb and craniofacial morphogenesis in mice deficient for interferon regulatory factor 6 (Irf6). *Nature genetics* **38**, 1335-1340

74. Parada Sanchez, M. (2012) Dissecting the role of the major cleft gene, IRF6 in primary palatogenesis In *Oral Biology* Vol. PhD, University of Washington, Seattle

75. Steeg, P. S., Bevilacqua, G., Kopper, L., Thorgeirsson, U. P., Talmadge, J. E., Liotta, L. A., and Sobel, M. E. (1988) Evidence for a novel gene associated with low tumor metastatic potential. *J Natl Cancer Inst* **80**, 200-204

76. Boissan, M., Dabernat, S., Peuchant, E., Schlattner, U., Lascu, I., and Lacombe, M. L. (2009) The mammalian Nm23/NDPK family: from metastasis control to cilia movement. *Mol Cell Biochem* **329**, 51-62

77. Boissan, M., and Lacombe, M. L. (2011) Learning about the functions of NME/NM23: lessons from knockout mice to silencing strategies. *Naunyn-Schmiedeberg's archives of pharmacology* **384**, 421-431

78. Hsu, T. (2010) NME genes in epithelial morphogenesis. *Naunyn-Schmiedeberg's archives of pharmacology*

79. Woolworth, J. A., Nallamothu, G., and Hsu, T. (2009) The Drosophila metastasis suppressor gene Nm23 homolog, awd, regulates epithelial integrity during oogenesis. *Mol Cell Biol* **29**, 4679-4690

80. Aktary, Z., Chapman, K., Lam, L., Lo, A., Ji, C., Graham, K., Cook, L., Li, L., Mackey, J. R., and Pasdar, M. (2010) Plakoglobin interacts with and increases the protein levels of metastasis suppressor Nm23-H2 and regulates the expression of Nm23-H1. *Oncogene* **29**, 2118-2129

81. Zhao, R., Gong, L., Li, L., Guo, L., Zhu, D., Wu, Z., and Zhou, Q. (2013) nm23-H1 is a negative regulator of TGF-beta1-dependent induction of epithelial-mesenchymal transition. *Exp Cell Res* **319**, 740-749

82. Tso, P. H., Wang, Y., Yung, L. Y., Tong, Y., Lee, M. M., and Wong, Y. H. (2013) RGS19 inhibits Ras signaling through Nm23H1/2-mediated phosphorylation of the kinase suppressor of Ras. *Cell Signal* **25**, 1064-1074

83. Leslie, E. J., Standley, J., Compton, J., Bale, S., Schutte, B. C., and Murray, J. C. (2013) Comparative analysis of IRF6 variants in families with Van der Woude syndrome and popliteal pterygium syndrome using public whole-exome databases. *Genet Med* **15**, 338-344

84. Sohn, W. J., Ji, Y. R., Kim, H. S., Gwon, G. J., Chae, Y. M., An, C. H., Park, H. D., Jung, H. S., Ryoo, Z. Y., Lee, S., and Kim, J. Y. (2012) Rgs19 regulates mouse palatal fusion by modulating cell proliferation and apoptosis in the MEE. *Mech Dev* **129**, 244-254

85. Hartsock, A., and Nelson, W. J. (2008) Adherens and tight junctions: structure, function and connections to the actin cytoskeleton. *Biochim Biophys Acta* **1778**, 660-669

86. Baum, B., and Georgiou, M. (2011) Dynamics of adherens junctions in epithelial establishment, maintenance, and remodeling. *The Journal of cell biology* **192**, 907-917

87. Boggetti, B., and Niessen, C. M. (2012) Adherens junctions in Mammalian development, homeostasis and disease: lessons from mice. *Subcell Biochem* **60**, 321-355

88. Ivanov, A. I., and Naydenov, N. G. (2013) Dynamics and regulation of epithelial adherens junctions: recent discoveries and controversies. *Int Rev Cell Mol Biol* **303**, 27-99

89. Schneeberger, E. E., and Lynch, R. D. (2004) The tight junction: a multifunctional complex. *Am J Physiol Cell Physiol* **286**, C1213-1228

90. Reynolds, A. B., Roesel, D. J., Kanner, S. B., and Parsons, J. T. (1989) Transformation-specific tyrosine phosphorylation of a novel cellular protein in chicken cells expressing oncogenic variants of the avian cellular src gene. *Mol Cell Biol* **9**, 629-638

91. Niessen, C. M., and Gottardi, C. J. (2008) Molecular components of the adherens junction. *Biochim Biophys Acta* **1778**, 562-571

92. Braga, V. M. (1999) Small GTPases and regulation of cadherin dependent cell-cell adhesion. *Mol Pathol* **52**, 197-202

93. Braga, V. M., Machesky, L. M., Hall, A., and Hotchin, N. A. (1997) The small GTPases Rho and Rac are required for the establishment of cadherin-dependent cell-cell contacts. *The Journal of cell biology* **137**, 1421-1431

94. Ridley, A. J., and Hall, A. (1992) The small GTP-binding protein rho regulates the assembly of focal adhesions and actin stress fibers in response to growth factors. *Cell* **70**, 389-399

95. Biggs, L. C., Rhea, L., Schutte, B. C., and Dunnwald, M. (2012) Interferon regulatory factor 6 is necessary, but not sufficient, for keratinocyte differentiation. *J Invest Dermatol* **132**, 50-58

96. Bos, J. L., Rehmann, H., and Wittinghofer, A. (2007) GEFs and GAPs: critical elements in the control of small G proteins. *Cell* **129**, 865-877

97. Saras, J., Franzen, P., Aspenstrom, P., Hellman, U., Gonez, L. J., and Heldin, C. H. (1997) A novel GTPase-activating protein for Rho interacts with a PDZ domain of the protein-tyrosine phosphatase PTPL1. *The Journal of biological chemistry* **272**, 24333-24338

98. Grossi, M., Hiou-Feige, A., Tommasi Di Vignano, A., Calautti, E., Ostano, P., Lee, S., Chiorino, G., and Dotto, G. P. (2005) Negative control of keratinocyte differentiation by Rho/CRIK signaling coupled with up-regulation of KyoT1/2 (FHL1) expression. *Proceedings of the National Academy of Sciences of the United States of America* **102**, 11313-11318

99. McMullan, R., Lax, S., Robertson, V. H., Radford, D. J., Broad, S., Watt, F. M., Rowles, A., Croft, D. R., Olson, M. F., and Hotchin, N. A. (2003) Keratinocyte differentiation is regulated by the Rho and ROCK signaling pathway. *Curr Biol* **13**, 2185-2189

100. Kaartinen, V., Haataja, L., Nagy, A., Heisterkamp, N., and Groffen, J. (2002) TGFbeta3-induced activation of RhoA/Rho-kinase pathway is necessary but not sufficient for epithelio-mesenchymal transdifferentiation: implications for palatogenesis. *International journal of molecular medicine* **9**, 563-570

101. Mertens, A. E., Pegtel, D. M., and Collard, J. G. (2006) Tiam1 takes PARt in cell polarity. *Trends Cell Biol* **16**, 308-316

102. Otsuki, Y., Tanaka, M., Yoshii, S., Kawazoe, N., Nakaya, K., and Sugimura, H. (2001) Tumor metastasis suppressor nm23H1 regulates Rac1 GTPase by interaction with Tiam1. *Proceedings of the National Academy of Sciences of the United States of America* **98**, 4385-4390

103. Diviani, D., Baisamy, L., and Appert-Collin, A. (2006) AKAP-Lbc: a molecular scaffold for the integration of cyclic AMP and Rho transduction pathways. *Eur J Cell Biol* **85**, 603-610

104. Medina, F., Carter, A. M., Dada, O., Gutowski, S., Hadas, J., Chen, Z., and Sternweis, P. C. (2013) Activated RhoA is a positive feedback regulator of the Lbc

family of Rho guanine nucleotide exchange factor proteins. *The Journal of biological chemistry* **288**, 11325-11333

105. Iwashita, S., Fujii, M., Mukai, H., Ono, Y., and Miyamoto, M. (2004) Lbc proto-oncogene product binds to and could be negatively regulated by metastasis suppressor nm23-H2. *Biochem Biophys Res Commun* **320**, 1063-1068

106. Hoshino, T., Shimizu, K., Honda, T., Kawakatsu, T., Fukuyama, T., Nakamura, T., Matsuda, M., and Takai, Y. (2004) A novel role of nectins in inhibition of the E-cadherin-induced activation of Rac and formation of cell-cell adherens junctions. *Mol Biol Cell* **15**, 1077-1088

107. Akhtar, N., and Hotchin, N. A. (2001) RAC1 regulates adherens junctions through endocytosis of E-cadherin. *Mol Biol Cell* **12**, 847-862

108. Lorenowicz, M. J., Fernandez-Borja, M., van Stalborch, A. M., van Sterkenburg, M. A., Hiemstra, P. S., and Hordijk, P. L. (2007) Microtubule dynamics and Rac-1 signaling independently regulate barrier function in lung epithelial cells. *Am J Physiol Lung Cell Mol Physiol* **293**, L1321-1331

109. Suzuki, K., Hu, D., Bustos, T., Zlotogora, J., Richieri-Costa, A., Helms, J. A., and Spritz, R. A. (2000) Mutations of PVRL1, encoding a cell-cell adhesion molecule/herpesvirus receptor, in cleft lip/palate-ectodermal dysplasia. *Nature genetics* **25**, 427-430

110. de Lima, R. L., Hoper, S. A., Ghassibe, M., Cooper, M. E., Rorick, N. K., Kondo, S., Katz, L., Marazita, M. L., Compton, J., Bale, S., Hehr, U., Dixon, M. J., Daack-Hirsch, S., Boute, O., Bayet, B., Revencu, N., Verellen-Dumoulin, C., Vikkula, M., Richieri-Costa, A., Moretti-Ferreira, D., Murray, J. C., and Schutte, B. C. (2009) Prevalence and nonrandom distribution of exonic mutations in interferon regulatory factor 6 in 307 families with Van der Woude syndrome and 37 families with popliteal pterygium syndrome. *Genet Med* **11**, 241-247

111. Qin, B. Y., Liu, C., Lam, S. S., Srinath, H., Delston, R., Correia, J. J., Derynck, R., and Lin, K. (2003) Crystal structure of IRF-3 reveals mechanism of autoinhibition and virus-induced phosphoactivation. *Nat Struct Biol* **10**, 913-921

112. Chang Foreman, H. C., Van Scoy, S., Cheng, T. F., and Reich, N. C. (2012) Activation of interferon regulatory factor 5 by site specific phosphorylation. *PLoS One* **7**, e33098

113. Kwa, M. Q., Nguyen, T., Huynh, J., Ramnath, D., De Nardo, D., Lam, P. Y., Reynolds, E. C., Hamilton, J. A., Sweet, M. J., and Scholz, G. M. (2014) Interferon regulatory factor 6 differentially regulates Toll-like receptor 2-dependent

chemokine gene expression in epithelial cells. *The Journal of biological chemistry* **289**, 19758-19768

114. Kwa, M. Q., Huynh, J., Aw, J., Zhang, L., Nguyen, T., Reynolds, E. C., Sweet, M. J., Hamilton, J. A., and Scholz, G. M. (2014) Receptor-interacting protein kinase 4 and interferon regulatory factor 6 function as a signaling axis to regulate keratinocyte differentiation. *The Journal of biological chemistry* **289**, 31077-31087

115. Laugel-Haushalter, V., Langer, A., Marrie, J., Fraulob, V., Schuhbaur, B., Koch-Phillips, M., Dolle, P., and Bloch-Zupan, A. (2012) From the transcription of genes involved in ectodermal dysplasias to the understanding of associated dental anomalies. *Mol Syndromol* **3**, 158-168

116. Ranta, R. (1986) A review of tooth formation in children with cleft lip/palate. *Am J Orthod Dentofacial Orthop* **90**, 11-18

117. Nawa, H., Oberoi, S., and Vargervik, K. (2008) Taurodontism and Van der Woude syndrome. Is there an association? *The Angle orthodontist* **78**, 832-837

118. Oberoi, S., and Vargervik, K. (2005) Hypoplasia and hypodontia in Van der Woude syndrome. *Cleft Palate Craniofac J* **42**, 459-466

119. Pegelow, M., Peyrard-Janvid, M., Zucchelli, M., Fransson, I., Larson, O., Kere, J., Larsson, C., and Karsten, A. (2008) Familial non-syndromic cleft lip and palate--analysis of the IRF6 gene and clinical phenotypes. *European journal of orthodontics* **30**, 169-175

120. Maas, R., and Bei, M. (1997) The genetic control of early tooth development. *Crit Rev Oral Biol Med* **8**, 4-39

121. Thesleff, I. (2006) The genetic basis of tooth development and dental defects. *American journal of medical genetics* **140**, 2530-2535

122. Lisi, S., Peterkova, R., Peterka, M., Vonesch, J. L., Ruch, J. V., and Lesot, H. (2003) Tooth morphogenesis and pattern of odontoblast differentiation. *Connect Tissue Res* **44 Suppl 1**, 167-170

123. Miletich, I., and Sharpe, P. T. (2003) Normal and abnormal dental development. *Human molecular genetics* **12 Spec No 1**, R69-73

124. Diekwisch, T. G. (2001) The developmental biology of cementum. *Int J Dev Biol* **45**, 695-706

125. Kumakami-Sakano, M., Otsu, K., Fujiwara, N., and Harada, H. (2014) Regulatory mechanisms of Hertwigs epithelial root sheath formation and anomaly correlated with root length. *Exp Cell Res* **325**, 78-82

126. Zeichner-David, M., Oishi, K., Su, Z., Zakartchenko, V., Chen, L. S., Arzate, H., and Bringas, P., Jr. (2003) Role of Hertwig's epithelial root sheath cells in tooth root development. *Dev Dyn* **228**, 651-663

127. Shimazu, Y., Sato, K., and Aoyagi, K. (2009) Hertwig's epithelial cells adn multi-root deelopment of molars in mice. *J Oral Biosci*, 210-217

128. Aoba, T., Komatsu, H., Shimazu, Y., Yagishita, H., and Taya, Y. (1998) Enamel mineralization and an initial crystalline phase. *Connect Tissue Res* **38**, 129-137;discussion 139-145

129. Bartlett, J. D., Ganss, B., Goldberg, M., Moradian-Oldak, J., Paine, M. L., Snead, M. L., Wen, X., White, S. N., and Zhou, Y. L. (2006) 3. Protein-protein interactions of the developing enamel matrix. *Curr Top Dev Biol* **74**, 57-115

130. Margolis, H. C., Beniash, E., and Fowler, C. E. (2006) Role of macromolecular assembly of enamel matrix proteins in enamel formation. *J Dent Res* **85**, 775-793

131. Simmer, J. P., and Hu, J. C. (2002) Expression, structure, and function of enamel proteinases. *Connect Tissue Res* **43**, 441-449

132. Bartlett, J. D. (2013) Dental enamel development: proteinases and their enamel matrix substrates. *ISRN Dent* **2013**, 684607

133. Gibson, C. W., Yuan, Z. A., Hall, B., Longenecker, G., Chen, E., Thyagarajan, T., Sreenath, T., Wright, J. T., Decker, S., Piddington, R., Harrison, G., and Kulkarni, A. B. (2001) Amelogenin-deficient mice display an amelogenesis imperfecta phenotype. *The Journal of biological chemistry* **276**, 31871-31875

134. Gibson, C. W., Li, Y., Daly, B., Suggs, C., Yuan, Z. A., Fong, H., Simmons, D., Aragon, M., Kulkarni, A. B., and Wright, J. T. (2009) The leucine-rich amelogenin peptide alters the amelogenin null enamel phenotype. *Cells Tissues Organs* **189**, 169-174

135. Hu, J. C., Lertlam, R., Richardson, A. S., Smith, C. E., McKee, M. D., and Simmer, J. P. (2011) Cell proliferation and apoptosis in enamelin null mice. *Eur J Oral Sci* **119 Suppl 1**, 329-337

136. Fukae, M., Tanabe, T., Uchida, T., Lee, S. K., Ryu, O. H., Murakami, C., Wakida, K., Simmer, J. P., Yamada, Y., and Bartlett, J. D. (1998) Enamelysin (matrix metalloproteinase-20): localization in the developing tooth and effects of pH and calcium on amelogenin hydrolysis. *J Dent Res* **77**, 1580-1588

137. Witkop, C. J., Jr. (1988) Amelogenesis imperfecta, dentinogenesis imperfecta and dentin dysplasia revisited: problems in classification. *J Oral Pathol* **17**, 547-553

138. Kim, J. W., Simmer, J. P., Hart, T. C., Hart, P. S., Ramaswami, M. D., Bartlett, J. D., and Hu, J. C. (2005) MMP-20 mutation in autosomal recessive pigmented hypomaturation amelogenesis imperfecta. *Journal of medical genetics* **42**, 271-275

139. Ozdemir, D., Hart, P. S., Ryu, O. H., Choi, S. J., Ozdemir-Karatas, M., Firatli, E., Piesco, N., and Hart, T. C. (2005) MMP20 active-site mutation in hypomaturation amelogenesis imperfecta. *J Dent Res* **84**, 1031-1035

140. Lu, Y., Papagerakis, P., Yamakoshi, Y., Hu, J. C., Bartlett, J. D., and Simmer, J. P. (2008) Functions of KLK4 and MMP-20 in dental enamel formation. *Biol Chem* **389**, 695-700

141. Bartlett, J. D., Beniash, E., Lee, D. H., and Smith, C. E. (2004) Decreased mineral content in MMP-20 null mouse enamel is prominent during the maturation stage. *J Dent Res* **83**, 909-913

142. Caterina, J. J., Skobe, Z., Shi, J., Ding, Y., Simmer, J. P., Birkedal-Hansen, H., and Bartlett, J. D. (2002) Enamelysin (matrix metalloproteinase 20)-deficient mice display an amelogenesis imperfecta phenotype. *The Journal of biological chemistry* **277**, 49598-49604

143. Bartlett, J. D., Yamakoshi, Y., Simmer, J. P., Nanci, A., and Smith, C. E. (2011) MMP20 cleaves E-cadherin and influences ameloblast development. *Cells Tissues Organs* **194**, 222-226

144. Hart, P. S., Hart, T. C., Michalec, M. D., Ryu, O. H., Simmons, D., Hong, S., and Wright, J. T. (2004) Mutation in kallikrein 4 causes autosomal recessive hypomaturation amelogenesis imperfecta. *Journal of medical genetics* **41**, 545-549

145. Wright, J. T., Torain, M., Long, K., Seow, K., Crawford, P., Aldred, M. J., Hart, P. S., and Hart, T. C. (2011) Amelogenesis imperfecta: genotype-phenotype studies in 71 families. *Cells Tissues Organs* **194**, 279-283

146. Simmer, J. P., Hu, Y., Richardson, A. S., Bartlett, J. D., and Hu, J. C. (2011) Why does enamel in Klk4-null mice break above the dentino-enamel junction? *Cells Tissues Organs* **194**, 211-215

147. Simmer, J. P., Hu, Y., Lertlam, R., Yamakoshi, Y., and Hu, J. C. (2009) Hypomaturation enamel defects in Klk4 knockout/LacZ knockin mice. *The Journal of biological chemistry* **284**, 19110-19121

148. Barron, M. J., Brookes, S. J., Draper, C. E., Garrod, D., Kirkham, J., Shore, R. C., and Dixon, M. J. (2008) The cell adhesion molecule nectin-1 is critical for normal enamel formation in mice. *Human molecular genetics* **17**, 3509-3520

149. Bartlett, J. D., Dobeck, J. M., Tye, C. E., Perez-Moreno, M., Stokes, N., Reynolds, A. B., Fuchs, E., and Skobe, Z. (2010) Targeted p120-catenin ablation disrupts dental enamel development. *PLoS One* **5**

150. Huang, Z., Kim, J., Lacruz, R. S., Bringas, P., Jr., Glogauer, M., Bromage, T. G., Kaartinen, V. M., and Snead, M. L. (2011) Epithelial-specific knockout of the Rac1 gene leads to enamel defects. *Eur J Oral Sci* **119 Suppl 1**, 168-176

151. Nishikawa, S., Tsukita, S., and Sasa, S. (1990) Localization of adherens junction proteins along the possible sliding interface between secretory ameloblasts of the rat incisor. *Cell Struct Funct* **15**, 245-249

152. Li, Y., Pugach, M. K., Kuehl, M. A., Peng, L., Bouchard, J., Hwang, S. Y., and Gibson, C. W. (2011) Dental enamel structure is altered by expression of dominant negative RhoA in ameloblasts. *Cells Tissues Organs* **194**, 227-231

153. Perez-Riverol, Y., Audain, E., Millan, A., Ramos, Y., Sanchez, A., Vizcaino, J. A., Wang, R., Muller, M., Machado, Y. J., Betancourt, L. H., Gonzalez, L. J., Padron, G., and Besada, V. (2012) Isoelectric point optimization using peptide descriptors and support vector machines. *J Proteomics* **75**, 2269-2274

154. Hsu, T. (2011) NME genes in epithelial morphogenesis. *Naunyn-Schmiedeberg's archives of pharmacology* **384**, 363-372

155. Graham, F. L., Smiley, J., Russell, W. C., and Nairn, R. (1977) Characteristics of a human cell line transformed by DNA from human adenovirus type 5. *J Gen Virol* **36**, 59-74

156. Zhou, Y. L., and Snead, M. L. (2000) Identification of CCAAT/enhancer-binding protein alpha as a transactivator of the mouse amelogenin gene. *The Journal of biological chemistry* **275**, 12273-12280

157. Sarkar, J., Simanian, E. J., Tuggy, S. Y., Bartlett, J. D., Snead, M. L., Sugiyama, T., and Paine, M. L. (2014) Comparison of two mouse ameloblast-like cell lines for enamel-specific gene expression. *Front Physiol* **5**, 277

158. Xu, Y., Zhou, Y. L., Erickson, R. L., Macdougald, O. A., and Snead, M. L. (2007) Physical dissection of the CCAAT/enhancer-binding protein alpha in regulating the mouse amelogenin gene. *Biochem Biophys Res Commun* **354**, 56-61

159. Chen, L. S., Couwenhoven, R. I., Hsu, D., Luo, W., and Snead, M. L. (1992) Maintenance of amelogenin gene expression by transformed epithelial cells of mouse enamel organ. *Arch Oral Biol* **37**, 771-778

160. Li, X., Venugopalan, S. R., Cao, H., Pinho, F. O., Paine, M. L., Snead, M. L., Semina, E. V., and Amendt, B. A. (2014) A model for the molecular underpinnings of tooth defects in Axenfeld-Rieger syndrome. *Human molecular genetics* **23**, 194-208

161. Rizos, M., and Spyropoulos, M. N. (2004) Van der Woude syndrome: a review. Cardinal signs, epidemiology, associated features, differential diagnosis, expressivity, genetic counselling and treatment. *European journal of orthodontics* **26**, 17-24

162. Jones, J. L., Canady, J. W., Brookes, J. T., Wehby, G. L., L'Heureux, J., Schutte, B. C., Murray, J. C., and Dunnwald, M. (2010) Wound complications after cleft repair in children with Van der Woude syndrome. *The Journal of craniofacial surgery* **21**, 1350-1353

163. Restivo, G., Nguyen, B. C., Dziunycz, P., Ristorcelli, E., Ryan, R. J., Ozuysal, O. Y., Di Piazza, M., Radtke, F., Dixon, M. J., Hofbauer, G. F., Lefort, K., and Dotto, G. P. (2011) IRF6 is a mediator of Notch pro-differentiation and tumour suppressive function in keratinocytes. *EMBO J* **30**, 4571-4585

164. Richardson, R. J., Dixon, J., Malhotra, S., Hardman, M. J., Knowles, L., Boot-Handford, R. P., Shore, P., Whitmarsh, A., and Dixon, M. J. (2006) Irf6 is a key determinant of the keratinocyte proliferation-differentiation switch. *Nature genetics* **38**, 1329-1334

165. Ozato, K., Tailor, P., and Kubota, T. (2007) The interferon regulatory factor family in host defense: mechanism of action. *The Journal of biological chemistry* **282**, 20065-20069

166. Tanaka, N., and Taniguchi, T. (2000) The interferon regulatory factors and oncogenesis. *Semin Cancer Biol* **10**, 73-81

167. Taniguchi, T., Ogasawara, K., Takaoka, A., and Tanaka, N. (2001) IRF family of transcription factors as regulators of host defense. *Annu Rev Immunol* **19**, 623-655

168. Mamane, Y., Heylbroeck, C., Genin, P., Algarte, M., Servant, M. J., LePage, C., DeLuca, C., Kwon, H., Lin, R., and Hiscott, J. (1999) Interferon regulatory factors: the next generation. *Gene* **237**, 1-14

169. Paun, A., and Pitha, P. M. (2007) The IRF family, revisited. *Biochimie* **89**, 744-753

170. Gritli-Linde, A. (2010) p63 and IRF6: brothers in arms against cleft palate. *The Journal of clinical investigation* **120**, 1386-1389

171. Vanbokhoven, H., Melino, G., Candi, E., and Declercq, W. (2011) p63, a story of mice and men. *J Invest Dermatol* **131**, 1196-1207

172. Tanaka, M., Kuriyama, S., and Aiba, N. (2012) Nm23-H1 regulates contact inhibition of locomotion, which is affected by ephrin-B1. *J Cell Sci* **125**, 4343-4353

173. Kosa, N. M., Haushalter, R. W., Smith, A. R., and Burkart, M. D. (2012) Reversible labeling of native and fusion-protein motifs. *Nat Methods* **9**, 981-984

174. Bailey, S. D., D'Auria, J. P., and Haushalter, J. P. (2013) Information on infantile colic on the World Wide Web. *J Pediatr Health Care* **27**, 443-450

175. Zhang, D., Lin, J., and Han, J. (2010) Receptor-interacting protein (RIP) kinase family. *Cell Mol Immunol* **7**, 243-249

176. Abdalla, E. M., and Morsy, H. (2011) Bartsocas-papas syndrome: unusual findings in the first reported egyptian family. *Case Rep Genet* **2011**, 428714

177. Kalay, E., Sezgin, O., Chellappa, V., Mutlu, M., Morsy, H., Kayserili, H., Kreiger, E., Cansu, A., Toraman, B., Abdalla, E. M., Aslan, Y., Pillai, S., and Akarsu, N. A. (2012) Mutations in RIPK4 cause the autosomal-recessive form of popliteal pterygium syndrome. *American journal of human genetics* **90**, 76-85

178. Mitchell, K., O'Sullivan, J., Missero, C., Blair, E., Richardson, R., Anderson, B., Antonini, D., Murray, J. C., Shanske, A. L., Schutte, B. C., Romano, R. A., Sinha, S., Bhaskar, S. S., Black, G. C., Dixon, J., and Dixon, M. J. (2012) Exome sequence identifies RIPK4 as the Bartsocas-Papas syndrome locus. *American journal of human genetics* **90**, 69-75

179. Holland, P., Willis, C., Kanaly, S., Glaccum, M., Warren, A., Charrier, K., Murison, J., Derry, J., Virca, G., Bird, T., and Peschon, J. (2002) RIP4 is an ankyrin repeat-containing kinase essential for keratinocyte differentiation. *Curr Biol* **12**, 1424-1428

180. Rountree, R. B., Willis, C. R., Dinh, H., Blumberg, H., Bailey, K., Dean, C., Jr., Peschon, J. J., and Holland, P. M. (2010) RIP4 regulates epidermal differentiation and cutaneous inflammation. *J Invest Dermatol* **130**, 102-112

181. Kwa, M. Q., Huynh, J., Reynolds, E. C., Hamilton, J. A., and Scholz, G. M. (2015) Disease-associated mutations in IRF6 and RIPK4 dysregulate their signalling functions. *Cell Signal* **27**, 1509-1516

182. Botti, E., Spallone, G., Moretti, F., Marinari, B., Pinetti, V., Galanti, S., De Meo, P. D., De Nicola, F., Ganci, F., Castrignano, T., Pesole, G., Chimenti, S., Guerrini, L., Fanciulli, M., Blandino, G., Karin, M., and Costanzo, A. (2011) Developmental factor IRF6 exhibits tumor suppressor activity in squamous cell carcinomas. *Proceedings of the National Academy of Sciences of the United States of America* **108**, 13710-13715

183. Lynch, C. C., Vargo-Gogola, T., Matrisian, L. M., and Fingleton, B. (2010) Cleavage of E-Cadherin by Matrix Metalloproteinase-7 Promotes Cellular Proliferation in Nontransformed Cell Lines via Activation of RhoA. *J Oncol* **2010**, 530745

184. Troyanovsky, R. B., Sokolov, E. P., and Troyanovsky, S. M. (2006) Endocytosis of cadherin from intracellular junctions is the driving force for cadherin adhesive dimer disassembly. *Mol Biol Cell* **17**, 3484-3493

185. Ivanov, A. I. (2008) Pharmacological inhibition of endocytic pathways: is it specific enough to be useful? *Methods Mol Biol* **440**, 15-33

186. Chiasson, C. M., Wittich, K. B., Vincent, P. A., Faundez, V., and Kowalczyk, A. P. (2009) p120-catenin inhibits VE-cadherin internalization through a Rho-independent mechanism. *Mol Biol Cell* **20**, 1970-1980

187. Ivanov, A. I., Nusrat, A., and Parkos, C. A. (2004) Endocytosis of epithelial apical junctional proteins by a clathrin-mediated pathway into a unique storage compartment. *Mol Biol Cell* **15**, 176-188

188. Palacios, F., Schweitzer, J. K., Boshans, R. L., and D'Souza-Schorey, C. (2002) ARF6-GTP recruits Nm23-H1 to facilitate dynamin-mediated endocytosis during adherens junctions disassembly. *Nat Cell Biol* **4**, 929-936

189. Paleotti, O., Macia, E., Luton, F., Klein, S., Partisani, M., Chardin, P., Kirchhausen, T., and Franco, M. (2005) The small G-protein Arf6GTP recruits the AP-2 adaptor complex to membranes. *The Journal of biological chemistry* **280**, 21661-21666

190. Guo, X., Wang, M., Jiang, J., Xie, C., Peng, F., Li, X., Tian, R., and Qin, R. (2013) Balanced Tiam1-rac1 and RhoA drives proliferation and invasion of pancreatic cancer cells. *Molecular cancer research : MCR* **11**, 230-239

191. Biggs, L. C., Naridze, R. L., DeMali, K. A., Lusche, D. F., Kuhl, S., Soll, D. R., Schutte, B. C., and Dunnwald, M. (2014) Interferon regulatory factor 6 regulates keratinocyte migration. *J Cell Sci* **127**, 2840-2848

192. Bruewer, M., Hopkins, A. M., Hobert, M. E., Nusrat, A., and Madara, J. L. (2004) RhoA, Rac1, and Cdc42 exert distinct effects on epithelial barrier via selective structural and biochemical modulation of junctional proteins and F-actin. *Am J Physiol Cell Physiol* **287**, C327-335

193. Jou, T. S., and Nelson, W. J. (1998) Effects of regulated expression of mutant RhoA and Rac1 small GTPases on the development of epithelial (MDCK) cell polarity. *The Journal of cell biology* **142**, 85-100

194. Wood, W., Jacinto, A., Grose, R., Woolner, S., Gale, J., Wilson, C., and Martin, P. (2002) Wound healing recapitulates morphogenesis in Drosophila embryos. *Nat Cell Biol* **4**, 907-912

195. Smith, B. J., Nidey, N., Miller, S. F., Moreno Uribe, L. M., Baum, C. L., Hamilton, G. S., 3rd, Wehby, G. L., and Dunnwald, M. (2014) Digital imaging analysis to assess scar phenotype. *Wound Repair Regen* **22**, 228-238

196. Ridley, A. J., and Hall, A. (1992) Distinct patterns of actin organization regulated by the small GTP-binding proteins Rac and Rho. *Cold Spring Harb Symp Quant Biol* **57**, 661-671

197. Liu, C., Liu, W., Palie, J., Lu, M. F., Brown, N. A., and Martin, J. F. (2002) Pitx2c patterns anterior myocardium and aortic arch vessels and is required for local cell movement into atrioventricular cushions. *Development* **129**, 5081-5091

198. Hu, J. C., Chun, Y. H., Al Hazzazzi, T., and Simmer, J. P. (2007) Enamel formation and amelogenesis imperfecta. *Cells Tissues Organs* **186**, 78-85

199. Miyata, M., Rikitake, Y., Takahashi, M., Nagamatsu, Y., Yamauchi, Y., Ogita, H., Hirata, K., and Takai, Y. (2009) Regulation by afadin of cyclical activation and inactivation of Rap1, Rac1, and RhoA small G proteins at leading edges of moving NIH3T3 cells. *The Journal of biological chemistry* **284**, 24595-24609

200. Kim, J. G., Moon, M. Y., Kim, H. J., Li, Y., Song, D. K., Kim, J. S., Lee, J. Y., Kim, J., Kim, S. C., and Park, J. B. (2012) Ras-related GTPases Rap1 and RhoA collectively induce the phagocytosis of serum-opsonized zymosan particles in macrophages. *The Journal of biological chemistry* **287**, 5145-5155

201. Wang, Y. C., Khan, Z., and Wieschaus, E. F. (2013) Distinct Rap1 activity states control the extent of epithelial invagination via alpha-catenin. *Developmental cell* **25**, 299-309

202. Jafarzadeh, H., Azarpazhooh, A., and Mayhall, J. T. (2008) Taurodontism: a review of the condition and endodontic treatment challenges. *International endodontic journal* **41**, 375-388

203. Biz, M. T., Marques, M. R., Crema, V. O., Moriscot, A. S., and dos Santos, M. F. (2010) GTPases RhoA and Rac1 are important for amelogenin and DSPP expression during differentiation of ameloblasts and odontoblasts. *Cell Tissue Res* **340**, 459-470

204. Hatakeyama, J., Fukumoto, S., Nakamura, T., Haruyama, N., Suzuki, S., Hatakeyama, Y., Shum, L., Gibson, C. W., Yamada, Y., and Kulkarni, A. B. (2009) Synergistic roles of amelogenin and ameloblastin. *J Dent Res* **88**, 318-322

205. Heymann, R., About, I., Lendahl, U., Franquin, J. C., Obrink, B., and Mitsiadis, T. A. (2002) E- and N-cadherin distribution in developing and functional human teeth under normal and pathological conditions. *Am J Pathol* **160**, 2123-2133

206. Alves Pereira, K. M., do Amaral, B. A., dos Santos, B. R., Galvao, H. C., Freitas Rde, A., and de Souza, L. B. (2010) Immunohistochemical expression of E-cadherin and beta-catenin in ameloblastomas and tooth germs. *Oral surgery, oral medicine, oral pathology, oral radiology, and endodontics* **109**, 425-431

207. Thesleff, I., and Jernvall, J. (1997) The enamel knot: a putative signaling center regulating tooth development. *Cold Spring Harb Symp Quant Biol* **62**, 257-267

208. Vaahtokari, A., Aberg, T., Jernvall, J., Keranen, S., and Thesleff, I. (1996) The enamel knot as a signaling center in the developing mouse tooth. *Mech Dev* **54**, 39-43

209. Lan, Y., Jia, S., and Jiang, R. (2014) Molecular patterning of the mammalian dentition. *Semin Cell Dev Biol* **25-26**, 61-70

210. Liu, F., Chu, E. Y., Watt, B., Zhang, Y., Gallant, N. M., Andl, T., Yang, S. H., Lu, M. M., Piccolo, S., Schmidt-Ullrich, R., Taketo, M. M., Morrisey, E. E., Atit, R., Dlugosz, A. A., and Millar, S. E. (2008) Wnt/beta-catenin signaling directs multiple stages of tooth morphogenesis. *Dev Biol* **313**, 210-224

211. Chen, J., Lan, Y., Baek, J. A., Gao, Y., and Jiang, R. (2009) Wnt/beta-catenin signaling plays an essential role in activation of odontogenic mesenchyme during early tooth development. *Dev Biol* **334**, 174-185

212. Sarkar, L., and Sharpe, P. T. (1999) Expression of Wnt signalling pathway genes during tooth development. *Mech Dev* **85**, 197-200

213. Srivastava, A. K., Pispa, J., Hartung, A. J., Du, Y., Ezer, S., Jenks, T., Shimada, T., Pekkanen, M., Mikkola, M. L., Ko, M. S., Thesleff, I., Kere, J., and Schlessinger, D. (1997) The Tabby phenotype is caused by mutation in a mouse homologue of the EDA gene that reveals novel mouse and human exons and encodes a protein (ectodysplasin-A) with collagenous domains. *Proceedings of the National Academy of Sciences of the United States of America* **94**, 13069-13074

214. Kristenova, P., Peterka, M., Lisi, S., Gendrault, J. L., Lesot, H., and Peterkova, R. (2002) Different morphotypes of functional dentition in the lower molar region of tabby (EDA) mice. *Orthod Craniofac Res* **5**, 205-214

215. Yang, J., Wang, S. K., Choi, M., Reid, B. M., Hu, Y., Lee, Y. L., Herzog, C. R., Kim-Berman, H., Lee, M., Benke, P. J., Lloyd, K. C., Simmer, J. P., and Hu, J. C. (2015) Taurodontism, variations in tooth number, and misshapened crowns in Wnt10a null mice and human kindreds. *Mol Genet Genomic Med* **3**, 40-58

216. Nadiri, A., Kuchler-Bopp, S., Haikel, Y., and Lesot, H. (2004) Immunolocalization of BMP-2/-4, FGF-4, and WNT10b in the developing mouse first lower molar. *J Histochem Cytochem* **52**, 103-112

217. Kim, T. H., Bae, C. H., Lee, J. C., Kim, J. E., Yang, X., de Crombrugghe, B., and Cho, E. S. (2015) Osterix regulates tooth root formation in a site-specific manner. *J Dent Res* **94**, 430-438

218. Bosshardt, D. D., and Nanci, A. (2004) Hertwig's epithelial root sheath, enamel matrix proteins, and initiation of cementogenesis in porcine teeth. *J Clin Periodontol* **31**, 184-192

219. Zhang, C., Cho, K., Huang, Y., Lyons, J. P., Zhou, X., Sinha, K., McCrea, P. D., and de Crombrugghe, B. (2008) Inhibition of Wnt signaling by the osteoblast-specific transcription factor Osterix. *Proceedings of the National Academy of Sciences of the United States of America* **105**, 6936-6941

220. Gadhia, K., McDonald, S., Arkutu, N., and Malik, K. (2012) Amelogenesis imperfecta: an introduction. *British dental journal* **212**, 377-379

221. Bartlett, J. D., and Simmer, J. P. (2014) Kallikrein-related peptidase-4 (KLK4): role in enamel formation and revelations from ablated mice. *Front Physiol* **5**, 240

222. Nagano, T., Kakegawa, A., Yamakoshi, Y., Tsuchiya, S., Hu, J. C., Gomi, K., Arai, T., Bartlett, J. D., and Simmer, J. P. (2009) Mmp-20 and Klk4 cleavage site preferences for amelogenin sequences. *J Dent Res* **88**, 823-828

223. Hartsough, M. T., Morrison, D. K., Salerno, M., Palmieri, D., Ouatas, T., Mair, M., Patrick, J., and Steeg, P. S. (2002) Nm23-H1 metastasis suppressor phosphorylation of kinase suppressor of Ras via a histidine protein kinase pathway. *The Journal of biological chemistry* **277**, 32389-32399

224. Chandrasekharan, D., and Ramanathan, A. (2014) Identification of a novel heterozygous truncation mutation in exon 1 of ARHGAP29 in an Indian subject with nonsyndromic cleft lip with cleft palate. *Eur J Dent* **8**, 528-532

225. Leslie, E. J., Mansilla, M. A., Biggs, L. C., Schuette, K., Bullard, S., Cooper, M., Dunnwald, M., Lidral, A. C., Marazita, M. L., Beaty, T. H., and Murray, J. C. (2012) Expression and mutation analyses implicate ARHGAP29 as the etiologic gene for the cleft lip with or without cleft palate locus identified by genome-wide

association on chromosome 1p22. *Birth Defects Res A Clin Mol Teratol* **94**, 934-942

226. Letra, A., Maili, L., Mulliken, J. B., Buchanan, E., Blanton, S. H., and Hecht, J. T. (2014) Further evidence suggesting a role for variation in ARHGAP29 variants in nonsyndromic cleft lip/palate. *Birth Defects Res A Clin Mol Teratol* **100**, 679-685

227. Peyrard-Janvid, M., Leslie, E. J., Kousa, Y. A., Smith, T. L., Dunnwald, M., Magnusson, M., Lentz, B. A., Unneberg, P., Fransson, I., Koillinen, H. K., Rautio, J., Pegelow, M., Karsten, A., Basel-Vanagaite, L., Gordon, W., Andersen, B., Svensson, T., Murray, J. C., Cornell, R. A., Kere, J., and Schutte, B. C. (2014) Dominant mutations in GRHL3 cause Van der Woude Syndrome and disrupt oral periderm development. *American journal of human genetics* **94**, 23-32

228. De Groote, P., Tran, H. T., Fransen, M., Tanghe, G., Urwyler, C., De Craene, B., Leurs, K., Gilbert, B., Van Imschoot, G., De Rycke, R., Guerin, C. J., Holland, P., Berx, G., Vandenabeele, P., Lippens, S., Vleminckx, K., and Declercq, W. (2015) A novel RIPK4-IRF6 connection is required to prevent epithelial fusions characteristic for popliteal pterygium syndromes. *Cell Death Differ* **22**, 1012-1024

229. Xue, H., Li, Y., Everett, E. T., Ryan, K., Peng, L., Porecha, R., Yan, Y., Lucchese, A. M., Kuehl, M. A., Pugach, M. K., Bouchard, J., and Gibson, C. W. (2013) Ameloblasts require active RhoA to generate normal dental enamel. *Eur J Oral Sci* **121**, 293-302

230. Peng, L., Li, Y., Shusterman, K., Kuehl, M., and Gibson, C. W. (2011) Wnt-RhoA signaling is involved in dental enamel development. *Eur J Oral Sci* **119 Suppl 1**, 41-49

231. Zhang, R., Yang, G., Wu, X., Xie, J., Yang, X., and Li, T. (2013) Disruption of Wnt/beta-catenin signaling in odontoblasts and cementoblasts arrests tooth root development in postnatal mouse teeth. *Int J Biol Sci* **9**, 228-236

232. Shibata, S., Dias, R. A., Hashimoto-Uoshima, M., Abe, T., and Yanagishita, M. (2007) Immunohistochemical localization of syndecan-1 in the dental follicle of postnatal mouse teeth. *J Periodontol* **78**, 1322-1328

233. Huang, X., McGann, J. C., Liu, B. Y., Hannoush, R. N., Lill, J. R., Pham, V., Newton, K., Kakunda, M., Liu, J., Yu, C., Hymowitz, S. G., Hongo, J. A., Wynshaw-Boris, A., Polakis, P., Harland, R. M., and Dixit, V. M. (2013) Phosphorylation of Dishevelled by protein kinase RIPK4 regulates Wnt signaling. *Science* **339**, 1441-1445

Curriculum Vitae

PART 1: General Information

Name: Emily Y. Chu, DDS

Education:
8/2002-5/2006: Washington University in St. Louis, BA, Biology and Mathematics
8/2006-7/2008: University of Washington, Graduate Non-matriculated student
8/2008-6/2012: University of Washington, DDS
6/2012-6/2015 University of Washington, PhD

Awards and Honors
Top Scholar Award from UW Graduate School (2008)
Summer Undergraduate Research Fellowship Poster Competition, 2nd Place, University of
Washington Research Day (2008)
University of Washington Research Advisory Committee IADR Travel Award
Summer Undergraduate Research Fellowship Poster Competition, 2nd Place, University of
Washington Research Day (2009)
Hatton Poster Competition, Junior Category finalist, AADR (2009)
Most Outstanding Presentation in Clinical Research award, Hinman Student Symposium (2009)
Quintessence Award for Research Achievement (2012)
Academy of General Dentistry (Washington Chapter) & William Howard Student Case
Presentation Competition Award, 1st place (2012)
Academy of Dental Materials Award (2012)
American Association of Oral Biologists Award (2012)
Warren Magnuson Scholar, School of Dentistry (2013)
University of Washington School of Dentistry Graduate Student/Trainee Research Day
Competition, 1st place (2014)
Hatton Poster Competition, Senior Category finalist, AADR (2015)

PART 2: Research/Clinical Training and Contributions

A. Narrative

Currently, I am in my seventh and concluding year of the University of Washington's DDS PhD program. So far, I have found the DDS PhD program to be challenging and stimulating. As I progressed through my educational career, I know that research and clinical practice are not mutually exclusive. Research justifies the treatment performed in the clinic, and clinical practice provides the application of the knowledge acquired from research. Although the primary focus may shift between research and clinic during the different stages of my training, certain aspects remain constant. I am constantly learning, and my commitment to both research and clinic has not waned. In fact, as I gain more experience, my determination to pursue my goals of becoming a scientist and a clinician has strengthened.

As a dual degree student, difficulties in establishing a proper balance between clinical and research responsibilities undoubtedly arise. Ever since I entered the program, I have been integrating the DDS and the PhD portions as much as possible. While completing DDS requirements, I took PhD classes simultaneously with my DDS coursework, used my vacations to complete research rotations, and stayed in contact with my research mentors. This enabled me to submit a successful F30 fellowship application shortly after completing my DDS and passing boards for dental license certification. To stay active in the clinic, I also work part-time in private practice as a General Dentist. To me, having the research and the clinical training fosters an appreciation for both. Because my time is limited, I feel privileged to be able to directly influence the welfare of others in clinic as well as contribute to the pursuit of scientific knowledge in the research lab.

Ultimately, in pursuing both the DDS and PhD degrees, I am aspiring to remain a part of the academic environment. I am hoping to become a tenure-track faculty member with roles in clinic, research, and teaching. Specifically, I believe that an academic institution has the unique capability to simultaneously promote many levels of learning and help members of the community that may not necessarily have access to care otherwise. To me, research is a critical component of patient care—the quality of life of many individuals is improved as the information gained from research leads to more effective treatments. Thus, I believe that by becoming an academic clinician and a researcher, I will be more equipped to make a positive difference in others' lives.

B. Funding	July 2013-July 2015	NIH-NIDDK F30 DK100280-02	PI Trainee: Emily Chu Sponsor: Timothy Cox Co-sponsor: Martha Somerman	Title: Regulation of orofacial ectodermal polarity by the CLP protein, IRF6.
	July 2014-July 2015	Cleft Palate Foundation Junior Investigator Research Grant	Recipient: Emily Chu Sponsor: Timothy Cox	Title: Regulation of orofacial ectodermal polarity by the CLP protein, IRF6.

C. Publications

Chu EY, Fong H, LaCourse MR, Foster BL, Somerman MJ, Cox TC. (*In progress*). IRF6 loss-of-function causes defects in enamel formation and root patterning.

Parada-Sanchez MT, Chu EY, Somerman MJ, Cox, TC. (*In progress*) Inteferon Regulatory Factor 6 (IRF6) interacts directly with NME1/NME2: novel insights into the molecular function of IRF6 in the pathogenesis of cleft lip/palate (CLP).

Lau WL, Linnes M, Chu EY, Foster BL, Bartley BA, Somerman MJ, Giachelli CM. (2013) High phosphate feeding promotes mineral and bone abnormalities in mice with chronic kidney disease. *Nephrol Dial Transplant* 28(1): 62-69.

Foster BL, Nagatomo KJ, Bamashmous SO, Tompkins KA, Fong H, Dunn D, Chu EY, Guenther C, Kingsley DM, Rutherford RB, Somerman MJ. (2011) The Progressive Ankylosis Protein Regulates Cementum Apposition and Extracellular Matrix Composition. *Cells Tissues Organs*. 194(5): 382-405.

Chu EY, Fong H, Blethen FA, Tompkins KA, Foster BL, Yeh K-D, Sitara D, Lanske B, Rutherford RB, and MJ Somerman. (2010). Ablation of systemic phosphate regulating gene fibroblast growth factor 23 (*Fgf23*) compromises the dento-alveolar complex. *Anat Rec* 293(7): 1214-26.

Lee MM, Chu EY, El-Abbadi MM, Foster BL, Tompkins KA, Giachelli CM, Somerman MJ. (2010). Characterization of mandibular bone in a mouse model of chronic kidney disease. *J Periodontol.* 81(2): 300-9.